

UC Davis

Technical Memoranda

Title

RAP and RAS in HMA Pilot Project on ELD 49: Material Testing, Observations, and Findings

Permalink

<https://escholarship.org/uc/item/8h67s9z0>

Authors

Harvey, John
Buscheck, Jeff
Brotschi, Julian
et al.

Publication Date

2023

DOI

10.7922/G2X065DD

RAP and RAS in HMA Pilot Project on ELD 49: Material Testing, Observations, and Findings

Authors:

John Harvey, Jeff Buscheck, Julian Brotschi, Mohammad Rahman,
Angel Mateos, and David Jones

Partnered Pavement Research Center (PPRC) Project 4.79 (DRISI Task 3819):
Guidance, Tests, and Specifications for High Recycled Asphalt Pavement/ Recycled Asphalt
Shingle Contents in HMA and RHMA Mixes

PREPARED FOR:

California Department of Transportation
Division of Research, Innovation, and System Information
Office of Materials and Infrastructure

PREPARED BY:

University of California
Pavement Research Center
UC Davis and UC Berkeley



TECHNICAL REPORT DOCUMENTATION PAGE

1. REPORT NUMBER UCPRC-TM-2020-04	2. GOVERNMENT ASSOCIATION NUMBER	3. RECIPIENT'S CATALOG NUMBER
4. TITLE AND SUBTITLE RAP and RAS in HMA Pilot Project on ELD 49: Material Testing, Observations, and Findings		5. REPORT PUBLICATION DATE January 2023
		6. PERFORMING ORGANIZATION CODE
7. AUTHOR(S) John Harvey (ORCID 0000-0002-8924-6212) Jeff Buscheck (ORCID 0000-0002-0930-6861) Julian Brotschi (ORCID 0000-0002-1752-2898) Mohammad Rahman (ORCID 0000-0001-7855-5346) Angel Mateos (ORCID 0000-0002-3614-2858) David Jones (ORCID 0000-0002-2938-076X)		8. PERFORMING ORGANIZATION REPORT NO. UCPRC-TM-2022-04 UCD-ITS-RR-22-123
9. PERFORMING ORGANIZATION NAME AND ADDRESS University of California Pavement Research Center Department of Civil and Environmental Engineering, UC Davis 1 Shields Avenue Davis, CA 95616		10. WORK UNIT NUMBER
		11. CONTRACT OR GRANT NUMBER 65A0788
12. SPONSORING AGENCY AND ADDRESS California Department of Transportation Division of Research, Innovation, and System Information P.O. Box 942873 Sacramento, CA 94273-0001		13. TYPE OF REPORT AND PERIOD COVERED Technical Memorandum May 2021 to June 2022
		14. SPONSORING AGENCY CODE
15. SUPPLEMENTAL NOTES doi:10.7922/G2X065DD		
16. ABSTRACT A pilot project for the inclusion of recycled asphalt shingles (RAS) in hot mix asphalt (HMA) was built on State Route 49 in El Dorado County in November 2021. Four mixes were included in short test sections: (1) a control mix with no RAS or recycled asphalt pavement (RAP), (2) a typically used mix with 10% RAP that was also used for construction of the rest of the overall project, (3) a mix with 3% RAS, and (4) a mix with 10% RAP and 3% RAS. This technical memorandum presents the laboratory test results from plant mix produced for job mix formula (JMF) verification and from two quality assurance (QA) samples taken during test section construction as well as observations of plant production and construction. The results showed that the mixes submitted for JMF verification and tested as part of QA all met the two performance-related specifications. Most of the QA samples had binder and mix testing results that were similar to or better than those of the JMF verification samples, though there were exceptions. There were no major problems during production or placement of the mixes. The existing roadway has highly variable thicknesses of remaining HMA after milling, and the remaining original HMA has transverse, wheelpath, and block cracks.		
17. KEYWORDS RAP, RAS, hot mix asphalt, pilot project		18. DISTRIBUTION STATEMENT No restrictions. This document is available to the public through the National Technical Information Service, Springfield, VA 22161
19. SECURITY CLASSIFICATION (of this report) Unclassified	20. NUMBER OF PAGES 118	21. PRICE None

Reproduction of completed page authorized

UCPRC ADDITIONAL INFORMATION

1. DRAFT STAGE Final	2. VERSION NUMBER 1
3. UCPRC STRATEGIC PLAN ELEMENT NUMBER 4.79	4. CALTRANS TASK NUMBER 3819
5. CALTRANS TECHNICAL LEAD AND REVIEWER(S) Saeed Pourtahmasb	6. FHWA NUMBER CA233819A
7. PROPOSALS FOR IMPLEMENTATION None	

8. RELATED DOCUMENTS
None

9. LABORATORY ACCREDITATION
The UCPRC laboratory is accredited by AASHTO re:source for the tests listed in this report



10. SIGNATURES

J. T. Harvey FIRST AUTHOR	J.T. Harvey TECHNICAL REVIEW	C. Fink EDITOR	J.T. Harvey PRINCIPAL INVESTIGATOR	S. Pourtahmasb CALTRANS TECH. LEAD	T. J. Holland CALTRANS CONTRACT MANAGER
------------------------------	---------------------------------	-------------------	--	--	--

Reproduction of completed page authorized

DISCLAIMER STATEMENT

This document is disseminated in the interest of information exchange. The contents of this report reflect the views of the authors who are responsible for the facts and accuracy of the data presented herein. The contents do not necessarily reflect the official views or policies of the State of California or the Federal Highway Administration. This publication does not constitute a standard, specification, or regulation. This report does not constitute an endorsement by the Department of any product described herein.

ACKNOWLEDGMENTS

The University of California Pavement Research Center acknowledges the following individuals and organizations who contributed to the project: Caltrans Office of Asphalt Pavement reviewers, DRISI project manager T. Joseph Holland, Construction and Materials staff in District 3, the staff of George Reed, Inc. who produced and placed the mix, the UCPRC laboratory and field staff, and UCPRC publications manager Camille Fink.

TABLE OF CONTENTS

LIST OF TABLES	vi
LIST OF FIGURES	vii
LIST OF ABBREVIATIONS	vii
LIST OF TEST METHODS CITED IN THIS REPORT.....	xiii
PROJECT OBJECTIVES	xvi
1. INTRODUCTION.....	1
1.1 Background of the Study	1
1.2 Problem Statements	2
1.3 Report Structure	3
1.4 Measurement Units	3
2. TESTING PLAN AND MATERIAL SAMPLING	4
2.1 Pilot Project Test Sections Overview and Pre-Overlay Observations	4
2.2 Mix Designs	6
2.3 Testing Plan.....	11
2.4 Material Sampling and Handling	11
2.4.1 Plant-Produced Material Sampling for Job Mix Formula Verification Testing....	11
2.4.2 Plant-Produced Material Sampling During Construction	12
2.4.3 Material Handling After Sampling	13
2.4.6 Binder Extraction	15
2.5 Test Methods	16
2.6 Binder Testing	17
2.6.1 Performance Grading	17
2.6.2 Frequency Sweep	18
2.6.3 Fourier Transform Infrared Spectroscopy.....	20
2.7 Mix Testing.....	21
2.7.1 Test Specimen Air Void Contents.....	22
2.7.2 Triaxial Dynamic Modulus	22
2.7.3 Flexural Dynamic Modulus	23
2.7.4 Fatigue Cracking Resistance.....	23
2.7.5 Fracture Cracking Resistance (SCB).....	24
2.7.6 Rutting Resistance	25
2.7.7 Indirect Tensile Cracking Resistance IDEAL-CT.....	25
2.7.8 Testing Done by Caltrans and Texas A&M University	28
3. BINDER TESTING RESULTS	29
3.1 Introduction	29
3.2 Binder Testing Results for JMF Verification Mix Samples.....	29
3.2.1 PG Grading.....	29
3.2.2 Frequency Sweep	34
3.2.3 FTIR Testing	34
3.3 Binder Testing Results from Quality Assurance Mix Samples.....	34
3.3.1 PG Grading.....	34
3.3.2 Frequency Sweep	39

3.3.3 FTIR Testing	43
4. MIX TESTING RESULTS.....	47
4.1 Introduction	47
4.2 Mix Test Variability.....	47
4.2.1 Overview	47
4.2.2 Variability of Test Results on This Pilot Project.....	49
4.3 Testing of Job Mix Formula Mixes Prior to Construction for JMF Verification.....	51
4.3.1 Mix Stiffness: Flexural and Triaxial Dynamic Modulus.....	51
4.3.2 Rutting Resistance: Repeated Load Triaxial Test (Unconfined and Confined)	55
4.3.3 Fatigue/Reflective Cracking Resistance: Four-Point Beam Test.....	58
4.3.4 Indirect Tensile Cracking Resistance: IDEAL-CT Test.....	61
4.3.5 Fracture Cracking Resistance: Semicircular Beam Test.....	63
4.4 Testing of Mixes Sampled During Construction for Quality Assurance	65
4.4.1 Mix Stiffness: Triaxial and Flexural Dynamic Modulus.....	65
4.4.2 Qualitative Assessment of Binder Blending from Comparison Binder and Mix Stiffness Rankings.....	70
4.4.3 Rutting Resistance: Repeated Load Triaxial Test (Unconfined and Confined)	72
4.4.4 Fatigue/Reflective Cracking Resistance: Four-Point Beam Test.....	76
4.4.5 Indirect Tensile Cracking Resistance: IDEAL-CT Test.....	81
4.4.6 Fracture Cracking Resistance: Semicircular Beam Test.....	84
5. OBSERVATIONS FROM CONSTRUCTION	88
5.1 Milling and Post-Milling Condition	88
5.2 Overlay Construction	88
5.2.1 Plant Operations.....	88
5.2.2 Paving	88
6. CONCLUSIONS AND RECOMMENDATIONS FROM THE ELD 49 PILOT PROJECT	95
6.1 Conclusions	95
6.1.1 Performance-Related Properties of the Four Mixes	95
6.1.2 The Four Mixes and Their Specifications	97
6.1.3 Construction of the Test Sections.....	97
6.2 Preliminary Recommendations	98
REFERENCES	99

LIST OF TABLES

Table 2.1: Pilot Project Test Section Location Lane and Post Miles and Mix Types from Project Special Provisions.....	4
Table 2.2: Non-Standard Special Provision (nSSP) Requirements for the Mixes	8
Table 2.3: Job Mix Formula Submittal by Contractor	9
Table 2.4: Job Mix Formula Verification Results from Caltrans	10
Table 2.5: Mix Samples for JMF Verification Testing by the UCPRC	11
Table 2.6: Mix Sampling, Storage, and Reheating-to-Compaction Temperature Procedures for ELD 49 Pilot Project Materials, Compared with AASHTO R30	14
Table 2.7: JMF Verification Testing Performed by UCPRC for Pilot Project	17
Table 2.8: Fracture Parameters from IDEAL-CT	28
Table 3.1. Continuous Binder Grading Results for JMF Verification and QA Samples	32
Table 4.1: Variability of Within-Sample Stiffness (MPa) and Coefficient of Variation for Dynamic Modulus at 20°C and 10 Hz.....	49
Table 4.2: Variability Of Within-Sample Stiffness (Repetitions To Flow Number or Failure) and Coefficient of Variation for Repeated Load Triaxial Test	49
Table 4.3: Variability of Within-Sample Tensile Strain at 1 Million Repetitions to Failure and Coefficient of Variation for Flexural Fatigue Test.....	50
Table 4.4: Variability of Within-Sample Fracture Test Parameter (IDEAL-CT Number or I-FIT Parameter) and Strength (mpa) and Coefficient of Variation.....	50
Table 4.5: Ranking of Extracted Binder and Mix Stiffnesses from Quality Assurance Testing	71

LIST OF FIGURES

Figure 2.1: Fatigue cracking in the wheelpaths, partly sealed with crack sealant.	5
Figure 2.2: Transverse and block cracking.....	5
Figure 2.3: Fatigue cracking in the wheelpath and extensive crack sealing.	6
Figure 2.4: Sampling from hot drop put in buckets and boxes for QA sampling (each person is sampling from a quadrant of the pile of hot mix).....	13
Figure 2.5: Loose plant mix samples stored in cardboard boxes in temperature-controlled environment before extraction.....	14
Figure 2.6: Closed-loop binder extraction system.....	16
Figure 2.7: Placing extraction cylinder with sample into extraction system.....	16
Figure 2.8: Example of modulus master curves (plotted by frequency at tested temperature).....	19
Figure 2.9: Example of modulus master curves (plotted by shifted frequency).	20
Figure 2.10: Example of normalized FTIR absorbance spectrum.....	21
Figure 2.11: Testing machine for IDEAL-CT with a specimen.....	26
Figure 2.12: Example load-displacement curve from IDEAL-CT.....	26
Figure 3.1: Continuous temperature binder grades for JMF verification sampled binders.	33
Figure 3.2: Delta T _c values for JMF samples (20-hour PAV specification value and for 40-hour PAV).....	33
Figure 3.3: Binder grades for JMF verification sampled binders normalized to Mix A (0% RAP, 0% RAS) control mix.	34
Figure 3.4: Continuous temperature binder grades for QA sampled binders by sample.	37
Figure 3.5: Average continuous temperature binder grades for QA sampled binders.	37
Figure 3.6: Delta T _c values by sample for QA samples (20 hour PAV specification value and for 40 hour PAV).....	38
Figure 3.7: Average Delta T _c values for QA samples (20 hour PAV specification value and for 40 hour PAV).....	38
Figure 3.8: Average binder grades for QA sampled binders normalized to Mix A (0% RAP 0% RAS) control mix.	39
Figure 3.9: Average frequency sweep master curves for QA sampled binders.	41
Figure 3.10: Frequency sweep master curves for both QA sampled binders.	41
Figure 3.11: Frequency sweep master curves for QA sampled binders normalized to Mix B (10% RAP, 0% RAS).....	42
Figure 3.12: Black Space plot for QA sampled binders with Glover-Rowe criteria.	42
Figure 3.13: Carbonyl area index changes after aging for QA sampled binders.	44
Figure 3.14: Sulfoxide area index changes after aging.	44
Figure 3.15: Carbonyl area for all binders versus Glover-Rowe parameter for all QA samples and aging conditions.	45
Figure 3.16: Carbonyl area for all binders versus G* sineδ at 10 Hz and 64°C for all QA samples and aging conditions.	45
Figure 3.17: Carbonyl area for all binders versus crossover modulus for all QA samples and aging conditions.	46
Figure 4.1: Flexural dynamic modulus master curves for JMF verification sampled mixes.	51

Figure 4.2: Flexural dynamic modulus master curves for JMF verification sampled mixes normalized to Mix A (0% RAP, 0% RAS).....	52
Figure 4.3: Black Space diagram for flexural dynamic modulus master curves for JMF verification sampled mixes.	52
Figure 4.4: Triaxial dynamic modulus master curves for JMF verification sampled mixes.	53
Figure 4.5: Triaxial dynamic modulus master curves for JMF verification sampled mixes normalized to Mix A (0% RAP, 0% RAS).....	54
Figure 4.6: Black Space diagram for triaxial dynamic modulus master curves for JMF verification sampled mixes.	54
Figure 4.7: Unconfined repeated load triaxial results for JMF verification mixes (flow number and permanent deformation at flow number).	56
Figure 4.8: Confined repeated load triaxial results for JMF verification mixes (flow number and permanent deformation at flow number).	56
Figure 4.9: Unconfined and confined repeated load triaxial results for JMF verification mixes (load cycles to 3% permanent strain).....	57
Figure 4.10: Unconfined and confined repeated load triaxial results for JMF verification mixes (load cycles to 5% permanent strain).....	57
Figure 4.11: Flexural fatigue results for JMF sampled mixes (Wohler curve).....	59
Figure 4.12: Extrapolation of flexural fatigue results for JMF sampled mixes (Wohler curve)....	60
Figure 4.13: Flexural fatigue results for JMF verification sampled mixes: repetitions to failure at different strain levels from Wohler curve regressions.....	60
Figure 4.14: Flexural fatigue results for JMF sampled mixes: repetitions to failure at different strain levels from Wohler curve regressions normalized to Mix A (0% RAP, 0% RAS).....	61
Figure 4.15: IDEAL-CT test results for JMF verification sampled mixes (CT number and post-peak slope).....	62
Figure 4.16: IDEAL-CT test results for JMF verification sample mixes (fracture energy and strength).....	63
Figure 4.17: I-FIT test results for JMF verification sample mixes (fracture energy and strength).....	64
Figure 4.18: I-FIT test results for JMF verification sample mixes (flexibility index and post-peak slope).....	64
Figure 4.19: Flexural dynamic modulus master curves for QA sampled mixes.....	66
Figure 4.20: Flexural dynamic modulus master curves for QA sampled mixes normalized to Mix A (0% RAP, 0% RAS) first sample (v1).....	67
Figure 4.21: Black Space diagram for flexural dynamic modulus master curves for QA sampled mixes.....	67
Figure 4.22: Triaxial dynamic modulus master curves for QA sampled mixes.....	68
Figure 4.23: Triaxial dynamic modulus master curves for QA sampled mixes normalized to Mix A (0% RAP, 0% RAS) first sample (v1).....	69
Figure 4.24: Black Space diagram for triaxial dynamic modulus master curves for QA sampled mixes.....	69
Figure 4.25: Unconfined repeated load triaxial results for QA sampled mixes (flow number and permanent deformation at flow number).....	73
Figure 4.26: Unconfined repeated load triaxial results for QA sampled mixes (average flow number and permanent deformation at flow number)	74

Figure 4.27: Confined repeated load triaxial results for QA sampled mixes (flow number and permanent deformation at flow number).....	74
Figure 4.28: Confined repeated load triaxial results for QA sampled mixes (average flow number and permanent deformation at flow number).	75
Figure 4.29: Unconfined repeated load triaxial results for JMF verification mixes: load cycles to 3% permanent strain.	75
Figure 4.30: Unconfined repeated load triaxial results for QA sampled mixes: load cycles to 5% permanent strain.	76
Figure 4.31: Flexural fatigue results for QA sampled mixes (Wohler curve).....	78
Figure 4.32: Extrapolation of flexural fatigue regression results for QA sampled mixes (Wohler curve).	78
Figure 4.33: Flexural fatigue results for all QA sampled mixes from Wohler curve regression normalized to Mix A.	79
Figure 4.34: Flexural fatigue results for Mix A comparing JMF with first and second QA samples at 300, 400, and 500 microstrain.....	79
Figure 4.35: Flexural fatigue results for Mix B comparing first and second QA samples (no JMF submittal for Mix B) at 300, 400, and 500 microstrain.	80
Figure 4.36: Flexural fatigue results for Mix C comparing JMF with first and second QA samples at 300, 400, and 500 microstrain.	80
Figure 4.37: Flexural fatigue results for Mix D comparing JMF with first and second QA samples at 300, 400, and 500 microstrain.....	81
Figure 4.38: IDEAL-CT test results for QA sampled mixes (IDEAL-CT number and post-peak slope).	82
Figure 4.39: Average IDEAL-CT test results for QA sampled mixes (IDEAL-CT number and post-peak slope).....	83
Figure 4.40: IDEAL-CT test results for QA sampled mixes (fracture energy and strength).	83
Figure 4.41: Average IDEAL-CT test results for QA sampled mixes (fracture energy and strength).....	84
Figure 4.42: I-FIT test results for QA sampled mixes (fracture energy and strength).....	85
Figure 4.43: Average I-FIT test results for QA sampled mixes (fracture energy and strength)....	86
Figure 4.44: I-FIT test results for QA sampled mixes (flexibility index and post-peak slope).....	86
Figure 4.45: Average I-FIT test results for QA sampled mixes (flexibility index and post-peak slope).....	87
Figure 5.1: Remnants of digouts remaining in asphalt after milling and milling down to aggregate base in half of the lane.	89
Figure 5.2: Cracking in remaining asphalt after milling.	90
Figure 5.3: Cracking in remaining asphalt after milling.	90
Figure 5.4: RAS in tote bags before mixing.....	91
Figure 5.5: Windrow pick up of a mix containing RAS.	91
Figure 5.6: One lane paved with a mix containing RAS (Mix C) and other lane with tack coat before overlay.	92
Figure 5.7: Windrowed RAP-RAS Mix D material.	92
Figure 5.8: Breakdown rolling.	93
Figure 5.9: Compacted mat.....	93

Figure 5.10: Close-up of compacted surface at density test location showing good characteristics and no evidence of segregation.	94
Figure 5.11: Sampling cores from new pavement.....	94

LIST OF ABBREVIATIONS

AASHTO	American Association of State Highway and Transportation Officials
AMPT	Asphalt mixture performance tester
ASTM	American Society for Testing and Materials
BBR	Bending beam rheometer
CA	Carbonyl area index
CalME	California Mechanistic-Empirical Design Software
Caltrans	California Department of Transportation
CG	Continuous grade
DSR	Dynamic shear rheometer
ELD	El Dorado
FAT	Beam fatigue test
FI	Flexibility index
FM	Flexural modulus
FS	Frequency sweep
FTIR	Fourier transform infrared
FTIR-ATR	Fourier transform infrared spectroscopy with attenuated total reflection
Gmb	Bulk specific gravity
Gmm	Theoretical maximum specific gravity
HMA	Hot mix asphalt
HWT	Hamburg Wheel Tracking
JMF	Job mix formula
MTOA	Medium-term oven aging
NMAS	Nominal maximum aggregate size
nSSP	Non-standard special provision
PAV	Pressurized aging vessel
PG	Performance grade
PPRC	Partnered Pavement Research Center

QA	Quality assurance
RAP	Recycled asphalt pavement
RAS	Recycled asphalt shingles
RHMA	Rubberized hot mix asphalt
RLT	Repeated load triaxial
RTFO	Rolling thin-film oven
RVE	Representative volume element
SCB	Semicircular bending test
SSD	Saturated surface dry
Superpave	SUperior PERforming asphalt PAVEmnt
TCE	Trichloroethylene
UCPRC	University of California Pavement Research Center

LIST OF TEST METHODS CITED IN THIS REPORT

AASHTO

- M 320 Standard Specification for Performance-Graded Asphalt Binder
- M 323 Standard Specification for Superpave Volumetric Mix Design
- PP 3 Standard Practice for Preparing Hot Mix Asphalt (HMA) Specimens by Means of the Rolling Wheel Compactor
- R 28 Standard Practice for Accelerated Aging of Asphalt Binder Using a Pressurized Aging Vessel (PAV)
- R 30 Standard Practice for Mixture Conditioning of Hot Mix Asphalt (HMA)
- T 84 Standard Method of Test for Specific Gravity and Absorption of Fine Aggregate
- T 85 Standard Method of Test for Specific Gravity and Absorption of Coarse Aggregate
- T 164 Standard Method of Test for Quantitative Extraction of Asphalt Binder from Hot-Mix Asphalt (HMA)
- T 166 Standard Method of Test for Bulk Specific Gravity (Gmb) of Compacted Hot Mix-Asphalt (HMA) Using Saturated Surface-Dry Specimens
- T 209 Standard Method of Test for Theoretical Maximum Specific Gravity (Gmm) and Density of Hot-Mix Asphalt (HMA)
- T 240 Standard Method of Test for Effect of Heat and Air on a Moving Film of Asphalt Binder (Rolling Thin-Film Oven Test)
- T 308 Standard Method of Test for Determining the Asphalt Binder Content of Hot Mix-Asphalt (HMA) by the Ignition Method
- T 312 Standard Method of Test for Preparing and Determining the Density of Asphalt Mix Specimens by Means of the Superpave Gyratory Compactor
- T 313 Standard Method of Test for Determining the Flexural Creep Stiffness of Asphalt Binder Using the Bending Beam Rheometer
- T 315 Standard Method of Test for Determining the Rheological Properties of Asphalt Binder Using a Dynamic Shear Rheometer
- T 316 Standard Method of Test for Viscosity Determination of Asphalt Binder Using Rotational Viscometer

- T 321 Standard Method of Test for Determining the Fatigue Life of Compacted Asphalt Mixtures Subjected to Repeated Flexural Bending
- T 331 Bulk Specific Gravity (Gmb) and Density of Compacted Hot Mix Asphalt (HMA) Using Automatic Vacuum Sealing Method
- T 378 Standard Method of Test for Determining the Dynamic Modulus and Flow Number for Asphalt Mixtures Using the Asphalt Mixture Performance Tester (AMPT)
- TP 124 Provisional Standard Method of Test for Determining the Fracture Potential of Asphalt Mixtures Using Semicircular Bend Geometry (SCB) at Intermediate Temperature

SI* (MODERN METRIC) CONVERSION FACTORS

APPROXIMATE CONVERSIONS TO SI UNITS

Symbol	When You Know	Multiply By	To Find	Symbol
LENGTH				
in.	inches	25.40	millimeters	mm
ft.	feet	0.3048	meters	m
yd.	yards	0.9144	meters	m
mi.	miles	1.609	kilometers	km
AREA				
in ²	square inches	645.2	square millimeters	mm ²
ft ²	square feet	0.09290	square meters	m ²
yd ²	square yards	0.8361	square meters	m ²
ac.	acres	0.4047	hectares	ha
mi ²	square miles	2.590	square kilometers	km ²
VOLUME				
fl. oz.	fluid ounces	29.57	milliliters	mL
gal.	gallons	3.785	liters	L
ft ³	cubic feet	0.02832	cubic meters	m ³
yd ³	cubic yards	0.7646	cubic meters	m ³
MASS				
oz.	ounces	28.35	grams	g
lb.	pounds	0.4536	kilograms	kg
T	short tons (2000 pounds)	0.9072	metric tons	t
TEMPERATURE (exact degrees)				
°F	Fahrenheit	(F-32)/1.8	Celsius	°C
FORCE and PRESSURE or STRESS				
lbf	pound-force	4.448	newtons	N
lbf/in ²	pound-force per square inch	6.895	kilopascals	kPa

APPROXIMATE CONVERSIONS FROM SI UNITS

Symbol	When You Know	Multiply By	To Find	Symbol
LENGTH				
mm	millimeters	0.03937	inches	in.
m	meters	3.281	feet	ft.
m	meters	1.094	yards	yd.
km	kilometers	0.6214	miles	mi.
AREA				
mm ²	square millimeters	0.001550	square inches	in ²
m ²	square meters	10.76	square feet	ft ²
m ²	square meters	1.196	square yards	yd ²
ha	hectares	2.471	acres	ac.
km ²	square kilometers	0.3861	square miles	mi ²
VOLUME				
mL	milliliters	0.03381	fluid ounces	fl. oz.
L	liters	0.2642	gallons	gal.
m ³	cubic meters	35.31	cubic feet	ft ³
m ³	cubic meters	1.308	cubic yards	yd ³
MASS				
g	grams	0.03527	ounces	oz.
kg	kilograms	2.205	pounds	lb.
t	metric tons	1.102	short tons (2000 pounds)	T
TEMPERATURE (exact degrees)				
°C	Celsius	1.8C + 32	Fahrenheit	°F
FORCE and PRESSURE or STRESS				
N	newtons	0.2248	pound-force	lbf
kPa	kilopascals	0.1450	pound-force per square inch	lbf/in ²

*SI is the abbreviation for the International System of Units. Appropriate rounding should be made to comply with Section 4 of ASTM E380.
(Revised April 2021)

PROJECT OBJECTIVES

This study is a continuation of PPRC Project 4.64 (Continued Development of Guidelines for Determining Binder Replacement in High RAP/RAS Content Mixes). The objective of this project is to develop guidelines for determining binder replacement rates in high RAP/RAS content mixes without the need for binder extraction and performance-related tests for use in routine mix design and construction quality control/quality assurance. This will be achieved through the following tasks:

- Task 1: Update literature review to include recently completed research.
- Task 2: Complete testing of high RAP and RAP/RAS mixes to determine their performance properties.
- Task 3: Complete testing of extracted and recovered RAP, RAP/RAS, and RAP/RAS/virgin binder blends to assess the effectiveness of different rejuvenators.
- Task 4: Complete investigation into the use of fine aggregate matrix mix testing to assess the fatigue performance of mixes and to predict binder properties.
- Task 5: Investigate long-term aging effects of high RAP and RAP/RAS mixes using different laboratory-aging protocols.
- Task 6: Monitor field performance of high RAP and RAP/RAS mixes, and use results to evaluate laboratory-aging protocols.
- Task 7: Prepare a research report with recommendations for use of RAP and RAP/RAS as binder replacement, and, if applicable, recommendations for accelerated wheel-load testing.

The results presented in this technical memorandum contribute to Tasks 2, 3, 5, and 6 by presenting the results of laboratory testing of binders and mixes for a pilot project on State Route 49 in El Dorado County (ELD 49), including sampling and testing for job mix formula (JMF) approval and sampling and testing of plant-sampled materials during construction of the test sections, as well as observations from construction.

1. INTRODUCTION

1.1 Background of the Study

The California Department of Transportation (Caltrans) is interested in finding, developing, and implementing approaches to reduce life cycle cost and improve life cycle environmental performance. Two approaches under investigation that offer the potential to advance these goals are the use of increased amounts of recycled asphalt pavement (RAP) and the use of recycled asphalt shingles (RAS) in hot mix asphalt (HMA) materials. Caltrans is investigating the performance of high RAP content mixes, meaning mixes containing more than 25% RAP. The University of California Pavement Research Center (UCPRC) has been investigating the use of higher percentages of RAP in HMA through laboratory testing of laboratory-prepared and field-sampled materials, observations of construction, and mechanistic-empirical simulations using the performance-related test properties for the mixes.

Previous and ongoing research at the UCPRC working with Caltrans and industry has identified potential concerns regarding using highly aged, stiff RAP. Research is underway at the UCPRC to study the impact of different RAP sources, varying RAP content, and the addition of rejuvenators to restore the properties of highly aged RAP on the performance-related properties of binders and mixes.

Several performance-related tests have been identified to assess the performance of these mixes, including rutting, stiffness, and fatigue. These performance-related tests include long-established tests such as Hamburg Wheel Tracking (HWT), repeated load triaxial (RLT), and four-point bending beam tests. Other recently developed tests, such as the semicircular bending (SCB) test and indirect tensile asphalt cracking test (IDEAL-CT), are also being assessed for their potential to provide a quick and simple indicator of mix performance for mix design and quality control/quality assurance (QC/QA) purposes.

Limited work had been done on binder replacement from RAS in California by the UCPRC, Caltrans, and industry prior to the pilot study presented in this technical memorandum. Limited

previous work by the UCPRC indicated poor results because of the lack of blending of the RAS and virgin binders due to the very heavy oxidation of the RAS source used (1).

This technical memorandum presents project information, materials testing data from tests performed by the UCPRC, and construction observations by the UCPRC from a pilot project on State Route 49 (ELD 49) in El Dorado County that included four mixes: (1) a control mix with no RAP or RAS, (2) a mix with a currently typical amount of RAP, (3) a mix with RAS, and (4) a mix with a currently typical amount of RAP and RAS.

1.2 Problem Statements

The following problem statements related to inclusion of RAS and RAP in HMA were identified for this project:

- The degree of blending between RAP, RAP/RAS, and virgin binders could be significant, particularly for mixes using highly aged RAP, typical of Inland Valley scenarios, and RAS. Incomplete blending could alter the properties of the mix because of less available binder and partial activation of the stiff RAP and/or RAS binder. The effects of potentially not achieving full blending need to be better understood to be effectively considered in mix design procedures and performance-related testing. This problem is addressed in this pilot project and report.
- Plant-produced mixes subjected to silo storage undergo additional blending and aging leading to increased stiffness, improved rutting, and reduced cracking and fatigue resistance. This outcome needs to be factored into mix design procedures and performance-related testing. This problem was not addressed in this pilot project or report because all materials were sampled without silo storage. Silo storage is addressed in a separate report.
- The impact of long-term aging on the performance of high RAP and RAP/RAS mixes with different rejuvenators needs to be fully investigated using various aging protocols. This problem was only addressed with respect to binder aging, and not mix aging. Mix aging will be addressed in the future through laboratory mix testing and later field sampling of this pilot project and will be documented in a separate report.

1.3 Report Structure

This technical memorandum includes the following chapters, which address the tasks discussed in Section 1.3:

- Chapter 2 details the test section layout, testing plan, material sampling, mix designs, and test method overview for the ELD 49 pilot project.
- Chapter 3 discuss the results from testing of binders from the pilot project mixes, addressing Task 3.
- Chapter 4 covers the testing of the mixes from the pilot project, including testing during the job mix formula (JMF) approval process and during construction, addressing Task 2 and setting the baseline for future testing of field mixed/field compacted specimens for Task 6.
- Chapter 5 presents initial field construction observations, collected in part through a partnership with Texas A&M University.
- Chapter 6 presents preliminary conclusions from this pilot project.
- Detailed data tables are not included in this technical memorandum. All data are available through the UCPRC Online Testing Service web application or in Excel tables. Contact the report's authors for access.

1.4 Measurement Units

Although Caltrans has returned to the use of US standard measurement units, metric units have always been used by the UCPRC in the design and layout of test tracks, and for laboratory, Heavy Vehicle Simulator, and field measurements and data storage. In this technical memorandum, both US and metric units (provided in parentheses after the US units) are provided in general discussion. In keeping with convention, metric units are used in laboratory data analyses and reporting, with some US units, where appropriate, to assist the reader. A conversion table is provided on page xv.

2. TESTING PLAN AND MATERIAL SAMPLING

2.1 Pilot Project Test Sections Overview and Pre-Overlay Observations

The test sections are within Caltrans project 03-2G1004, ELD 49, just south of Placerville. The beginning and ending post miles of the four test sections are shown in Table 2.1. The test sections are in a hilly area with alternating steep ascents and descents as well as sharp horizontal curvatures.

Table 2.1: Pilot Project Test Section Location Lane and Post Miles and Mix Types from Project Special Provisions

Pilot Project Test Sections ^a			
Type ^b	Begin Post Mile	End Post Mile	Lane Number
0% RAP and RAS	13.100	13.289	1
3% RAS	13.289	13.478	1
10% RAP	13.478	13.668	1
3% RAS and 10% RAP	13.668	13.857	1

^aSee project plans for details.

^bPercentages are by weight of aggregate with a maximum binder replacement of 15% from RAS and 10% from RAP.

The existing pavement had age-related cracking (transverse and block cracks) and load-related fatigue cracking in the wheelpaths, shown in Figure 2.1 and Figure 2.2. Some of the fatigue cracking had been addressed intermittently through previous digouts or extensive crack sealing in the wheelpaths, shown in Figure 2.3. The thickness of the existing pavement varied, depending on previous overlay thicknesses, feathering of the thickness toward the edges of the traveled way, slope changes, patching, and digouts. Milling, plant operations, and overlay construction are discussed in Chapter 5.



Figure 2.1: Fatigue cracking in the wheelpaths, partly sealed with crack sealant.



Figure 2.2: Transverse and block cracking.



Figure 2.3: Fatigue cracking in the wheelpath and extensive crack sealing.

2.2 Mix Designs

All the mixes were designed to meet Caltrans specifications for $\frac{1}{2}$ in. nominal maximum aggregate size (NMAS) specifications and the non-standard special provisions (nSSP) for the contract. The nSSP requirements are shown in Table 2.2. The mix design requirements are the same as those in the Caltrans Standard Specifications, except for the following:

- The gyratory compaction requirements (N_{design} , VMA) and gradation requirements for the mix with RAS are waived.
- The moisture susceptibility test dry strength of the RAS mix has a maximum value as well as a minimum value.
- Delta T_c values are specified for all mixes.
- The IDEAL-CT value of the RAS mix must be greater than or equal to that of the virgin mix (with no RAP or RAS).
- I-FIT and flexural fatigue testing are required for information only.

The JMF submittals JMF from the contractor for the four mixes are shown in Table 2.3. The information in the table comes from the CEM 3511/3512 forms submitted by the contractor prior to the collection of JMF verification samples. One aggregate source, one RAP source, and one RAS source were used by the contractor to produce the mix designs included in the pilot

sections. The aggregate was a crushed granite from the Sierra Nevada mountain range. The binder grade of the virgin asphalt used in the mixes containing RAS and/or RAP was PG 58-22 and that of the control mix with no RAP or RAS was PG 64-16. The contractor used the softer binder and rejuvenating agents to match the high temperature grade of the control mix.

The JMF submittal verification information from Caltrans for the four mixes is shown in Table 2.4. This information comes from the CEM 3513 forms completed by the Caltrans district lab or its consultants. The results shown are within the allowable arrangements, and no adjustments needed to be made.

Table 2.2: Non-Standard Special Provision (nSSP) Requirements for the Mixes

39-2.12B(2) Type A Hot Mix Asphalt—RAS Mix Design

The mix design for Type A HMA—RAS must comply with the requirements shown in the following table:

Quality characteristic	Test method	Requirement	
		HMA Virgin Mix and HMA with less than 15% RAP	HMA Mix with RAS
Air voids content (%)	AASHTO T 269 ^a	$N_{initial} > 8.0$ $N_{design} = 4.0$ ($N_{design} = 5.0$ for 1-inch aggregate) $N_{max} > 2.0$	Report value at N_{design} gyrations on job mix formula (JMF) submittal form
Gyration compaction (no. of gyrations)	AASHTO T 312	$N_{initial} = 8$ $N_{design} = 85.0$ $N_{max} = 130$	$N_{initial} = 8$ $N_{design} = 85.0$ $N_{max} = 130$
Voids in mineral aggregate (min, %) ^b Gradation: No. 4 3/8-inch 1/2-inch 3/4-inch 1-inch with NMAS = 1-inch with NMAS = 3/4-inch	MS-2 Asphalt Mixture Volumetrics	16.5–19.5 15.5–18.5 14.5–17.5 13.5–16.5 13.5–16.5 14.5–17.5	Report value on JMF submittal form
Dust proportion	MS-2 Asphalt Mixture Volumetrics	0.6–1.3	0.6–1.3
Hamburg wheel track (min number of passes at 0.5-inch rut depth) Binder grade: PG 58 PG 64 PG 70 PG 76 or higher	California Test 389 ^c	10,000 15,000 20,000 25,000	10,000 15,000 20,000 25,000
Hamburg wheel track (min number of passes at the inflection point) Binder grade: PG 58 PG 64 PG 70 PG 76 or higher	California Test 389 ^c	10,000 10,000 12,500 15,000	10,000 10,000 12,500 15,000
Moisture susceptibility (min, psi, dry strength)	AASHTO T 283 ^c	100	100–300
Moisture susceptibility (min, psi, wet strength)	AASHTO T 283 ^d	70	70
Recovered asphalt from HMA Mix	Must comply with section 92 ^e	Must comply with project specified PG binder	Must comply with project specified PG binder
Delta Tc (°C)	ASTM D7643 ^{f,g}	≥ -5.0	≥ -5.0
IDEAL CT	ASTM D8225	Report only	≥ the virgin mix value
I-FIT	AASHTO TP 124 ^g	Report only ^h	Report only ^h
Bending Beam Fatigue (psi)	AASHTO T 321 ^g	Report only ^h	Report only ^h
Repeated Load Triaxial test (psi)	AASHTO T 378 ^g	Report only ^h	Report only ^h

^aCalculate the air voids content of each specimen using AASHTO T 275, Method A, to determine bulk specific gravity. Use AASHTO T 209, Method A, to determine theoretical maximum specific gravity. Use a digital manometer and pycnometer when performing AASHTO T 209.

^bMeasure bulk specific gravity using AASHTO T 275, Method A.

^cTest plant-produced Type A HMA.

^dFreeze thaw required.

^ePerform binder extraction and recovery for HMA mix with RAS under AASHTO T 164 and ASTM D5404.

^fDelta Tc must be performed on virgin binder and extracted binder from HMA mix with RAP or RAS. For pilot project, run test at 20 hours for information only in addition to 40 hours.

^gContractor to provide and deliver loose mix samples to the Engineer.

^hEmail to RAS@dot.ca.gov.

Table 2.3: Job Mix Formula Submittal by Contractor

Parameter		1/2 in. NMAS							
		Control Mixes (No RAS)				Mixes with RAS			
		Control		Conventional		RAS Only		RAP and RAS Blend	
		0% RAP		10% RAP		0% RAP		10% RAP	
		0% RAS		0% RAS		3% RAS		3% RAS	
		JMF Design	JMF Limits	JMF Design	JMF Limits	JMF Design	JMF Limits	JMF Design	JMF Limits
Grading (% passing sieve)	1"	100	100	100	100	100	100	100	100
	3/4"	100	100	100	100	100	100	100	100
	1/2"	96	91–100	96	91–100	97	92–100	96	91–100
	3/8"	88	83–93	87	82–92	88	83–93	86	81–91
	#4	63	58–68	61	56–66	62	57–67	60	55–65
	#8	45	40–50	43	38–48	44	39–49	40	35–45
	#200	5.5	3.5–7.5	4.7	2.7–6.7	5.4	3.4–7.4	5.5	3.5–7.5
RAS content (% by weight of aggregate)		0	—	0	—	3	—	3	—
RAP content (% by weight of aggregate)		0	—	10	—	0	—	10	—
Base asphalt binder performance grade		64-16	64	64-16	64	58-22	64	58-22	64
Rejuvenator type		—	—	—	—	Tall Oil	—	Tall Oil	—
Rejuvenator dosage (% by weight of binder)		0	0	0	—	0.25	—	1.00	—
Binder content (% by weight of mix)		5.0	4.7–5.5	4.7	4.4–5.2	5.0	4.7–5.5	5.0	4.7–5.5
Recycled binder content (% binder in mix)		0	—	0.52	—	0.44	—	0.87	—
Estimated binder replacement excluding rejuvenator (% of total binder)		0	—	11.2	—	8.7	—	17.5	—
Estimated binder replacement including rejuvenator (% of total binder)		0	—	11.2	—	8.8	—	17.7	—
Number of gyrations		85	85	85	85	85	85	85	85
Air void content (%)		4.2	2.5–5.5	3.9	2.5–5.5	3.9	2.5–5.5	3.8	2.5–5.5
Voids in mineral aggregate (%)		15.7	13.5	14.8	13.5	15.5	13.5	15.7	13.5
Dust proportion		1.14	0.6–1.3	1.05	0.6–1.3	1.22	0.6–1.3	1.22	0.6–1.3
Hamburg (rut depth [mm] at # passes)		2.1 @20,000	<12.5 @15,000	3.3 @15,000	<12.5 @15,000	2.36 @25,000	<12.5 @15,000	1.46 @25,000	<12.5 @15,000
Moisture susceptibility, dry strength (psi)		234	>100	226	>100	287	>100	287	>100
Moisture susceptibility, wet strength (psi)		168	>70	137	>70	—	>70	—	>70

Table 2.4: Job Mix Formula Verification Results from Caltrans

Parameter	1/2 in. NMAS							
	Control Mixes (No RAS)				Mixes with RAS			
	Control		Conventional		RAS Only		RAP and RAS Blend	
	0% RAP		10% RAP		0% RAP		10% RAP	
	0% RAS		0% RAS		3% RAS		3% RAS	
	QA Verified	JMF Limits	QA Verified	JMF Limits	QA Verified	JMF Limits	QA Verified	JMF Limits
Grading (% passing sieve)	1"	100	100	100	100	100	100	100
	3/4"	100	100	100	100	100	100	100
	1/2"	96	91–100	96	91–100	97	92–100	96
	3/8"	87	83–93	86	82–92	89	83–93	86
	#4	66	58–68	60	56–66	62	57–67	60
	#8	47	40–50	43	38–48	45	39–49	43
	#200	4.8	3.5–7.5	5.4	2.7–6.7	5.6	3.4–7.4	3.9
RAS content (% by weight of aggregate)	0	—	0	—	3	—	3	—
RAP content (% by weight of aggregate)	0	—	10	—	0	—	10	—
Base asphalt binder performance grade	64-16	64	64-16	64	58-22	64	58-22	64
Rejuvenator Type	—	—	—	—	Tall Oil	—	Tall Oil	—
Rejuvenator Dosage (% by weight of binder)	0	0	0	—	0.25	—	1.00	—
Binder content (% by weight of mix)	5.3	4.7–5.5	4.7	4.7–5.5	5.3	4.7–5.5	4.9	4.7–5.5
Recycled Binder Content (% binder in mix)	0	—	0.52	—	0.44	—	0.87	—
Estimated Binder Replacement excluding Rejuvenator (% of total binder)	0	—	11.1	—	8.2	—	17.8	—
Estimated Binder Replacement including Rejuvenator (% of total binder)	0	—	11.1	—	8.3	—	18.0	—
Number of gyrations	85	85	85	85	85	85	85	85
Air void content (%)	3.5	2.5–5.5	4.1	2.5–5.5	3.5	2.5–5.5	3.9	2.5 – 5.5
Voids in mineral aggregate (%)	14.5	13.5	13.8	13.5	14.0	13.5	14.0	13.5
Dust proportion	1.1	0.6–1.3	1.3	0.6–1.3	1.3	0.6–1.3	0.9	0.6 – 1.3
Hamburg (rut depth [mm] at # passes)	9.2 @20,000	<12.5 @15,000	6.98 @20,000	<12.5 @15,000	4.9 @20,000	<12.5 @15,000	4.64 @20,000	<12.5 @15,000
Moisture susceptibility, dry strength (psi)	165	>100	179	>100	153	>100	198	> 100
Moisture susceptibility, wet strength (psi)	128	>70	138	>70	135	>70	177	> 70

2.3 Testing Plan

Laboratory testing covered both binder and mix testing during both JMF approval and construction. The sampling, test methods, and testing factorials are discussed in the following sections.

2.4 Material Sampling and Handling

Sampling for JMF verification and QA was completed in coordination with asphalt plant operations and quality control groups to ensure the quality of materials and safety for all involved.

2.4.1 Plant-Produced Material Sampling for Job Mix Formula Verification Testing

Three JMF submittals were verified in the period from July 2021 to October 2021 by the UCPRC: (1) the control mix with no RAP or RAS (Mix A), (2) the mix with RAS (Mix C), and (3) the mix with RAP and RAS (Mix D). The fourth test section mix, which was used to pave the rest of the project as well, had RAP (Mix B) and was previously verified by the District 3 laboratory. Approximately six tons of material were sampled for UCPRC testing when District 3 sampled for its testing.

Mix B was used in a test section and on the rest of the project. Mix B was a conventional ½ in. HMA Type A with 12% RAP, verified through the normal Caltrans system. The three mixes for JMF verification testing (Mixes A, C, and D) by the UCPRC for the pilot project sections are shown in Table 2.5.

Table 2.5: Mix Samples for JMF Verification Testing by the UCPRC

Mix Type	UCPRC HMA Mix Identifier	Date Sampled	Location Sampled	Samples Taken By
1/2" Type A HMA - RAS - virgin control	4.79-Mix A-ROS0	7/22/2021	George Reed Clements, Batch Plant	UCPRC and George Reed staff
1/2" Type A HMA - RAS - with less than 15% RAP control	4.79-Mix B-R10S0	Not sampled	Not sampled	Not sampled
1/2" Type A HMA - RAS - with RAS only	4.79-Mix C-ROS3	9/29/2021	George Reed Clements, Batch Plant	UCPRC and George Reed staff
1/2" Type A HMA - RAS - with less than 15% RAP/ RAS	4.79-Mix D-R10S3	9/29/2021	George Reed Clements, Batch Plant	UCPRC and George Reed staff

For all samples, the mixes for JMF verification were produced in a batch plant in two- to six-ton increments with no silo storage or additional processing of the mix and were loaded directly into a loader bucket. When the loader placed the mix in a large pile for sampling, a small stock was formed and then flattened into a sampling pad. The pad was split into four quadrants and mix was shoveled from each of the four quadrants, into four or more 5-gallon buckets. The buckets were not run through the quartermaster for reduction to a smaller sample at the plant. Use of the quartermaster at the plant was not done because of the large amount of material that must be collected for all the performance-related tests used on this project and the four mixes that had to be sampled in a short period of time. Instead, the buckets were brought to the UCPRC laboratory, and then when mix was needed to produce samples for a given type of test, buckets were randomly taken from the total set of buckets, reheated, and combined and resplit in three or more passes using the quartermaster to the final amount needed for the number of specimens. The 5-gallon buckets were sealed and immediately transported to the UCPRC's Davis laboratory for storage and processing. The materials were labeled and stored in an outdoor, shaded area prior to laboratory processing.

2.4.2 Plant-Produced Material Sampling During Construction

Plant-produced mixes for the four mixes were sampled at the plant during construction. The sampling for the production QA testing was performed similarly to the JMF process (Figure 2.4) and split across two days. During production, the boxes of mix for volumetric verification by Caltrans were collected at the same time, by the contractor, for all parties and a 5-gallon bucket or 3.5-gallon bucket (changed from the use of 5-gallon buckets during the project to reduce weight and facilitate handling) was used with a quartermaster splitter following CT 125 to collect representative boxes. The materials for determining the performance grades (PGs) of the binders for the UCPRC were collected by box and all other UCPRC samples were collected by 3.5-gallon bucket.

Two mixes were paved on November 2, 2021, with approximately 360 tons of production for each test section. The plant first shipped out Mix A ($\frac{1}{2}$ in. HMA with 0% RAP and 0% RAS) and samples were taken after approximately 100 and 300 tons, a sampling pattern that was repeated for the other three mixes. The mix production and sampling followed the same

process used for JMF sampling. The next mix produced on November 2, 2021, was Mix B ($\frac{1}{2}$ in. HMA with 10% RAP). The other two mixes were paved on November 3, 2021. The first mix on that day was Mix C ($\frac{1}{2}$ in. HMA with 3% RAS only), followed by Mix D ($\frac{1}{2}$ in. HMA with 3% RAS and 10% RAP).



Figure 2.4: Sampling from hot drop put in buckets and boxes for QA sampling (each person is sampling from a quadrant of the pile of hot mix).

2.4.3 Material Handling After Sampling

Storage and Reheating-to-Compaction

As mentioned in the sampling discussion, the mixes were all sampled in sealed 5-gallon or 3.5-gallon steel cans or cardboard boxes. The cardboard boxes for binder extraction were stored inside the asphalt binder laboratory at temperatures between 60°F and 80°F (15°C to 27°C) for up to 60 days prior to extraction (Figure 2.5). The buckets for mix testing were stored in an outdoor, shaded receiving area at temperatures between 50°F and 100°F (10°C to 38°C).



Figure 2.5: Loose plant mix samples stored in cardboard boxes in temperature-controlled environment before extraction.

The laboratory reheating-to-compaction procedure was discussed with the contractor and the procedures labeled as “ELD 49” in Table 2.6 were agreed to for this project. The AASHTO R30 procedure for laboratory mixed material is included as a reference. AASHTO R30 does not provide specific procedures for reheating for compaction or laboratory aging of plant-produced mix.

Table 2.6: Mix Sampling, Storage, and Reheating-to-Compaction Temperature Procedures for ELD 49 Pilot Project Materials, Compared with AASHTO R30

Activity	ELD 49	Activity	AASHTO R30
Sampling (bucked or box)	—	Components pre-heated	1–4 hours
Transport and storage (cooled)	—	Loose mixed in lab	4 minutes
Bucket/box reheating (workable at 135°C ^a)	4 hours	Conditioned at 135°C ^b	4 hours
Split to compaction mass	0.25 hours	Flipped every hour	—
Loose mix in pan to compaction temperature	1–2 hours	Loose Mix in Pan to Compaction Temp	0.5 hours

^a Material starts from room temperature.

^b Material starts at mixing temperature (140°C or higher).

All materials for mix tests other than flexural beam testing were stored prior to being reheated and compacted as specimens within 21 days of sampling. Materials for flexural beams were stored for up to a maximum of 60 days before specimen preparation. After compaction and cutting to final dimensions, specimens for tests other than flexural beam testing were tested

within 14 days. Specimens for flexural beam testing were tested within 90 days. All specimens were stored indoors at temperatures between 60°F and 80°F (15°C to 27°C).

Medium-Term Mix Aging

No medium-term aging to determine mix properties after initial construction was performed at the time of writing of this technical memorandum because a protocol had not yet been finalized. The mix tests for which medium-term aging in the field is important (stiffness, fatigue, and fracture tests) will be repeated after medium-term aging, and the results will be included in a future report.

2.4.4 Binder Extraction

To determine the PG grade and the Delta T_c parameter of each JMF verification and QA subplot, binder was extracted following ASTM D8159 and ASTM D5405 procedures with the use of an automated asphalt extraction unit and rotary evaporator (Figure 2.6 and Figure 2.7).

To obtain loose mix, sufficient cardboard sample boxes were minimally reheated to 110°C and the loose mix was split down to begin processing. The automated extraction process of eight to nine wash cycles for a complete trichloroethylene (TCE) solvent extraction took approximately 90 minutes to run. Extraction was performed on a minimum of four 2,000 to 2,200 g replicates of loose mix to obtain enough recovered asphalt for D7643 PG grading, with 20- and 40-hour pressurized aging vessel (PAV) long-term aging.

Following the solvent extraction process, the recovered asphalt binder and TCE solvent solution were stored in 500 mL glass jars for no more than two days prior to recovery. To remove the TCE solvent and recover the asphalt binder, a rotary evaporator was used, following ASTM D5404. The recovery process took approximately 100 minutes in a heated silicone fluid bath under continuously flowing nitrogen gas to minimize oxidation. After all the TCE was removed from the recovered asphalt binder, the glass flask was turned upside down and heated to 163°C to remove all binder. The sample was then transferred to a metal tin, and PG grading began.

The recovered asphalt binder from loose mix produced in the asphalt plant was assumed to have undergone aging like that caused by the rolling thin-film oven (RTFO) test (AASHTO T240),

and no further short-term aging was applied for PG grading. The 20-hour PAV aging and then 40-hour PAV aging immediately followed, and the Delta T_c parameter was calculated per ASTM D7643 using the low temperature bending beam rheometer (BBR) results in either an Excel worksheet or a transmittal database such as StonemontQC.



Figure 2.6: Closed-loop binder extraction system.



Figure 2.7: Placing extraction cylinder with sample into extraction system.

2.5 Test Methods

JMF verification testing performed by the UCPRC is shown in Table 2.7.

Table 2.7: JMF Verification Testing Performed by UCPRC for Pilot Project

Test Type	Test Method	Material Tested	Goal
Binder true grade with Delta T _c	AASHTO R29	Binder extracted from plant-sampled mix	Binder PG grade
IDEAL-CT indirect tension	ASTM D8225	Laboratory-compacted plant mix	Intermediate cracking tolerance
Semicircular beam I-FIT	AASHTO TP124 (updated)	Laboratory-compacted plant mix	Intermediate cracking tolerance
Repeated load triaxial	AASHTO T378	Laboratory-compacted plant mix	Dynamic modulus (stiffness) and permanent deformation
Four-point flexural beam	AASHTO T321	Laboratory-compacted plant mix	Dynamic modulus (stiffness) and fatigue life

2.6 Binder Testing

Binder testing included the following (an overview of the methods and data interpretation is discussed in the following sections):

- Performance grade (PG)
- Frequency sweep (FS) tests to evaluate binder stiffness
- Fourier transform infrared (FTIR) spectroscopy tests to track changes in binder chemistry after aging

These tests were all performed on binders extracted from the QA samples, while only PG tests were performed on the binders from the JMF verification samples.

2.6.1 Performance Grading

A dynamic shear rheometer (DSR) was used to determine the high and intermediate temperature binder PG. Short-term aging of the binders was not simulated in an RTFO because binders were extracted from mixes that were plant produced. Long-term aging of the binder was simulated in a PAV following the AASHTO R 28 method for 20 hours, and additional PAV specimens were aged 40 hours. The low temperature PGs were determined on PAV-aged binders using a BBR, following AASHTO T 313.

2.6.2 Frequency Sweep

A symmetric sigmoidal fit function was used to convert the frequency sweep data into a master curve at the reference temperature using the fit function in Equation 2.1 (2). The midpoint of the temperature testing range was selected as the reference temperature (i.e., 40°C):

$$\log|E^*| = \delta + \frac{\alpha}{1+e^{\beta+\gamma\log\omega f_r}} \quad (2.1)$$

Where:

$|E^*|$: magnitude of complex modulus (kPa)

α : fitting parameter (the high asymptote of the master curve)

δ : fitting parameter (the lower asymptote of the master curve)

β, γ : fitting parameters (the slope of the transition region of the master curve)

ω : frequency (Hz)

f_r : reduced frequency, which is the shifted frequency at the reference temperature from the frequency at the test temperature (Hz)

Equation 2.1 can be used to generate a binder master curve by substituting the complex modulus (E^*) with the shear complex modulus (G^*). The reduced frequency can be calculated using the Arrhenius equations (Equation 2.2 and Equation 2.3), which are based on the time-temperature superposition (1):

$$\log f_r = \log f + \log \alpha_T \quad (2.2)$$

$$\log \alpha_T = \frac{E_a}{R(\ln 10)} \left(\frac{1}{T} - \frac{1}{T_r} \right) \quad (2.3)$$

Where:

f : frequency sweep test loading frequency (Hz)

α_T : shift factor as a function of temperature in Kelvin (°K)

E_a : activation energy (Jol/Molar)

T : test temperature (°K)

T_r : reference temperature ($^{\circ}\text{K}$)

R : ideal gas constant, 8.314 J/ ($^{\circ}\text{K}$ molar)

Measured dynamic moduli can be horizontally shifted into a single master curve at the reference temperature using the above equations. The shift factor (α_T) can be determined using the solver function in Excel by minimizing the sum of squares error between the predicted and measured dynamic moduli. Figure 2.8 and Figure 2.9 show examples of the fitting procedure.

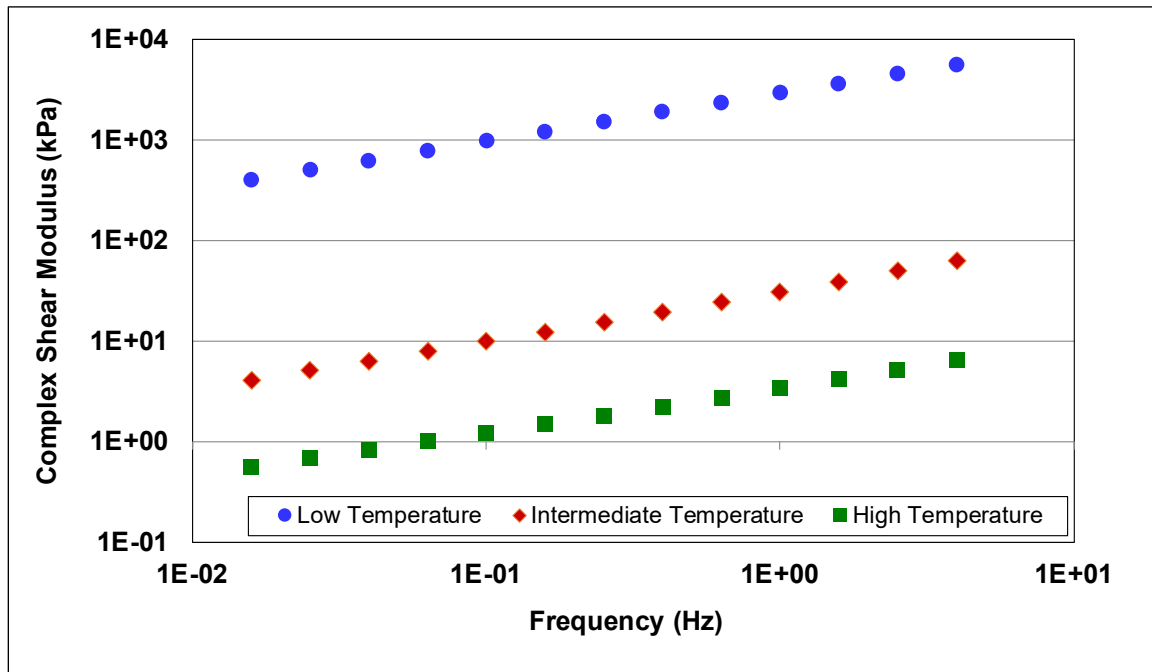


Figure 2.8: Example of modulus master curves (plotted by frequency at tested temperature).

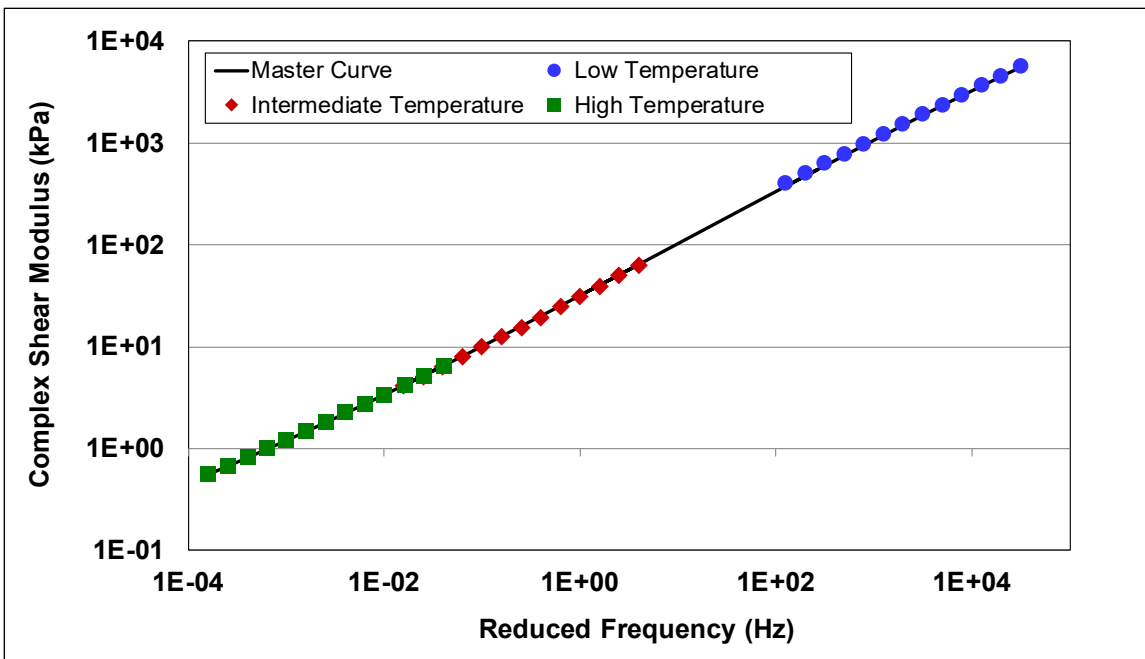


Figure 2.9: Example of modulus master curves (plotted by shifted frequency).

2.6.3 Fourier Transform Infrared Spectroscopy

Chemical component changes in the control and blended binders were evaluated using Fourier transform infrared spectroscopy with attenuated total reflection (FTIR-ATR). The spectra measured by the FTIR were recorded in a reflective mode, from 4,000 to 400 cm^{-1} , at a resolution of 4 cm^{-1} . Each measurement included 24 scans, and an average value was recorded. Nine replicate measurements were taken to ensure that representative measurements were collected for each binder sample. The carbonyl component was used to track oxidative aging, which is usually defined by the peak at 1,680 cm^{-1} (3-6). The tangential integration of the component area index was calculated between the upper and lower wavenumbers (1,675 and 1,750 cm^{-1}).

The spectra were normalized using the aliphatic band at 2,923 cm^{-1} to eliminate any variability introduced by the operator and any background impacts between repeat measurements. This aliphatic band structure is not affected by aging over time (6,7). The chemical component area index was then integrated from the normalized spectra using Equation 2.4 (6). Figure 2.10 shows an example of a spectrum and the respective component.

$$I_i = \int_{w_{l,i}}^{w_{u,i}} a(w) dw - \frac{a(w_{u,i}) + a(w_{l,i})}{2} \times (w_{u,i} - w_{l,i}) \quad (2.4)$$

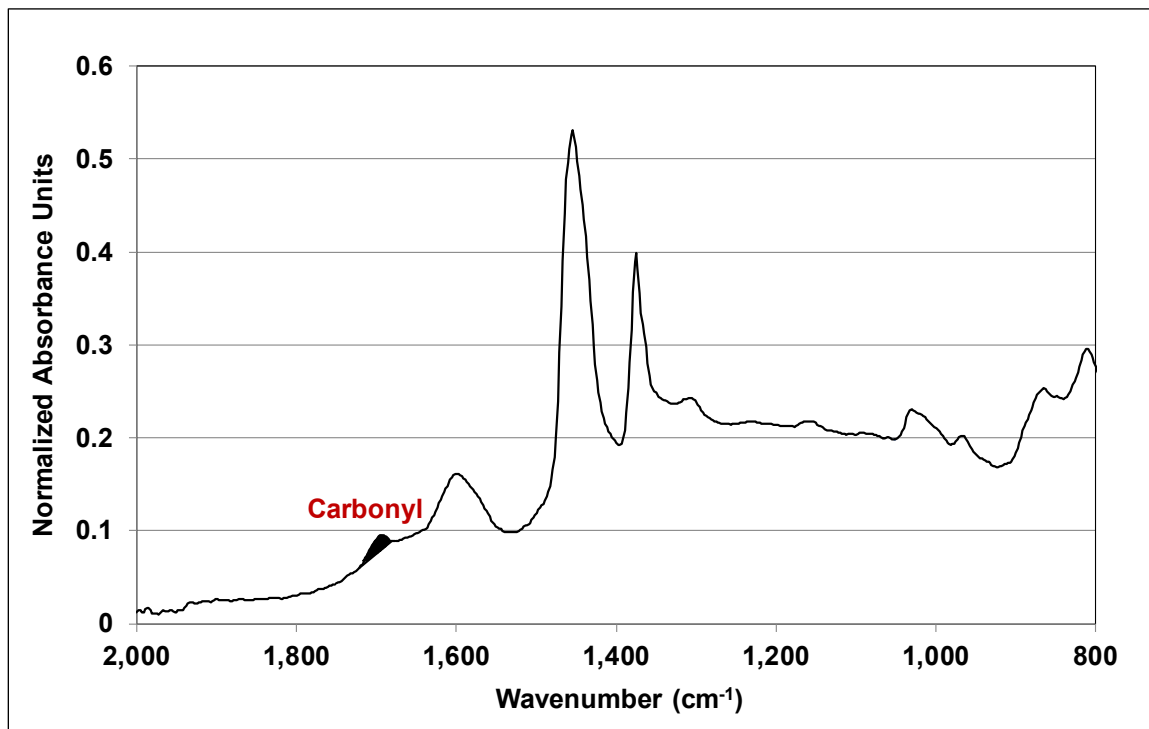
Where:

I_i : index of area i

$w_{l,i}$: lower wavenumber integral limit of area i

$w_{u,i}$: upper wave number integral limit of area i

$a(w)$: absorbance as a function of wavenumber



Note: Plot shows tangential integration with carbonyl areas.

Figure 2.10: Example of normalized FTIR absorbance spectrum.

2.7 Mix Testing

Mix testing included the following (an overview of the methods and data interpretation is discussed below):

- Dynamic modulus (DM, AASHTO T 378; specimens prepared in a gyratory compactor)
- Flexural modulus (FM, AASHTO T 321; specimens prepared using a rolling wheel compactor)

- Repeated load triaxial (RLT, flow number, AASHTO T 378; specimens prepared in a gyratory compactor)
- Beam fatigue (FAT, AASHTO T 321; specimens prepared using a rolling wheel compactor)
- Semicircular bend cracking test (SCB, AASHTO TP 124, specimens prepared in a gyratory compactor)
- IDEAL-CT indirect tensile strength test (IDEAL-CT, ASTM D 8225, specimens prepared in a gyratory compactor)

2.7.1 Test Specimen Air Void Contents

The bulk densities of the IDEAL-CT specimens were determined according to AASHTO T 166 (saturated surface-dry [SSD] method). The bulk densities of the beam, asphalt mix performance tester (AMPT), and SCB specimens were determined according to AASHTO T 331 (CoreLok). Theoretical maximum specific gravity (Gmm) was determined according to AASHTO T 209. All specimens for all tests were compacted to 7% air voids with a 0.5% tolerance around that target.

2.7.2 Triaxial Dynamic Modulus

Triaxial dynamic modulus testing followed AASHTO T 378 using an AMPT with specimens prepared in a gyratory compactor.

Specimens were tested at 4°C, 21°C, 38°C, and 54°C and at frequencies between 25 and 0.1 Hz. Measured dynamic moduli and phase angles were horizontally shifted into a master curve at 20°C using Equation 2.2, Equation 2.3, and the Williams-Landel-Ferry shift function (8) in Equation 2.5.

$$\log(\alpha_T) = \frac{-C_1(T-T_r)}{C_2+(T-T_r)} \quad (2.5)$$

Where:

α_T : shift factor as a function of temperature T

T: test temperature in Kelvin (°K)

T_r : reference temperature in Kelvin (°K)

C1 and C2: fitting parameters

2.7.3 Flexural Dynamic Modulus

Flexural beam frequency sweep testing followed AASHTO T 321 using a beam fatigue apparatus and beams prepared using a rolling wheel compactor.

Specimens were tested at 10°C, 20°C, and 30°C and at frequencies between 15 and 0.01 Hz. A sinewave frequency was applied to produce a tensile strain of 100 μ strain on the longitudinal surface of the beam. The measured stiffnesses and phase angles were horizontally shifted into master curves at 20°C using Equation 2.2, Equation 2.3, and Equation 2.5. Flexural stiffnesses were used in the *Cal/ME* simulations discussed in Chapter 8.

2.7.4 Fatigue Cracking Resistance

Fatigue cracking resistance testing followed AASHTO T 321 on beams prepared using a rolling wheel compactor. Beam specimens are subjected to four-point bending by applying sinusoidal loading at three different strain levels (high, intermediate, and low) at a frequency of 10 Hz and temperature of 20°C. The fatigue life for each strain level was selected by multiplying the maximum stiffness value for that strain level by the number of cycles at which that stiffness value occurred.

In this study, the testing approach currently specified in AASHTO T 321 was modified to optimize the quantity and quality of the data collected. Replicate specimens were first tested at high and medium strain levels to develop an initial regression relationship between fatigue life and strain (Equation 2.6). Strain levels were selected, based on experience, to achieve fatigue lives between 10,000 and 100,000 load cycles at high strains and between 300,000 and 500,000 load cycles for medium strains. Additional specimens were then tested at lower strain levels selected based on the results of the initial linear regression relationship to achieve a fatigue life of about 1 million load repetitions. The final regression relationship was then refined to accommodate the measured stiffness at the lower strain level.

$$\ln(N) = A + B \times \ln(\varepsilon) \quad (2.6)$$

Where:

N : fatigue life (number of cycles)

ε : strain level (μ strain)

A and B: model parameters

Test results can also be used to generate the material fatigue response in the *Ca/ME* simulations when used with flexural stiffness master curves to calculate estimated strains in the pavement. Flexural fatigue results can be directly compared without *Ca/ME* simulation when taking into consideration that laboratory test results will generally correspond with field fatigue or reflective cracking performance for overlays thinner than about 62 mm (0.2 ft.) but may not correspond with expected field performance for thicker layers of asphalt. For thicker layers, the interaction of the pavement structure, traffic loading, temperature, and mix stiffness with the controlled-strain beam fatigue results needs to be simulated using mechanistic analysis to rank mixes for expected field performance.

2.7.5 Fracture Cracking Resistance (SCB)

Fracture cracking resistance was assessed in terms of the fracture energy, strength, and flexibility index determined from the SCB test following AASHTO TP 124 on gyratory-compacted specimens.

Tests were run at 25°C with four replicates. Flexibility index, fracture energy, and strength were determined using Equation 2.7, Equation 2.8, and Equation 2.9, respectively. Potential differences in notch properties in the specimen (i.e., the notch ending in the mastic, in the fine aggregate matrix, or against a large aggregate or within a large aggregate) were taken into consideration when assessing variability between replicate test results (9).

$$G_f = \frac{W_f}{Area_{lig}} \times 10^6 \quad (2.7)$$

$$\sigma = \frac{L_p}{2rt} \quad (2.8)$$

$$FI = A \times \frac{G_f}{|Spp|} \quad (2.9)$$

Where:

G_f : fracture energy (Joule/m²)

W_f : work of fracture (Joule)

$Area_{lig}$: ligament area (mm^2)

σ : strength of the SCB specimen

L_p : peak load applied during the test

r : radius of the SCB specimen

t : thickness of the SCB specimen

Fl : flexibility index

A : correlation parameter, a typical value is 0.01

S_{pp} : post-peak slope

2.7.6 Rutting Resistance

Permanent deformation resistance testing followed AASHTO T 378 using an AMPT with specimens prepared in a gyratory compactor. The RLT parameters assessed included flow number and the number of cycles to reach 5% permanent axial strain. Specimens were tested with no confinement under a deviator stress of 483 kPa (10-12). Given that the addition of RAP tends to stiffen mixes and therefore improve rutting resistance, HWT tests were not done in addition to the RLT tests.

2.7.7 Indirect Tensile Cracking Resistance IDEAL-CT

IDEAL-CT used the same apparatus as the SCB testing but with a different specimen fixture, shown in Figure 2.11. A loading rate of 50 mm/min was applied until the tested specimen reached failure. An example of a test result from IDEAL-CT is illustrated in Figure 2.12.

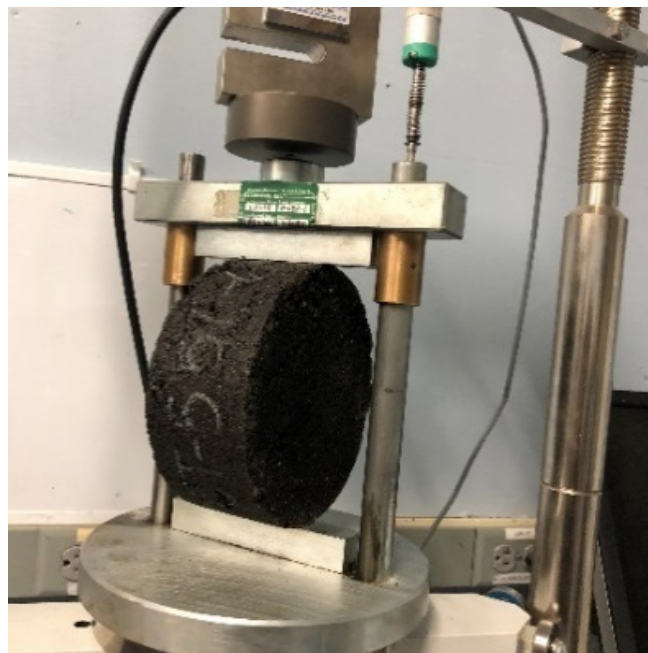


Figure 2.11: Testing machine for IDEAL-CT with a specimen.

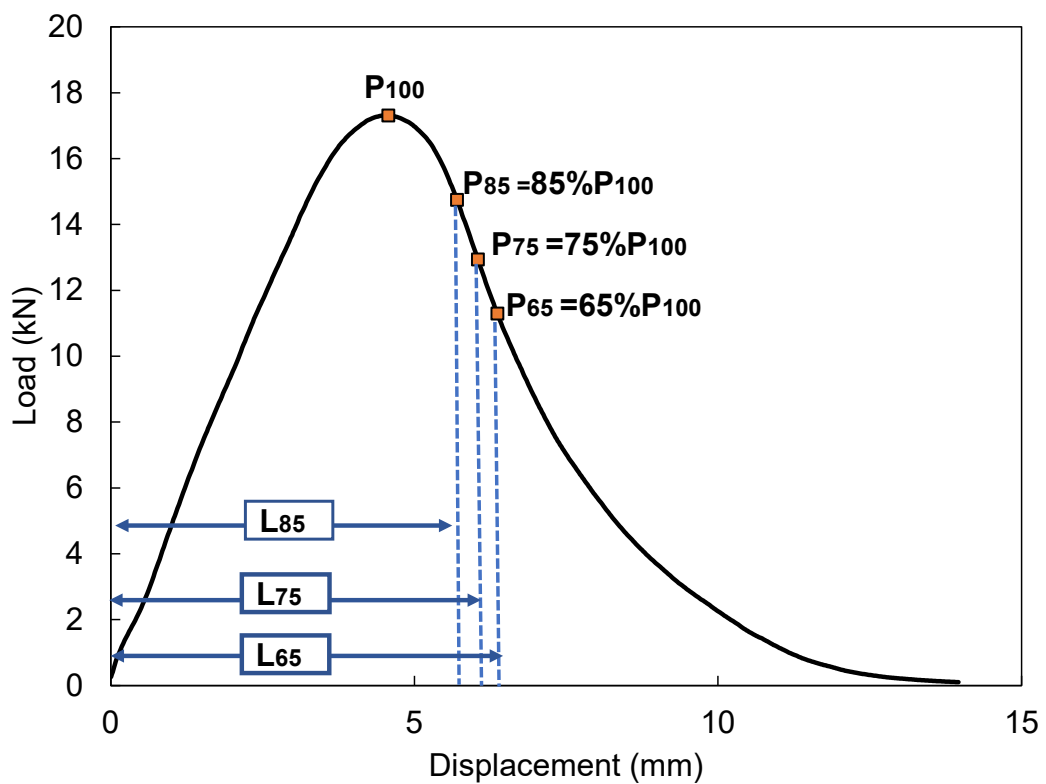


Figure 2.12: Example load-displacement curve from IDEAL-CT.

Fracture parameters obtained from IDEAL-CT are shown in Table 2.8, along with definitions. The two parameters of primary interest are the IDEAL-CT parameter, which is intended to relate to cracking and which the UCPRC has found correlates very well with flexural stiffness at 10 Hz and 20°C, and the Strength parameter, which has also been found to have a strong correlation with flexural stiffness but half the test variability of the IDEAL-CT parameter.

Table 2.8: Fracture Parameters from IDEAL-CT

Parameters	Equations
$ m_{75} $: post-peak slope (N/m)	$ m_{75} = \left \frac{P_{85} - P_{65}}{I_{85} - I_{65}} \right $ <p>Where: P_{85} = 85% of peak load P_{65} = 65% of peak load I_{85} = deformation at P_{85} I_{65} = deformation at P_{65}</p>
l_{75} (mm)	Displacement at 75% of the peak load after the peak
G_f : failure energy (J/m^2)	$G_f = \frac{W_f}{D \times t} \times 10^6$ <p>Where: W_f = area under load-displacement curve (J) t = thickness (mm) D = diameter (mm)</p>
CT_{index} : cracking tolerance index	$CT_{index} = \frac{t}{62} \times \frac{l_{75}}{D} \times \frac{G_f}{ m_{75} } \times 10^6$
Strength	$\text{Strength} = \frac{\text{Peak load}}{2rt}$

2.7.8 Testing Done by Caltrans and Texas A&M University

Testing for volumetric properties for JMF verification and during QA was completed by Caltrans. Additional mix and binder testing using sample from QA was completed by Texas A&M University. Neither of these sets of results are included in this technical memorandum.

3. BINDER TESTING RESULTS

3.1 Introduction

This chapter discusses the binder testing results on the blended binders extracted from the four mixes, including extracted binders from the mixes sampled during JMF verification and extracted binders from the two samples from each mix during construction QA. Summary plots are presented in the text, while more detailed, tabulated results are available in the UCPRC online laboratory testing system.

It should be noted that binder extracted from mixes results in complete blending of the virgin binder, RAP binder, and rejuvenating agent and that this complete diffusion may not have occurred in the mix at the time of sampling.

3.2 Binder Testing Results for JMF Verification Mix Samples

3.2.1 PG Grading

Table 3.1 summarizes the true grades of the binders at high, intermediate, and low temperatures and also for low temperatures at a non-standard 40 hours of PAV aging for the samples taken during JMF verification and during QA. JMF verification samples were only taken for Mix A (0% RAP, 0% RAS), Mix C (0% RAP, 3% RAS), and Mix D (10% RAP, 3% RAS). Mix B (10% RAP, 0% RAS) had been previously submitted for JMF verification because it is the mix that was being used on the rest of the project outside of the test sections.

The continuous high temperature grade is defined as the temperature where the unaged binder's $G^*/\sin(\delta)$ value equals 1.00 kPa and the RTFO-aged binder's $G^*/\sin(\delta)$ value equals 2.20 kPa. For the JMF verification and QA testing performed for the pilot project, the binder was extracted from a plant-produced mix, so there was no virgin binder test results for the blend and "plant-produced" results are presented in place of RTFO-aged results. Intermediate temperature grading is defined as the temperature where the 20-hour PAV-aged binder $G^*\times\sin(\delta)$ values equal the maximum allowable stiffness of 5,000 kPa, as specified in AASHTO M 320. The low temperature grading is defined as the warmest of the following two temperatures using 20-hour PAV-aged binder: (1) the temperature where the creep stiffness

(300 MPa) occurs or (2) the temperature where the lowest minimum allowable m-value (0.300) occurs.

The JMF results in Table 3.1 and the plot of JMF results in Figure 3.1 show that Mix A had the lowest high temperature true grade, Mix C had the highest, and Mix D fell in between. Mixes C and D had a PG 58 base binder while Mix A had a PG 64 binder, but the addition of RAS (Mix C) and RAP and RAS (Mix D) and rejuvenating agent resulted in Mixes C and D having high temperature true grades that were higher than those of Mix A: 5.6°C higher for Mix C and 3.8°C higher for Mix D. The specification (Table 2.2) calls for Mixes C and D to have PGs that are the same as the control mix, which were not met because Mixes C and D have high temperature true grades of 70. However, a higher high temperature true grade indicates better rutting performance at high temperatures, which is the intent of the PG grading specification. Therefore, while Mixes C and D did not meet the specification, they can be expected to have better rutting performance than Mix A, assuming complete blending of the RAP, RAS, rejuvenating agent, and virgin binder in those mixes.

As shown in the Table 3.1 JMF verification results and Figure 3.1, the control Mix A binder had the lowest average true grade low temperature, followed by Mix C and then Mix D, and the difference between Mix A and Mix D is 3.3°C. All the binders met the low temperature binder specification of -22°C.

For the intermediate temperature true grade, the Table 3.1 JMF verification results and Figure 3.1 show that the results are similar, with rank order from softest to stiffest of (1) Mix A, (2) Mix D, and (3) Mix C. The difference in intermediate temperature grade between Mixes A and D is 1.4°C. For thin overlays, less than about 0.2 to 0.25 ft. (60 to 75 mm) thick, softer binders at intermediate temperatures will tend to provide longer fatigue and reflective cracking lives. The opposite is true as overlay or new asphalt layer thicknesses increase above about 0.2 to 0.25 ft. (60 to 75 mm), with stiffer binders generally providing increasingly better fatigue and reflective cracking lives as the thickness increases. These results indicate similar performance for Mixes A, C, and D, assuming that the binders become fully blended in the mix.

The average Delta T_c results for 20- and 40-hour PAV-aged specimens are shown in Table 3.1 and Figure 3.2 for the JMF samples. Control Mix A had more positive Delta T_c values than the mixes with RAP and RAS, indicating that its low temperature performance is controlled more by creep slope than stiffness, which is considered an indication of better performance with regard to long-term age-related low temperature and block cracking. Additional PAV aging to 40 hours to simulate very long-term aging performance showed that Mix C suffered the most from the detrimental effects of very long-term aging, while Mixes A and D had less long-term aging. All the JMF verification sampled binders met the specification for a Delta T_c value greater than -5.0.

Figure 3.3 shows PG true grade temperatures normalized to those of Mix A, showing that Mixes C and D had slightly better high temperature true grades, slightly worse low temperature true grades, and slightly worse intermediate temperature true grades (for this thin overlay application).

Table 3.1. Continuous Binder Grading Results for JMF Verification and QA Samples

Mix, Sample	Sample Type	20HR PG Grade	40HR PG Grade	PG True Grade (20HR PAV) ^a	20HR ΔTc (°C)	PG True Grade (40HR PAV)	40HR ΔTc (°C)	ΔTc (°C) from 20HR to 40HR
Plant-MixA (1/2", 0% RAP, 0% RAS)	JMF	PG 64-28	PG 64-22	66.2-28.7 (22.1)	1.1	CG 66.2-25.5 (25)	-1.4	2.5
Plant-MixC (1/2", 0% RAP, 3% RAS)	JMF	PG 70-22	PG 70-22	71.8-27.5 (23.9)	-0.8	CG 71.8-22.8 (26.9)	-4.8	4
Plant-MixD (1/2", 10% RAP, 3% RAS)	JMF	PG 70-22	PG 70-22	70.0-25.4 (23.5)	-2.7	CG 70.0-22.5 (26.8)	-4.4	1.7
Plant-MixA (1/2", 0% RAP, 0% RAS)	QA Sample 1 (v1)	PG 64-22	PG 64-22	67.3-26.9 (23.2)	-1.7	CG 67.3-22 (27)	-4.8	3.1
Plant-MixA (1/2", 0% RAP, 0% RAS)	QA Sample 2 (v2)	PG 64-22	PG 64-22	68.4-25.5 (23.5)	-2.1	CG 68.4-21.4 (26.6)	-6.5	4.4
Plant-MixB (1/2", 10% RAP, 0% RAS)	QA Sample 1 (v1)	PG 70-22	PG 70-22	72.6-24.5 (26)	-2.6	CG 72.6-19.3 (29.2)	-7.0	4.4
Plant-MixB (1/2", 10% RAP, 0% RAS)	QA Sample 2 (v2)	PG 70-22	PG 70-22	72.1-23.3 (27)	-2.2	CG 72.1-19.8 (29.3)	-4.8	2.6
Plant-MixC (1/2", 0% RAP, 3% RAS)	QA Sample 1 (v1)	PG 70-22	PG 70-22	73.7-26.4 (23.8)	-2.6	CG 73.7-20.5 (27.5)	-7.7	5.1
Plant-MixC (1/2", 0% RAP, 3% RAS)	QA Sample 2 (v2)	PG 70-22	PG 70-22	73.9-24.9 (24.2)	-4.9	CG 73.9-21.1 (27.4)	-6.5	1.6
Plant-MixD (1/2", 10% RAP, 3% RAS)	QA Sample 1 (v1)	PG 70-22	PG 70-22	75.8-23.7 (28.9)	-3.6	CG 75.8-18.9 (28.8)	-8.4	4.8
Plant-MixD (1/2", 10% RAP, 3% RAS)	QA Sample 2 (v2)	PG 76-22	PG 76-22	76.5-24.4 (26.5)	-4.1	CG 76.5-19.4 (28.5)	-8.0	3.9

^a Also known as continuous grade (CG), shown as [high temperature, low temperature, (intermediate temperature)].

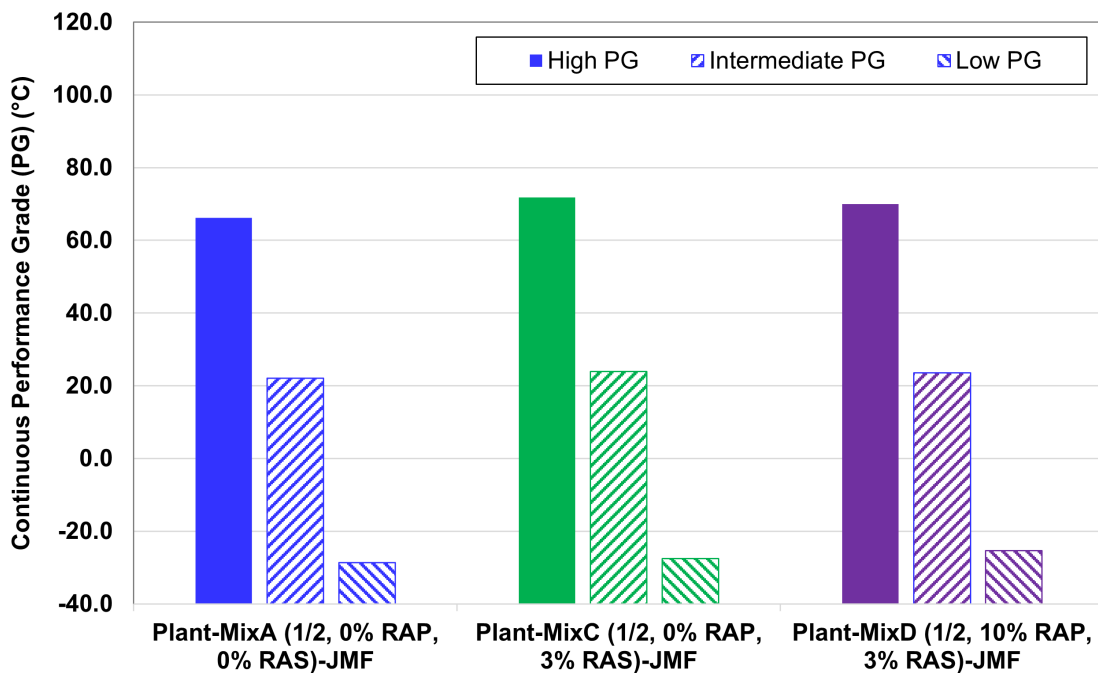


Figure 3.1: Continuous temperature binder grades for JMF verification sampled binders.

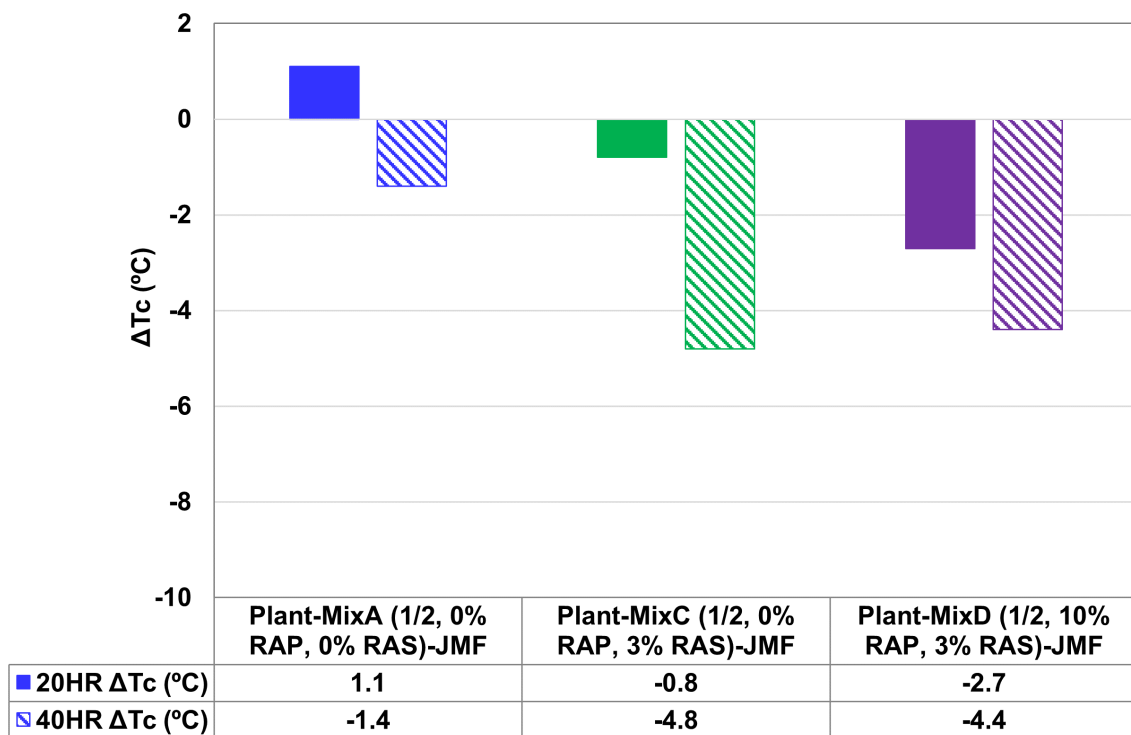


Figure 3.2: Delta T_c values for JMF samples (20-hour PAV specification value and for 40-hour PAV).

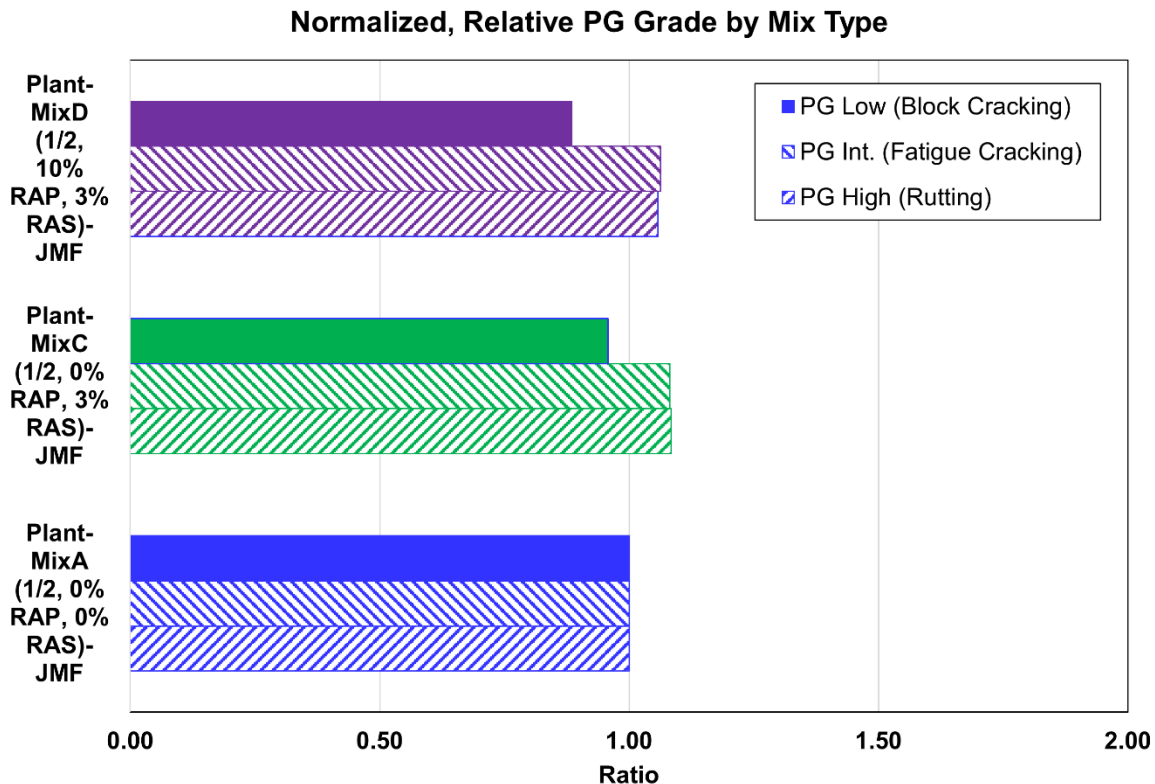


Figure 3.3: Binder grades for JMF verification sampled binders normalized to Mix A (0% RAP, 0% RAS) control mix.

3.2.2 Frequency Sweep

Frequency sweep testing was not performed on JMF verification sampled binders.

3.2.3 FTIR Testing

FTIR testing was not performed on JMF verification sampled binders.

3.3 Binder Testing Results from Quality Assurance Mix Samples

3.3.1 PG Grading

Table 3.1 and Figure 3.4 show that the true grade temperatures were consistent between the two QA samples. Figure 3.5 shows results averaged between the two QA samples, and that the control Mix A (0% RAP, 0% RAS) binder had the lowest average true grade high temperatures, followed by Mix B (10% RAP), Mix C (3% RAS), and Mix D (10% RAP, 3% RAS). The mixes with RAP, RAS, and RAP/RAS had higher average high binder true grade temperatures, indicating better resistance to rutting than the control, Mix A, which had no RAP or RAS. The difference in

high temperature grade between Mix A and Mix D is large, approximately 9°C. Mixes C and D meet requirements for PG 70 binder and, therefore, did not meet the specified requirements for this pilot project that they have the same high temperature true grade as the control Mix A, PG 64. The intention of the specification was to limit the high binder true grade temperatures of the mixes with RAS to limit their stiffness at intermediate and low temperatures, though a higher high binder true grade temperature indicates better rutting performance at high temperatures.

For the intermediate binder true grade temperatures, Table 3.1 and Figure 3.5 show that the rank order from softest to stiffest is the following: (1) Mix A, (2) Mix C, (3) Mix B, and (4) Mix D. The difference in intermediate temperature grade between Mixes A and D is approximately 4°C. A higher intermediate binder true grade temperature indicates that the mix will be stiffer at intermediate temperatures, which for thin overlays such as those on this pilot project, will often produce lower fatigue and reflective cracking resistance. These results indicate that the Mixes B, C, and D with RAP and RAS may have slightly lower fatigue and reflective cracking resistance than the control Mix A when used in thin asphalt layers, even though Mix A has a lower high temperature PG true grade and poorer rutting performance.

Figure 3.5 shows that the ranking for average low temperature from lowest true grade to highest is the following: (1) Mix A, (2) Mix C, (3) Mix B, and (4) Mix D. These results indicate that the binders with RAP and RAS had stiffnesses that were somewhat greater or had creep compliance at low temperatures that was somewhat less than the virgin binder (Mix A). The difference in the low temperature true grade of Mixes B and D and that of Mix A was small, approximately 2°C.

The Delta T_c results for 20- and 40-hour PAV-aged specimens are shown in Figure 3.6 for the two QA samples and averaged in Figure 3.7. Control Mix A had more positive Delta T_c values than the mixes with RAP and RAS, and the average order from most positive to most negative is the following: (1) Mix A, (2) Mix B, (3) Mix C, and (4) Mix D. A less negative Delta T_c value (if none are positive, as is the case for these four mixes) indicates that there is less difference between the critical stiffness temperature controlling the binder true grade temperature and

the critical creep compliance temperature, which indicates better resistance to block cracking after long-term aging than does a more negative Delta T_c value. In this case, the results indicate that the mixes with RAS (Mixes C and D) were more likely to have long-term block cracking than are those without RAS (Mixes A and B). The difference between Mixes A and D for the standard 20-hour PAV aging is 2°C, which is small, and 2.5°C for the severe 40-hour PAV aging, which is also relatively small.

The binder test results from the QA samples showed that the Delta T_c values of Mixes C and D as well as Mix B, the typical mix that was used on the rest of the project, all were above the minimum specified value of -5.0 for 20-hour PAV-aged samples.

Figure 3.8 summarizes the binder true grade temperatures normalized to Mix A. The results show that the other three mixes with RAP and RAS had higher high binder true grade temperatures, indicating better rutting performance; higher intermediate binder true grade temperatures, indicating slightly lower fatigue and reflective cracking resistance for thin overlays; and higher low binder true grade temperatures, indicating lower resistance to low temperature cracking.

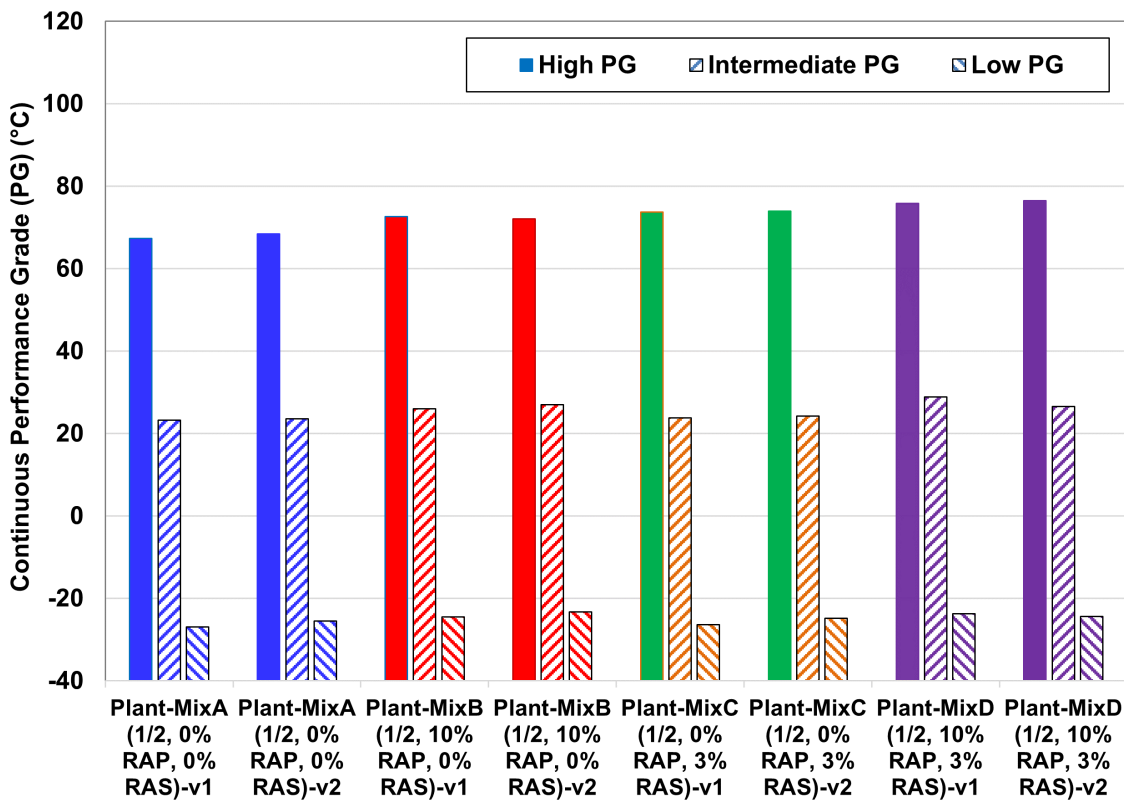


Figure 3.4: Continuous temperature binder grades for QA sampled binders by sample.

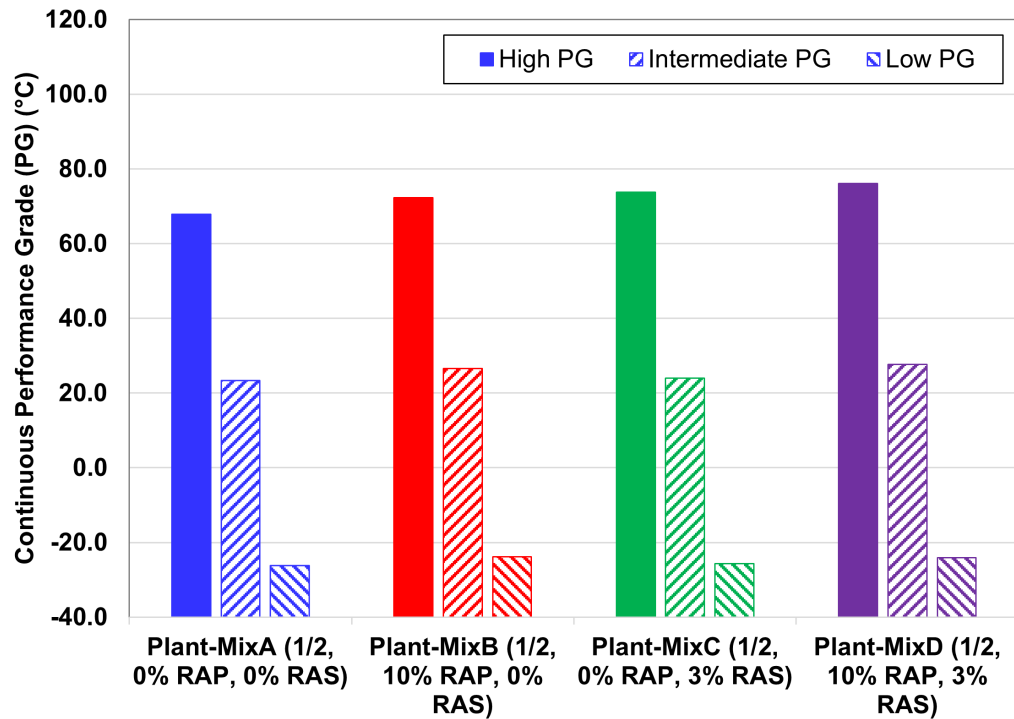


Figure 3.5: Average continuous temperature binder grades for QA sampled binders.

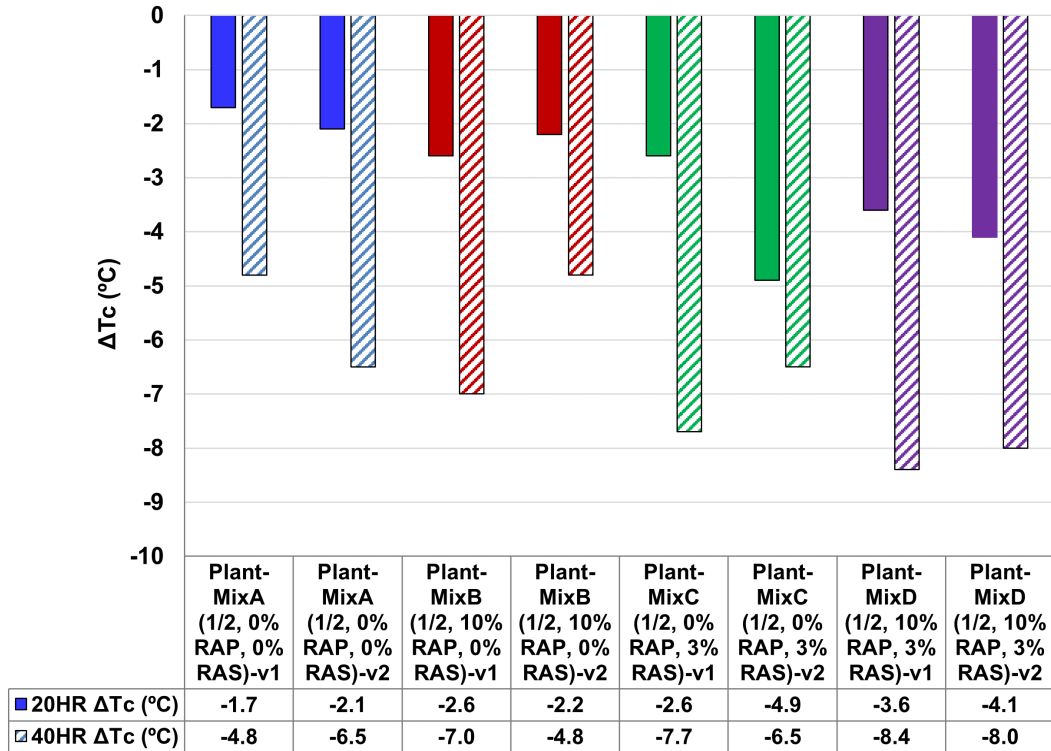


Figure 3.6: Delta T_c values by sample for QA samples (20 hour PAV specification value and for 40 hour PAV).

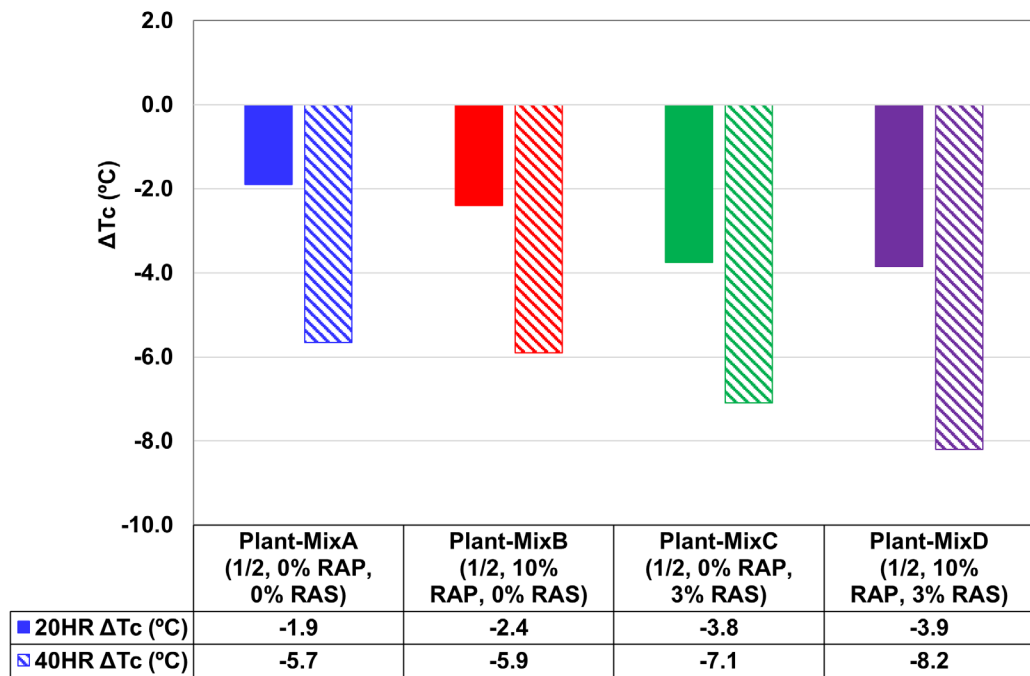


Figure 3.7: Average Delta T_c values for QA samples (20 hour PAV specification value and for 40 hour PAV).

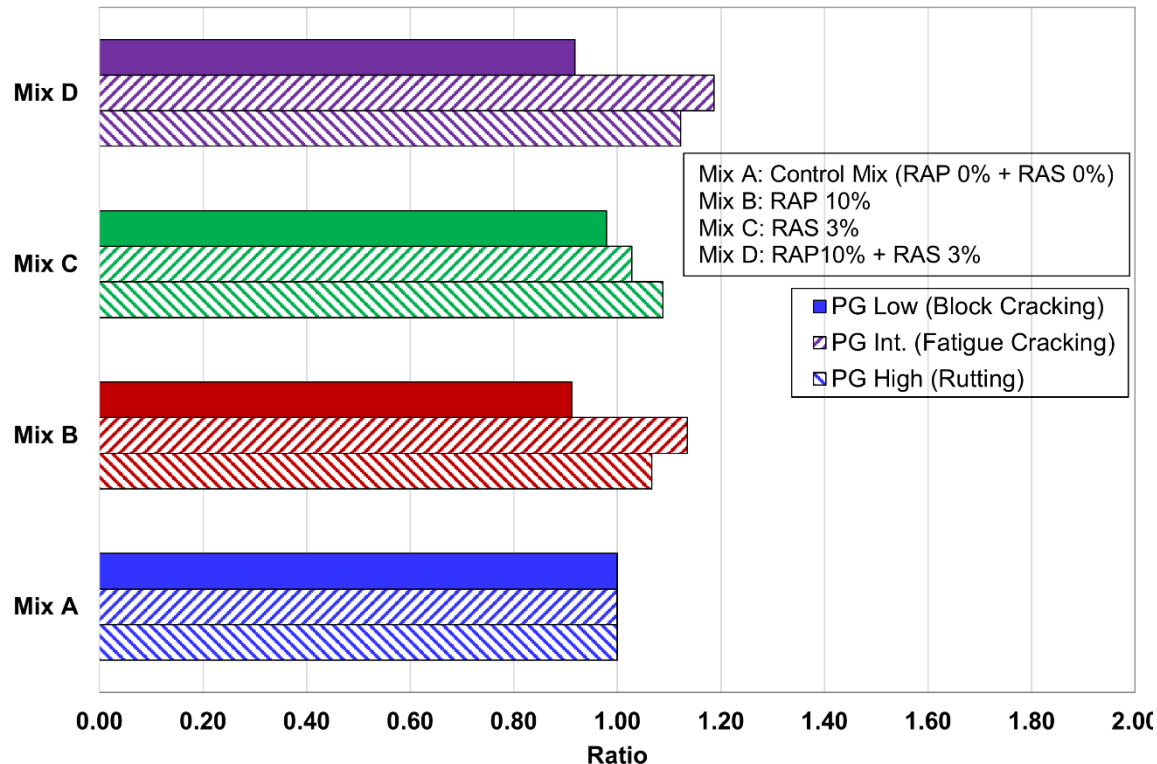


Figure 3.8: Average binder grades for QA sampled binders normalized to Mix A (0% RAP 0% RAS) control mix.

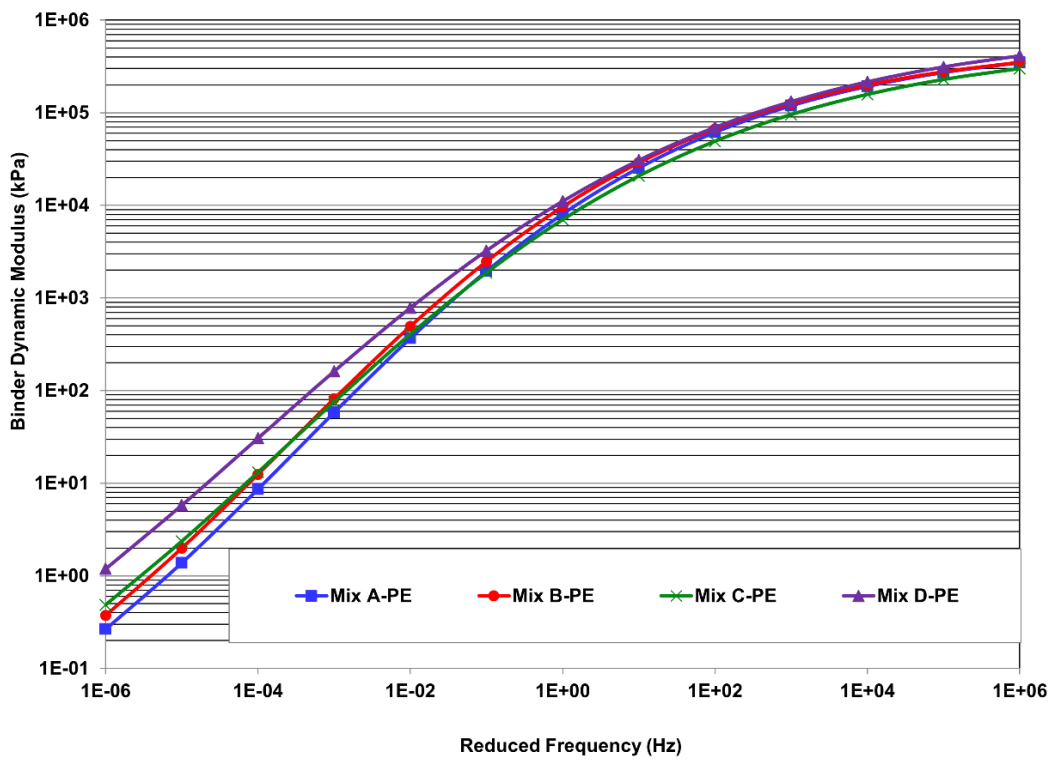
3.3.2 Frequency Sweep

The average binder dynamic stiffness master curves from the QA sampled materials are shown in Figure 3.9. The results are averages of four total tests, two for each of the two QA samples. The results are similar for QA sampled binders for Mixes A, B, C, and D at frequencies of 1 Hz and faster, associated with intermediate and low temperature cracking. Mix D, with RAP and RAS, was much stiffer than the control Mix A which had no RAP or RAS at reduced frequencies between 0.000001 and 1 Hz, associated with rutting performance, indicating potential for much better rutting performance. Mixes B and C were somewhat stiffer than Mix A, indicating potential for somewhat better rutting resistance.

Figure 3.10 shows the two QA samples (averaged for the two replicates from each sample). The binder stiffness master curve results for the QA samples for each mix are similar to each other, indicating little variability within each test section.

Figure 3.11 shows binder stiffnesses versus reduced frequency normalized to the Mix A QA sampled binder. As noted previously, all the QA sampled binders had similar stiffnesses at frequencies of 1 Hz and faster, within +/- 15% of each other, as shown in Figure 3.10 and Figure 3.11.

Figure 3.12 shows a Black Space diagram (stiffness versus phase angle) with stiffness at a reduced temperature of 15°C and a reduced frequency of 8 (10^{-4}) Hz for three aging conditions: (1) plant mixed, (2) 20-hour PAV aged, and (3) 40-hour PAV aged. Imposed on the plot are the Glover-Rowe thresholds that have been identified to correlate with an increased risk of long-term aging-related block cracking (13). Both QA samples of binder from paving are shown on the plot for the four pilot project mixes. The results show that Mix A with no RAP or RAS in it crosses into the transition zone only for the 40-hour PAV-aged samples. The 20-hour PAV-aged samples are in the transition zone for all the other three mix samples, except for one sample of Mix B. The 40-hour PAV-aged samples for Mix D show the greatest risk for block cracking with extreme aging, while the results for Mixes B and C were similar. These results indicate that Mix A has the least risk of block cracking with extreme aging, while the other three mixes, and especially Mix D, are at greater risk.



Note: PE indicates plant mix extracted.

Figure 3.9: Average frequency sweep master curves for QA sampled binders.

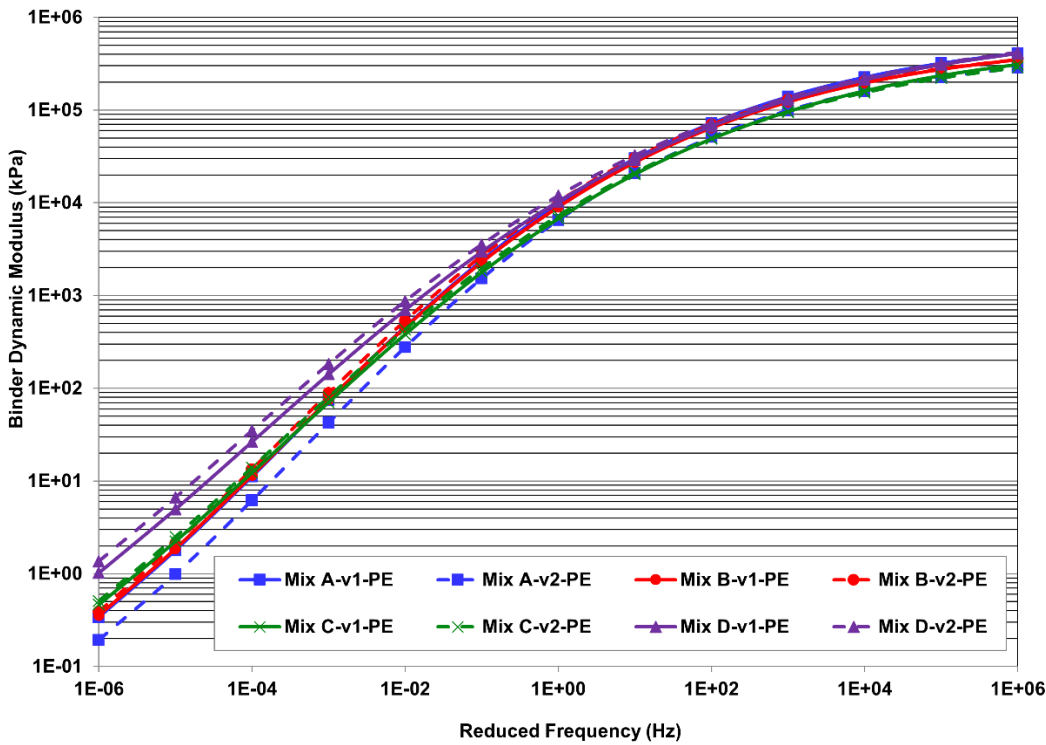


Figure 3.10: Frequency sweep master curves for both QA sampled binders .

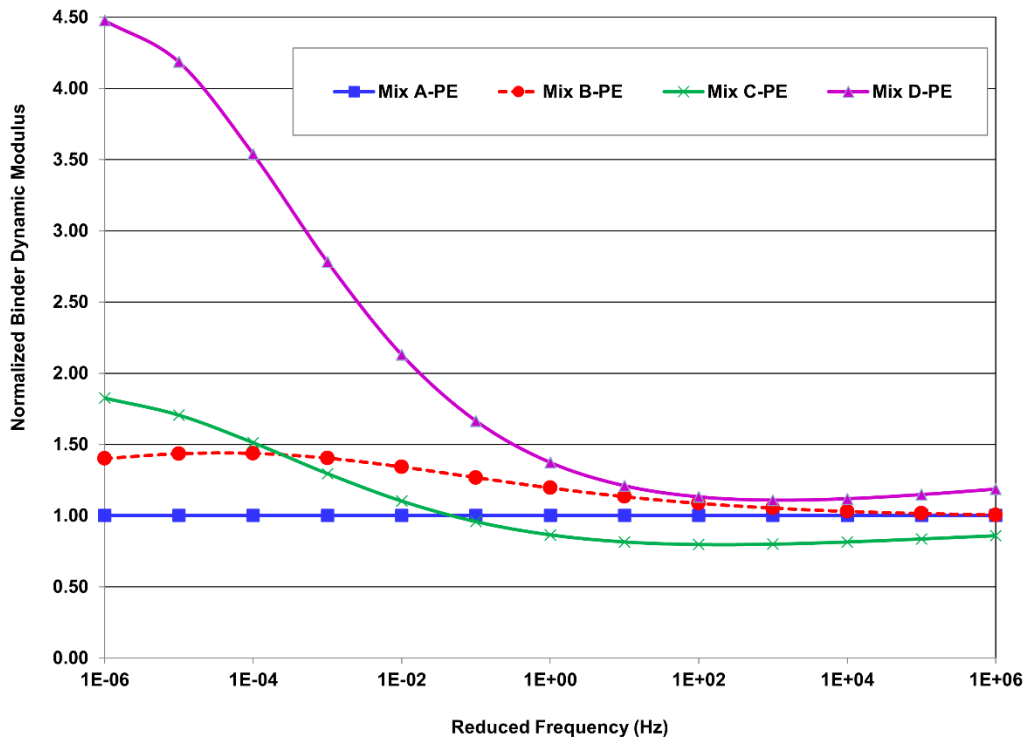


Figure 3.11: Frequency sweep master curves for QA sampled binders normalized to Mix B (10% RAP, 0% RAS).

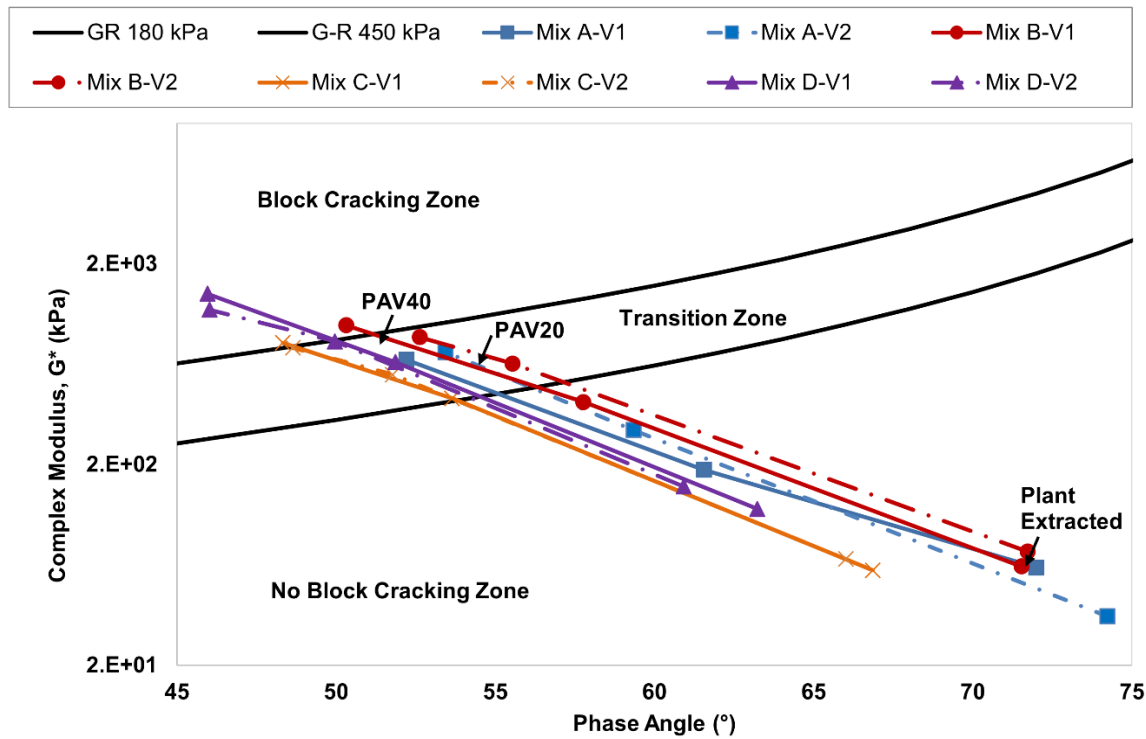


Figure 3.12: Black Space plot for QA sampled binders with Glover-Rowe criteria.

3.3.3 FTIR Testing

The QA samples binders were tested with the FTIR after plant mixing and 20- and 40-hour PAV aging. Figure 3.13 plots the carbonyl (CA) indices of the binders for these three conditions for both QA samples. The results show that Mix A had the least carbonyl (aging products) after plant mixing, followed by Mix B, Mix C, and Mix D, as expected. The carbonyl contents of all four mixes increased with PAV aging, also as expected, and the results were similar between QA samples for each mix. After PAV aging, the carbonyl indexes of Mixes B and C became more similar.

Figure 3.14 shows the sulfoxide indexes for each of the binders. For this less important aging product index, the sulfoxide contents were similar for all four mixes after plant mixing and after PAV aging.

Previous research by the UCPRC (2) and before that by other organizations (primarily Glover and others at Texas A&M University [14]) shows that carbonyl content is a good indicator of the changes in binder performance indicators with different amounts of aging for rutting at high temperatures and for stiffness related to different types of cracking at lower temperatures. This can be seen for the four mixes included in this project that were QA sampled during paving (three aging conditions each of two QA samples on four mixes). The results show a strong correlation versus the Glover-Rowe criteria (Figure 3.15), stiffness at 64°C and 10 Hz (Figure 3.16), and the crossover modulus (Figure 3.17). The crossover modulus is the stiffness at which the phase angle is 45 degrees, with decreasing crossover modulus indicating less ability to relax stresses under thermal contraction. The results show how the risk of block cracking increases with aging, the risk of rutting decreases, and the risk of low temperature cracking increases. It is interesting that the correlation remains strong despite different base binders being used in the mixes, RAP and RAS being present or not, and different dosages of rejuvenating agent.

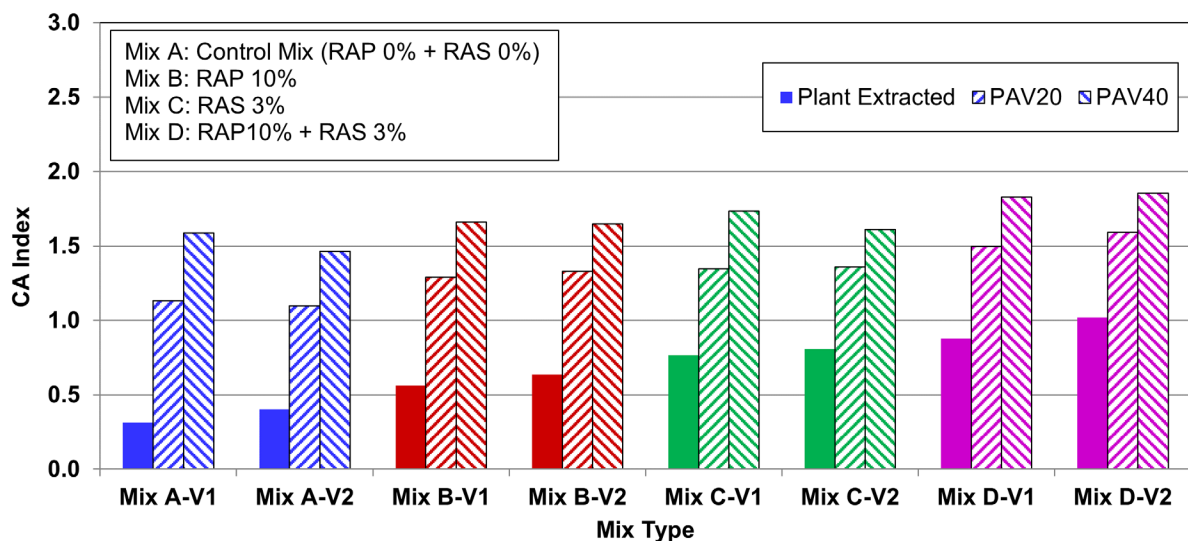


Figure 3.13: Carbonyl area index changes after aging for QA sampled binders.

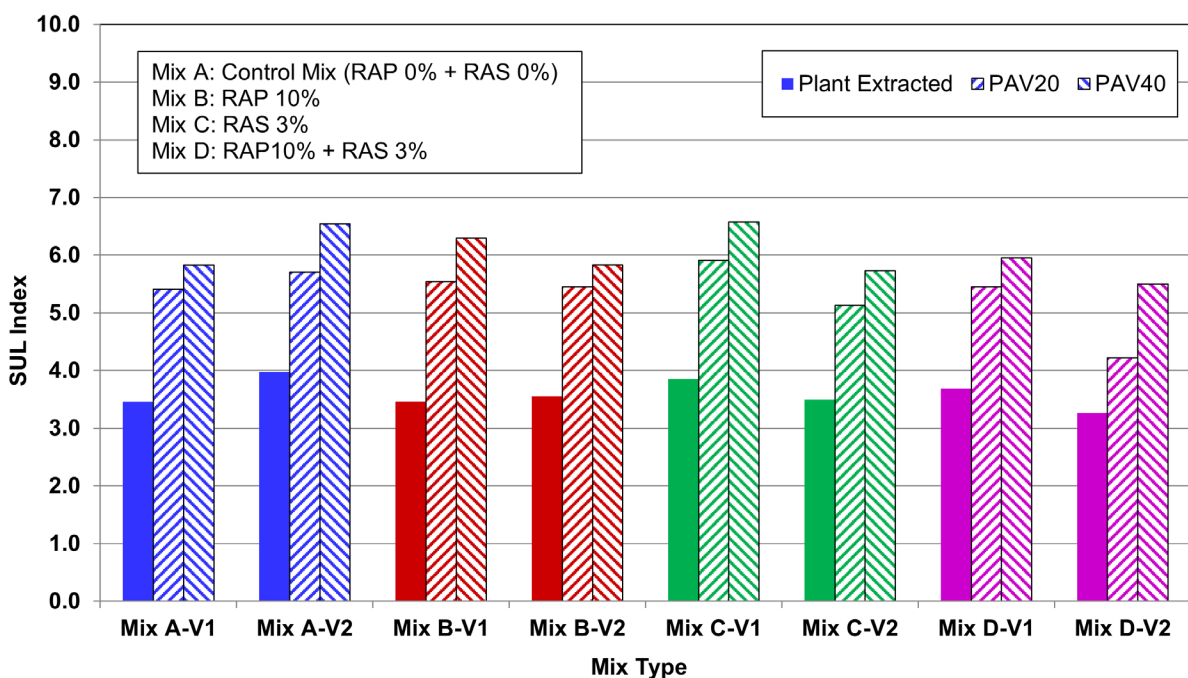


Figure 3.14: Sulfoxide area index changes after aging.

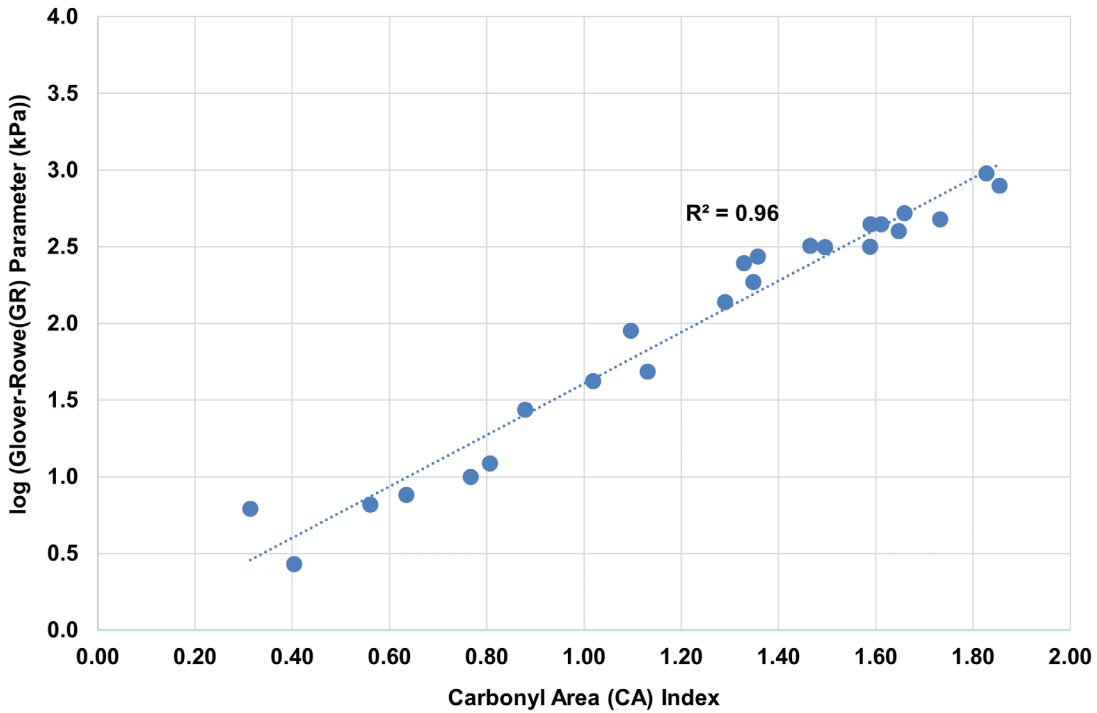


Figure 3.15: Carbonyl area for all binders versus Glover-Rowe parameter for all QA samples and aging conditions.

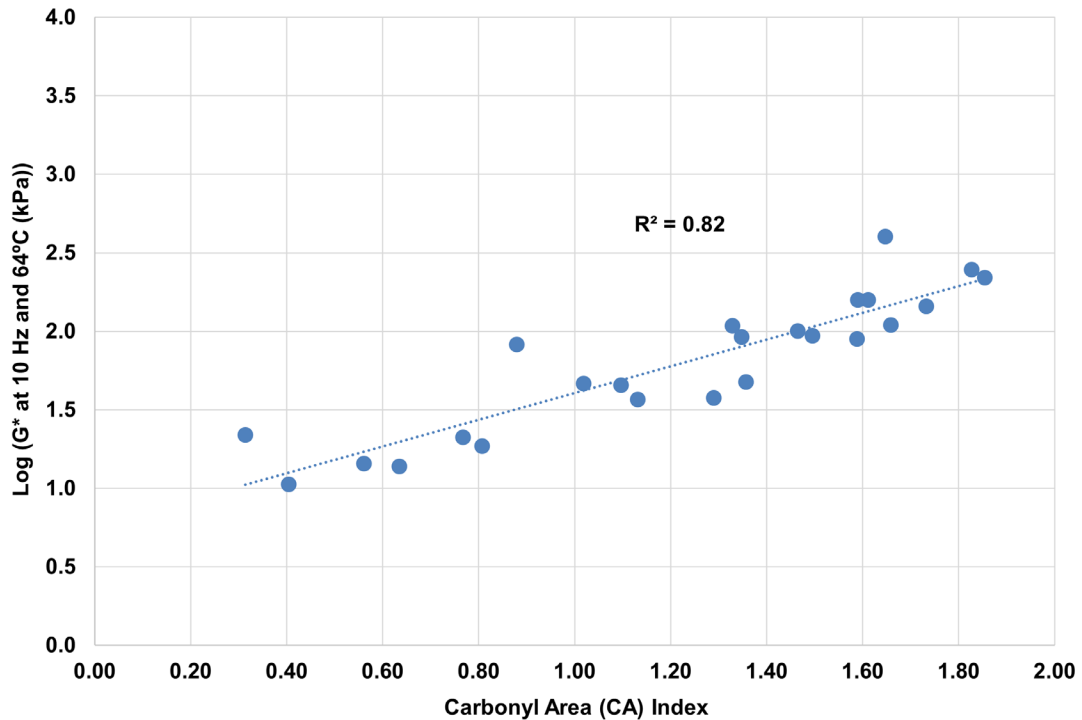


Figure 3.16: Carbonyl area for all binders versus G* sine δ at 10 Hz and 64°C for all QA samples and aging conditions.

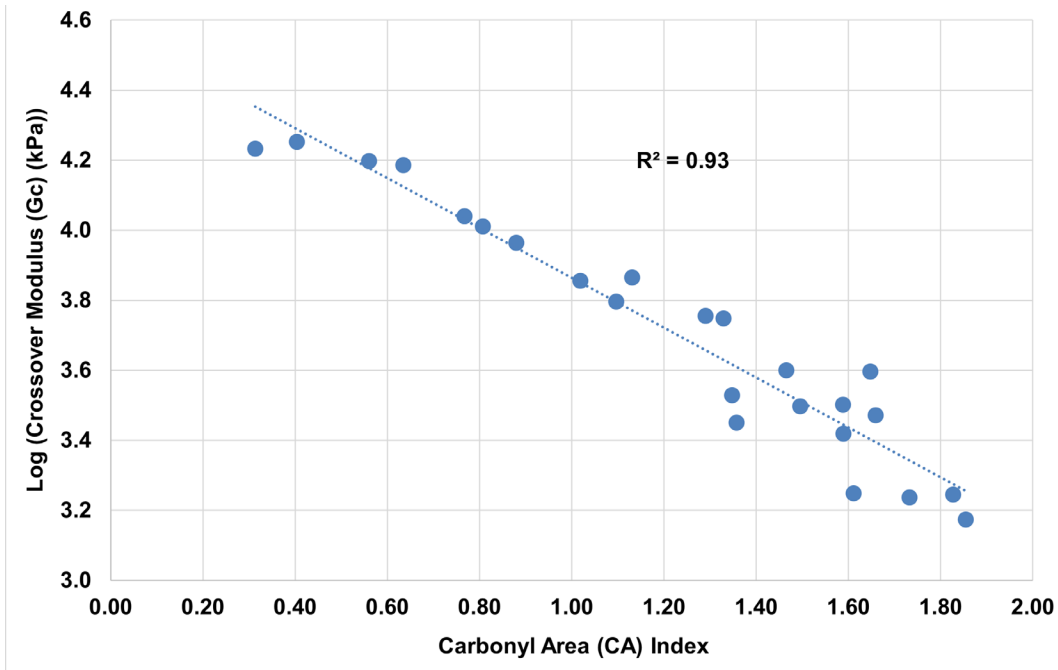


Figure 3.17: Carbonyl area for all binders versus crossover modulus for all QA samples and aging conditions.

4. MIX TESTING RESULTS

4.1 Introduction

This chapter discusses mix testing results for plant-produced JMF verification and QA sampled mixes. Mix designs and test method details are discussed in Chapter 2 and are not repeated in this chapter.

4.2 Mix Test Variability

4.2.1 Overview

It is desirable that pavement materials tests are sensitive to materials variables in the same way that the material performance in the field is sensitive to the same variables, and that the repeatability of the test is high (in other words, that the test variance is low). A few asphalt concrete mix distresses are related to monotonic loading conditions, particularly fracture from low temperature cracking or of long-term aged asphalt at intermediate temperatures as tested by fracture. The variability of monotonic tests is generally consistent regardless of the test value once operator and equipment inconsistencies are controlled.

The distresses of rutting and fatigue are caused by phenomena related to repeated loading. Assessments of mix properties for rutting and fatigue are generally considered to require a repeated load test to obtain the best mix characterization for permanent deformation (rutting) and damage or cracking under repeated traffic loading (fatigue) (15,16). The variability of repeated load tests is high when considered in terms of the standard deviation of the test. However, the sensitivity of repeated load tests to mix variables such as tensile strain (fatigue) or shear stress (rutting), binder stiffness and type, air void content, and aggregate gradation is very high, sufficiently similar to mix sensitivity in the field to predict rutting and fatigue performance when used with a mechanistic-empirical simulation framework (17). It has been shown that repeated load tests can discern the differences in expected performance between different mixes (or compaction levels, loading times, or temperatures) because the sensitivity of the tests to these variables is high (i.e., the change in the mean test result when a mix variable changes is greater than the variability for a given set of mix variables) (18). It has also been

found that the variability of repeated load tests is not constant, but rather it increases as the number of repetitions to failure increases such that the coefficient of variation (standard deviation of repetitions to a given damage state or failure divided by mean repetitions) is approximately a constant.

The calculated variability of repeated load test results can be reduced and changed to a relatively constant variability, as opposed to a constant coefficient of variation, by changing the definition of the test result parameter from the number of repetitions to reach the failure state to instead be the stress or strain state that results in a given number of repetitions to the failure state. This has been done in Caltrans performance-related specifications for the flexural fatigue test, where the specification parameter has been changed from the repetitions at a given tensile strain to instead be the tensile strain that results in 1 million cycles to failure. The test method is the same, except that the strains are selected to produce approximately 1 million repetitions to failure at the lowest strain used for a given mix. This has also reduced the time necessary to complete testing for a mix.

Methods of minimizing variability of test results for all types of asphalt concrete performance-related tests include consistent materials handling to have uniform aging, consistent air voids, consistent specimen dimensions, calibrated equipment, and certified testing staff. Once these sources of variability are controlled, inherent test variability is typically influenced by considerations of representative volume element (RVE) for the composite material (ratio of largest particle size to least specimen dimension), and the sensitivity of the results to the location of the critical stress state relative to the random locations of larger aggregate particles in the specimen.

Variabilities of mix test results on this pilot project were generally consistent with those for the same tests on other projects. Within-sample variability values are shown for the following tests performed on this pilot project during both JMF approval (where applicable) and QA testing: mix stiffness at 20°C and 10 Hz (flexural and axial tests), repeated load triaxial tests (confined and unconfined), four-point beam repetitions to failure at a given strain (lowest strain used), IDEAL-CT parameter and strength, and I-FIT parameter and strength. The variability data shown

for each test is within-sample, meaning that the JMF sample and the two QA samples are each treated as a different sample. Test variability for all tests will be assessed once all the pilot projects are completed.

4.2.2 Variability of Test Results on This Pilot Project

The average within-sample variabilities of the flexural and triaxial dynamic moduli at 10 Hz and 20°C from the frequency sweep tests are shown in Table 4.1.

Table 4.1: Variability of Within-Sample Stiffness (MPa) and Coefficient of Variation for Dynamic Modulus at 20°C and 10 Hz

Test	Replicate tests (range for samples)	Average Standard Deviation (MPa)	Minimum Coefficient of Variation ^a	Maximum Coefficient of Variation ^a	Average Coefficient of Variation ^a
Flexural dynamic modulus at 10 Hz, 20°C	3	283	0.02	0.11	0.05
Triaxial dynamic modulus at 10 Hz, 20°C	3	373	0.02	0.09	0.05

^a Std dev/mean.

The average within-sample variabilities of the unconfined and confined repeated load triaxial test results are shown in Table 4.2.

Table 4.2: Variability Of Within-Sample Stiffness (Repetitions To Flow Number or Failure) and Coefficient of Variation for Repeated Load Triaxial Test

Test	Replicate tests (range)	Average Standard Deviation (repetitions)	Minimum Coefficient of Variation ^a	Maximum Coefficient of Variation ^a	Average Coefficient of Variation ^a
Unconfined Flow Number	5-6	113	0.09	0.40	0.19
Confined Flow Number	5-6	5,975	0.03	0.53	0.35
Unconfined to 3% permanent strain	5-6	283	0.06	0.50	0.23
Confined to 3% permanent strain	5-6	6,939	0.41	0.53	0.26

^a Std dev/mean.

The average within-sample variabilities of the flexural fatigue beam test results are shown in Table 4.3.

Table 4.3: Variability of Within-Sample Tensile Strain at 1 Million Repetitions to Failure and Coefficient of Variation for Flexural Fatigue Test

Test	Replicate tests (range)	Average Standard deviation (repetitions to failure)	Minimum Coefficient of Variation ^a	Maximum Coefficient of Variation ^a	Average Coefficient of Variation ^a
Repetitions to failure at 370-375 $\mu\epsilon$	3-4 at each strain level	352,604	0.11	0.85	0.35

^a Std dev/mean.

The average within-sample variabilities of the indirect tension (IDEAL-CT) and semicircular beam (I-FIT) fracture test results are shown in Table 4.4.

Table 4.4: Variability of Within-Sample Fracture Test Parameter (IDEAL-CT Number or I-FIT Parameter) and Strength (mpa) and Coefficient of Variation

Test	Replicate test range	Average Standard deviation (parameter or psi)	Minimum Coefficient of Variation ^a	Maximum Coefficient of Variation ^a	Average Coefficient of Variation ^a
IDEAL-CT Number	3-5	27.8	0.12	0.38	0.23
IDEAL-CT Strength (psi)	3-5	10.6	0.03	0.09	0.06
I-FIT parameter	4-6	1.26	0.08	0.96	0.33
SCB Strength (psi)	4-6	20.1	0.04	0.34	0.09

^a Std dev/mean.

The within-sample test variabilities found in this project are within the ranges of those found in other projects. As noted previously, the variability of each of these tests will be assessed in future pilot projects and other test programs.

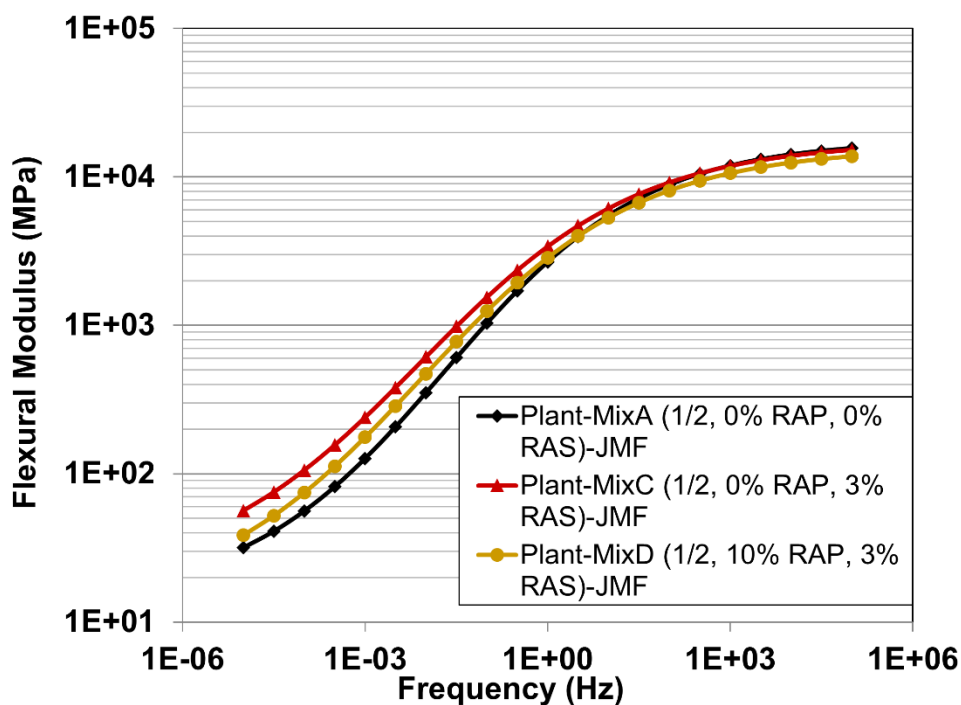
4.3 Testing of Job Mix Formula Mixes Prior to Construction for JMF Verification

4.3.1 Mix Stiffness: Flexural and Triaxial Dynamic Modulus

Flexural Dynamic Modulus Frequency Sweep Results

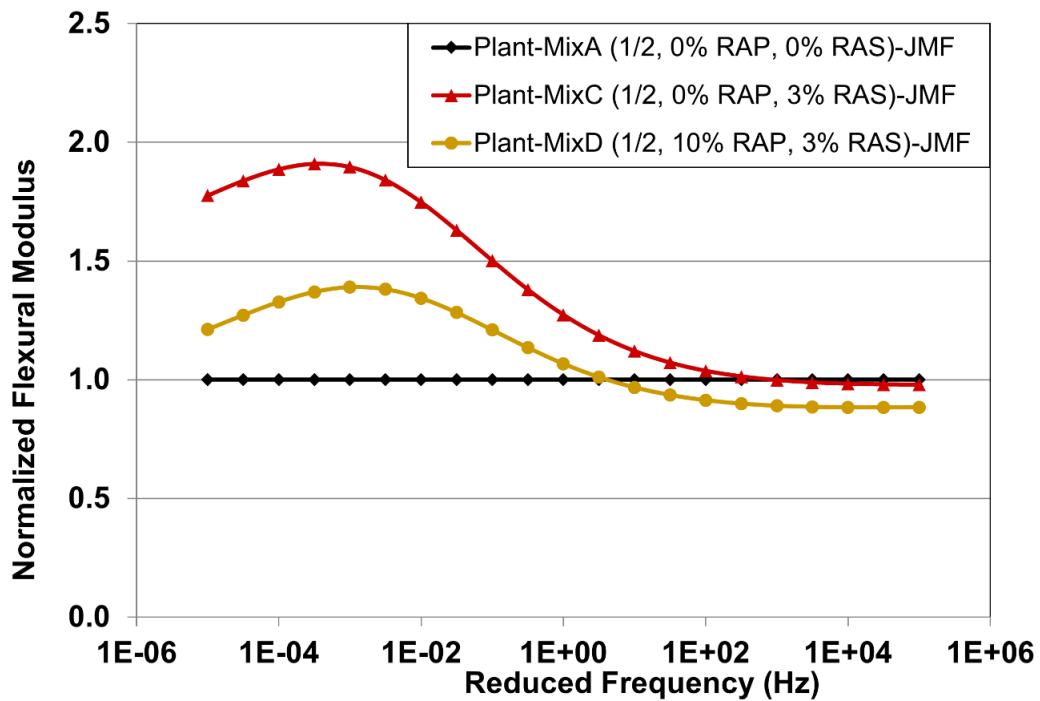
The flexural dynamic modulus curves from JMF verification sample testing for Mixes A, C, and D are shown in Figure 4.1. The mix stiffness results generally replicate those from binder testing, as expected with all the mixes having similar stiffnesses at reduced frequencies of approximately 1 Hz and faster and increasing differentiation at reduced frequencies less than 1 Hz. Below 1 Hz, Mix A is the softest, Mix C is the stiffest, and Mix D is in between them, shown in Figure 4.2 where the master curves are normalized to that of Mix A.

Figure 4.3 shows the Black Space diagram for the JMF verification samples for Mixes A, C, and D. Mix A has a higher phase angle at slower frequencies (when lower stiffnesses are occurring) than the other two mixes, indicating greater propensity for viscous flow and less elastic recovery at those frequencies.



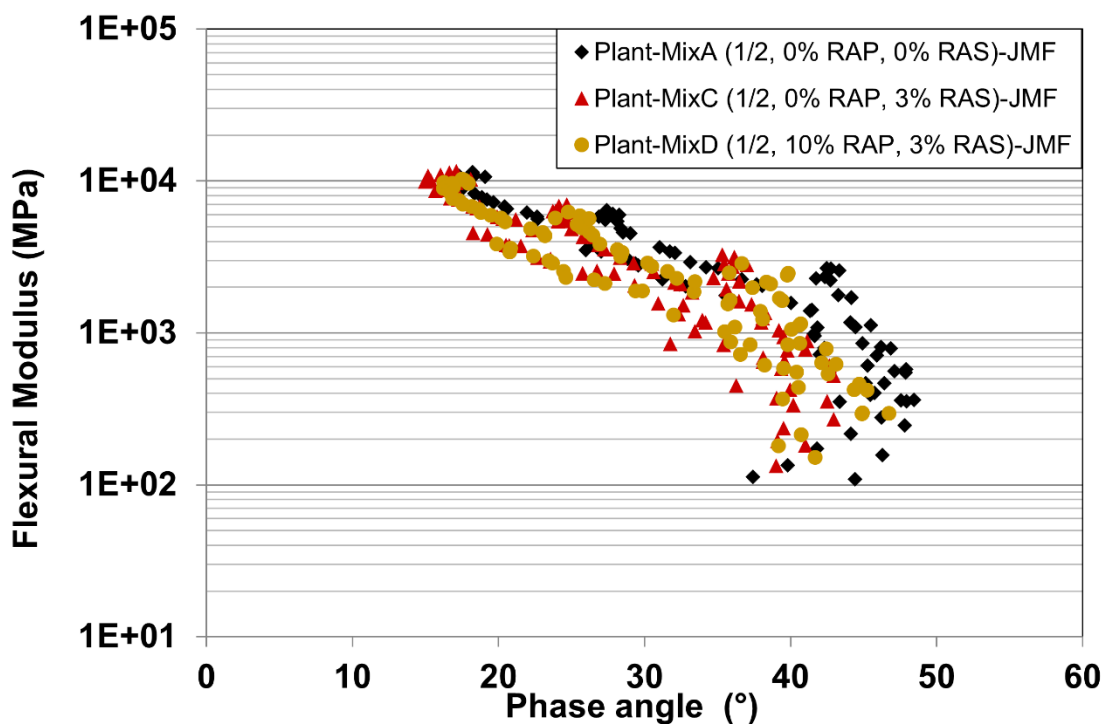
Note: MixB not tested.

Figure 4.1: Flexural dynamic modulus master curves for JMF verification sampled mixes.



Note: MixB not tested.

Figure 4.2: Flexural dynamic modulus master curves for JMF verification sampled mixes normalized to Mix A (0% RAP, 0% RAS).



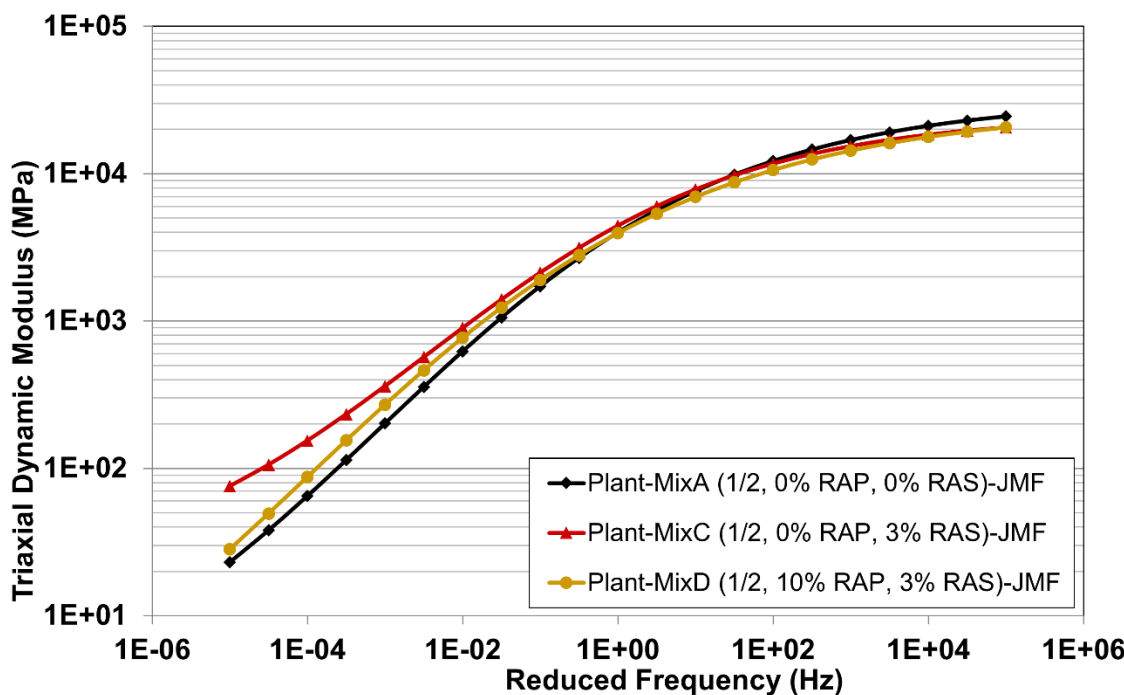
Note: MixB not tested.

Figure 4.3: Black Space diagram for flexural dynamic modulus master curves for JMF verification sampled mixes.

Triaxial Dynamic Modulus Frequency Sweep Results

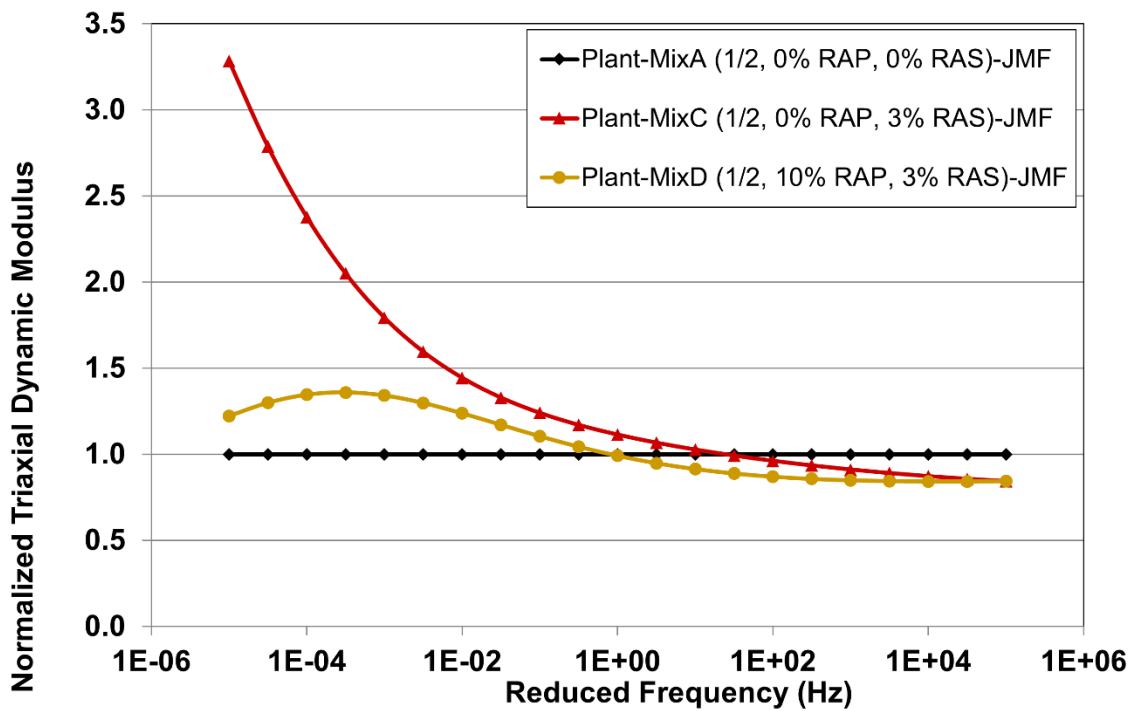
Figure 4.4 shows the master mix stiffness curves for the JMF verification samples for Mixes A, C, and D, and Figure 4.5 shows the master stiffness curves for Mixes C and D normalized to that of Mix A. Figure 4.6 is the Black Space diagram for the three mix binders. The stiffness master curves are consistent with those found from the flexural frequency sweeps, as expected.

As expected, the stiffnesses from the triaxial frequency sweeps shown in these figures are not always the same as those found from the flexural sweeps shown previously, and the triaxial stiffnesses are generally somewhat greater. This difference is expected because asphalt bound materials are stiffer in the combination of compressive and shear stresses found in the triaxial configuration compared with the flexural stress state, which is dominated by the effects of tensile stresses. There are also cross-anisotropic differences in the orientation of the aggregates between the horizontal plane of the mix, tested by flexural loading, versus the vertical direction, affecting more the results from loading in the triaxial configuration. At the fastest and slowest frequencies, the triaxial stiffnesses are up to about 80% greater than the flexural stiffnesses, as expected.



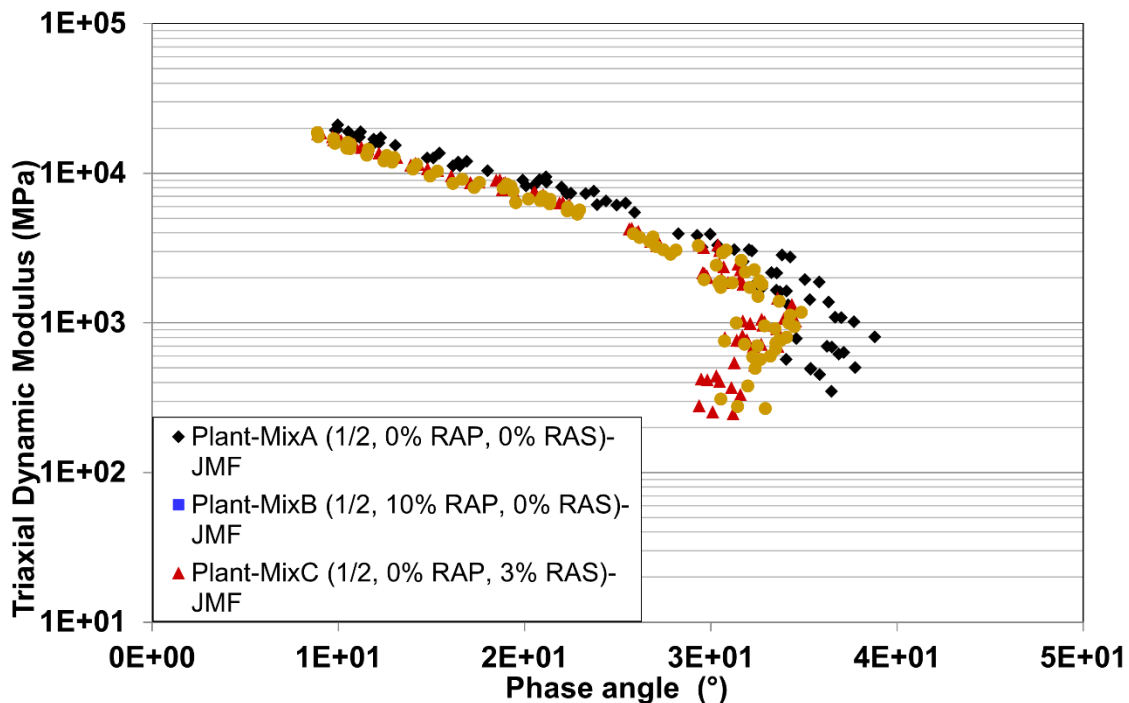
Note: MixB not tested.

Figure 4.4: Triaxial dynamic modulus master curves for JMF verification sampled mixes.



Note: MixB not tested.

Figure 4.5: Triaxial dynamic modulus master curves for JMF verification sampled mixes normalized to Mix A (0% RAP, 0% RAS).



Note: MixB not tested.

Figure 4.6: Black Space diagram for triaxial dynamic modulus master curves for JMF verification sampled mixes.

4.3.2 Rutting Resistance: Repeated Load Triaxial Test (Unconfined and Confined)

Repeated load triaxial (RLT) test results for the JMF verification samples for Mixes A, C, and D are shown for unconfined conditions in Figure 4.7 and confined conditions in Figure 4.8. Figure 4.9 and Figure 4.10 compare the unconfined and confined results.

Figure 4.7 shows that Mix A with no RAP and no RAS has the lowest number of unconfined load repetitions to reaching a “flow” condition, indicating rapid axial permanent deformation, and followed by Mix D and then Mix C. The permanent axial deformation at the flow condition is similar for all three mixes. Figure 4.8 shows that all three had similar average repetitions to the flow condition when in the confined condition. The permanent axial deformations at the flow condition were lowest for Mix C and similar for Mixes A and D.

The flow condition was originally postulated to relate to a critical level of densification under traffic at which permanent deformation accelerates (19) but has also been postulated and observed to often be related to internal cracking (20), which is not a phenomenon expected to be related to rutting in the field. On the other hand, the permanent axial deformation versus load repetitions in the RLT has been shown to generally correlate with repeated shear at constant height test results, which in turn are well correlated with field rutting performance (21).

The RLT repetitions to 3% permanent axial strain for the unconfined and confined conditions shown in Figure 4.9 indicate that for rutting resistance Mix A had the worst expected performance, Mix C had the best expected performance, and Mix D fell in between for both confined and unconfined RLT tests. These results are generally consistent with the stiffness results at slower frequencies (also related to higher temperatures) from the triaxial and flexural frequency sweep results. The repetitions to 5% permanent axial strain, shown in Figure 4.10, indicates similar results to the 3% permanent axial strain comparison for the unconfined state, and all the tests were stopped at 20,000 repetitions before reaching 5% strain.

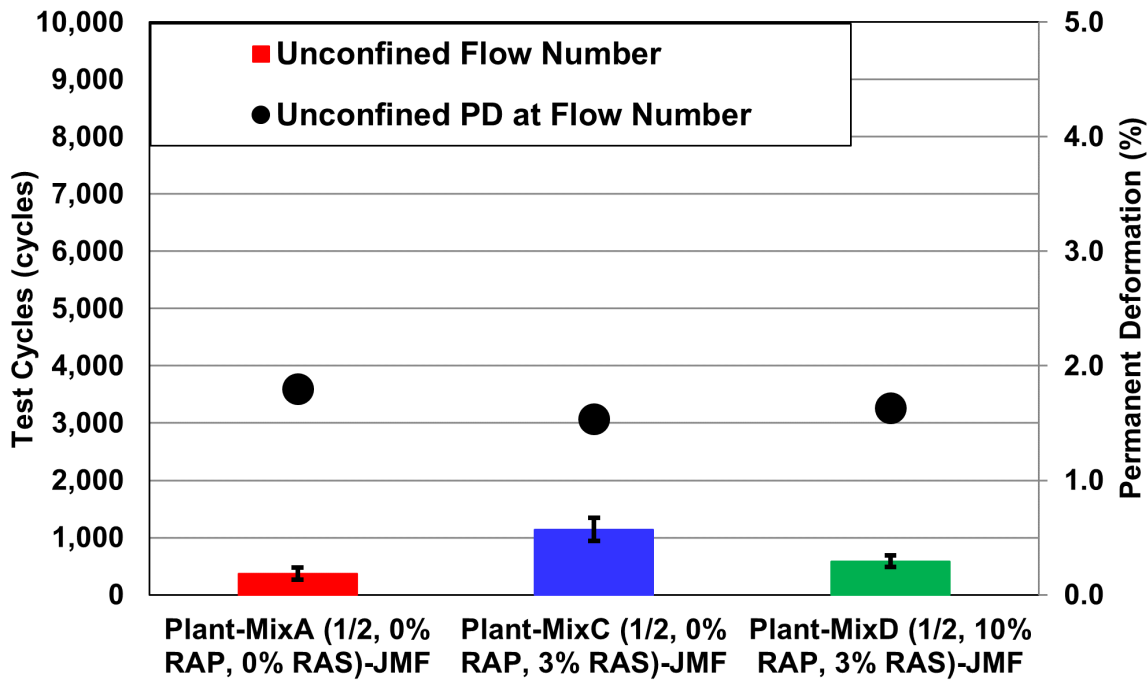


Figure 4.7: Unconfined repeated load triaxial results for JMF verification mixes (flow number and permanent deformation at flow number).

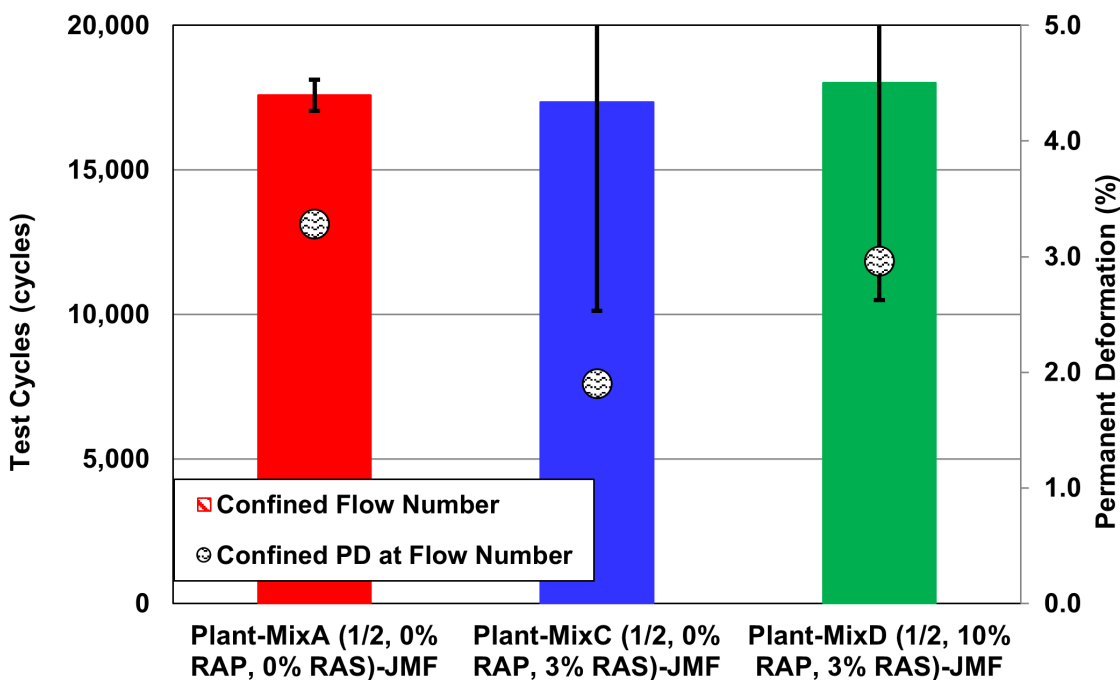


Figure 4.8: Confined repeated load triaxial results for JMF verification mixes (flow number and permanent deformation at flow number).

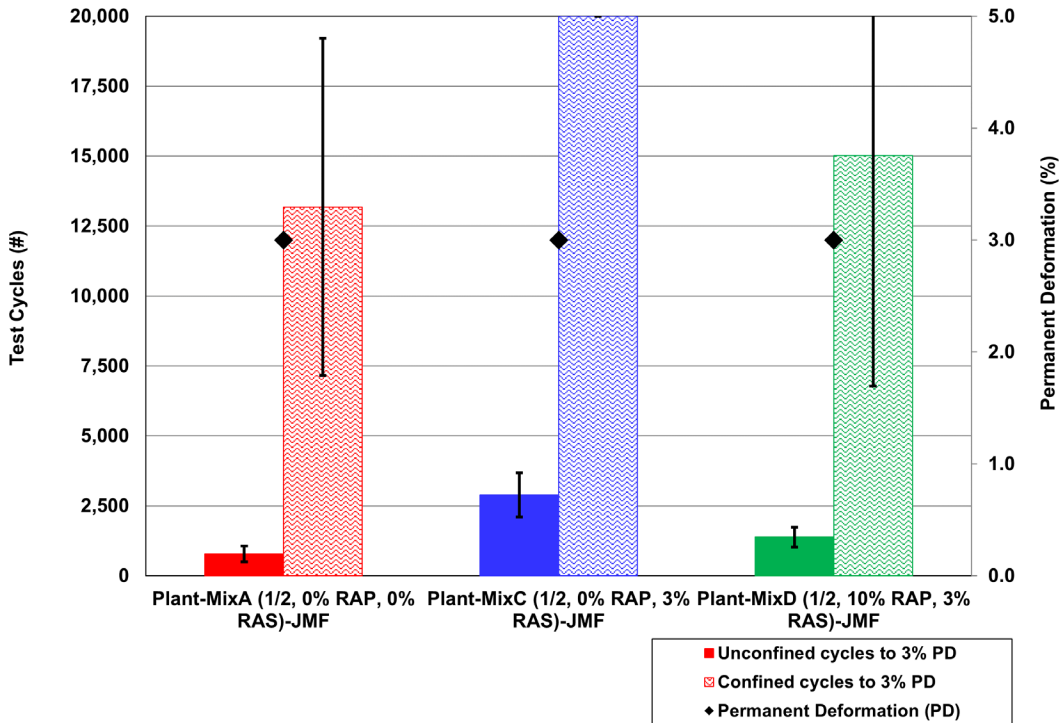


Figure 4.9: Unconfined and confined repeated load triaxial results for JMF verification mixes (load cycles to 3% permanent strain).

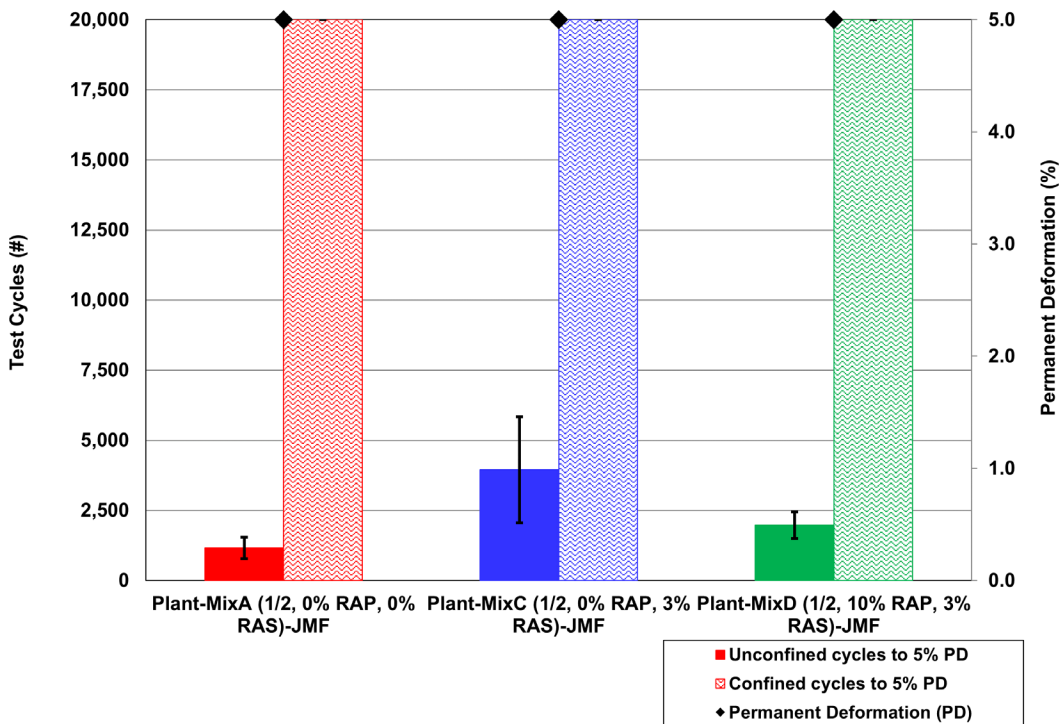


Figure 4.10: Unconfined and confined repeated load triaxial results for JMF verification mixes (load cycles to 5% permanent strain).

4.3.3 Fatigue/Reflective Cracking Resistance: Four-Point Beam Test

Four-point flexural beam fatigue test results from JMF verification samples for Mixes A, C, and D are shown as a Wohler curve of log fatigue life versus log tensile strain versus in Figure 4.11; by strain level from the regression of the Wohler curve results in Figure 4.12; and normalized to the results of the control Mix A in Figure 4.13. It should be noted that all the laboratory tests were run in controlled deformation mode, and the laboratory fatigue life is applicable to thin asphalt layers for pavement fatigue life and pavement reflective cracking life for thin overlays of cracked pavements. For thicker asphalt layers used in new or reconstructed pavement or overlays, the pavement fatigue life will depend on the interaction of asphalt mix stiffness, which influences the tensile strains causing fatigue or reflective cracking, and the fatigue life at a given tensile strain.

The results in shown in Figure 4.11 indicate that at most tensile strains Mix D (10% RAP and 3% RAS) has better fatigue life compared with Mix A (0% RAP, 0% RAS) and Mix C (0% RAP, 3% RAS), with Mixes D and C having approximately the same fatigue life near the lowest strain level tested, 300 microstrain. Mix C appears to have better fatigue performance at high test strain levels than Mix A, while Mix A has better fatigue lives at lower test strain levels than Mix D. Figure 4.12 shows the same results as in Figure 4.11 with the regression equation trends extrapolated to larger and smaller tensile strains than the range of test strains. The fatigue equations are as follows:

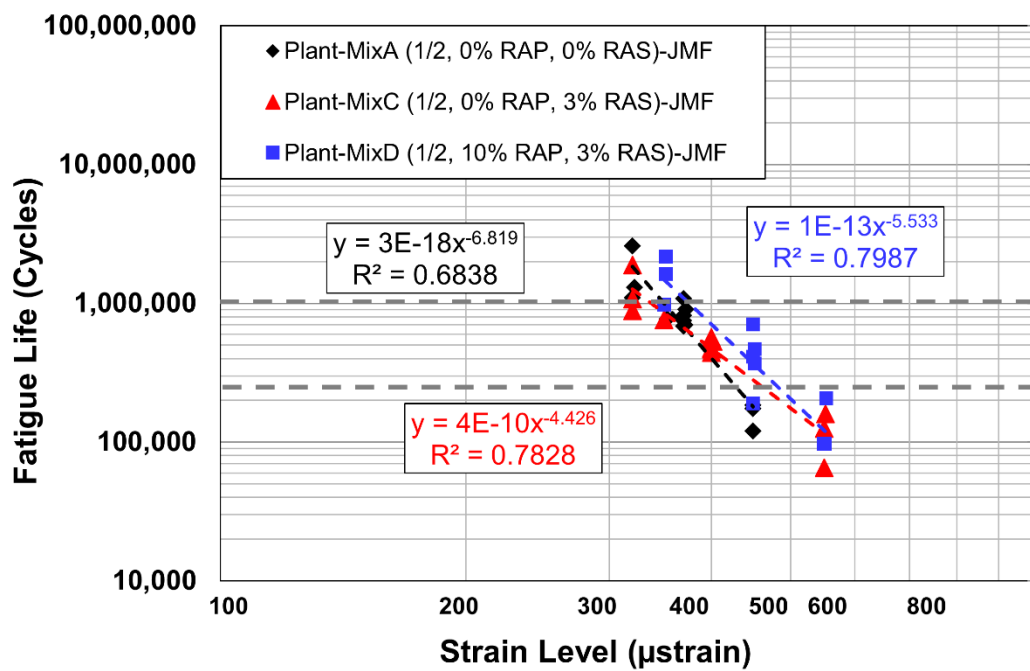
- Mix A: $N_f = 2.2287E+23 * \varepsilon_t^{-6.819}$
- Mix C: $N_f = 1.54939E+17 * \varepsilon_t^{-4.426}$
- Mix D: $N_f = 1.75992E+20 * \varepsilon_t^{-5.534}$

Where N_f is the fatigue life in the flexural fatigue test and ε_t is the tensile strain

In general, the linear relationship between the log of the fatigue life and the log of the tensile strain shown on the Wohler curve holds down to tensile strains in the 100 to 200 microstrain range, provided the materials are not polymer or rubber modified. In the case of polymer and rubber-modified materials, very long fatigue lives occur at strains in that range. The extrapolated results in Figure 4.12 indicate that at tensile strains in the 200 to 300 microstrain range Mixes A and D, with RAP and RAS, tend to have longer fatigue lives than Mix C with RAS

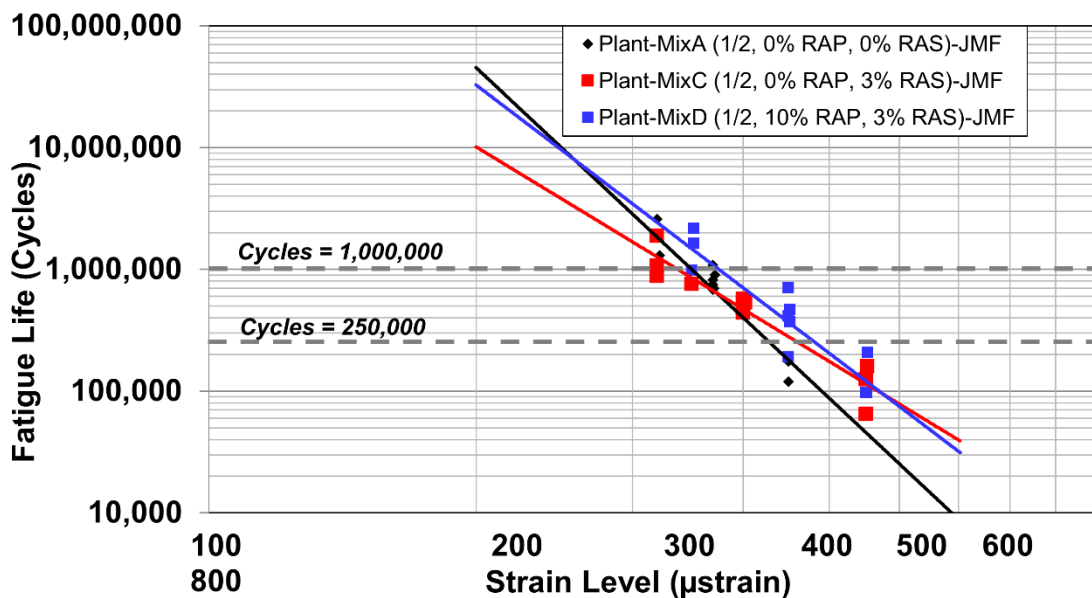
only. The results indicate a greater strain sensitivity for Mixes A and C, which results in longer fatigue lives at lower strains, and shorter fatigue lives at high strains compared with Mix D, which appears to be less strain sensitive.

Figure 4.13 shows the results of the regression lines for the fatigue lives versus the range of test tensile strains. Figure 4.14 shows the fatigue lives of Mixes C and D normalized by the fatigue life of Mix A for the range of strains tested. The better performance of Mixes C and D with recycled RAS and/or RAP at higher strains and decreasing performance at lower strains of those mixes relative to that of Mix A can be seen. It should be noted that in thicker pavements and overlays, strains would be less than 300 microstrain for most traffic load and asphalt temperature conditions.



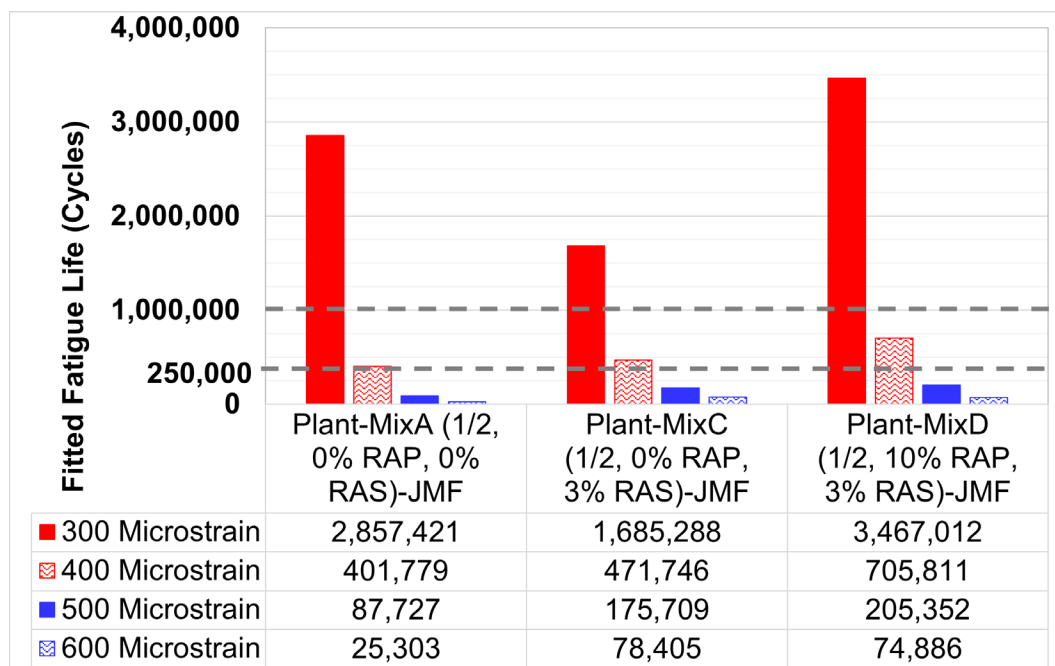
Note: MixB not tested.

Figure 4.11: Flexural fatigue results for JMF sampled mixes (Wohler curve).



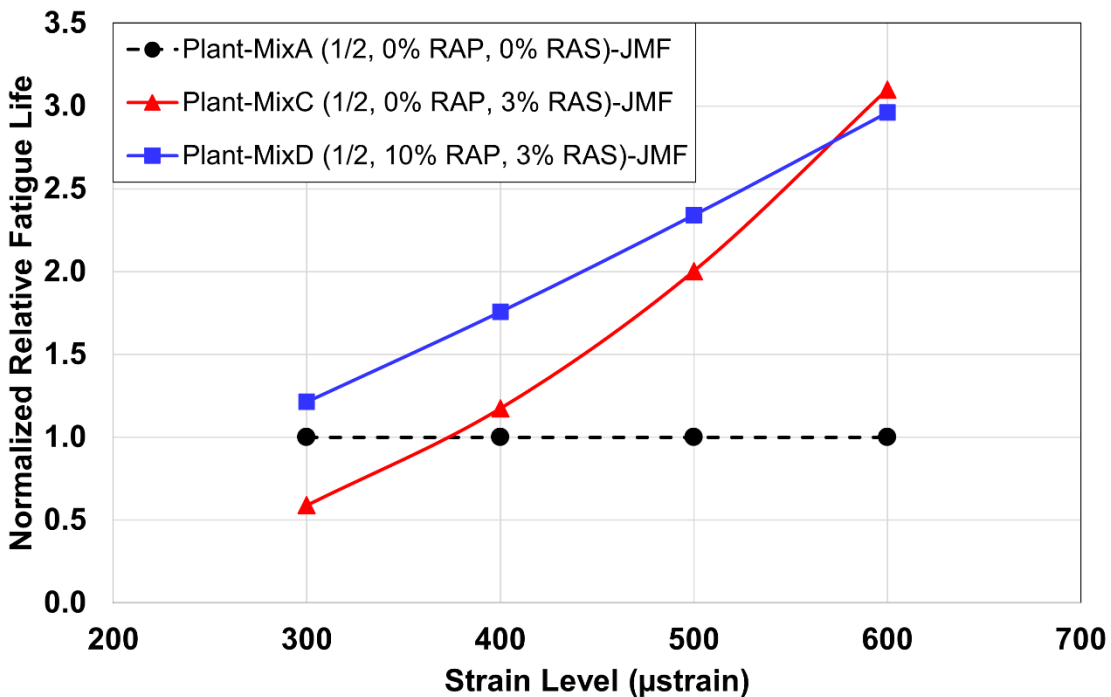
Note: MixB not tested.

Figure 4.12: Extrapolation of flexural fatigue results for JMF sampled mixes (Wohler curve).



Note: MixB not tested.

Figure 4.13: Flexural fatigue results for JMF verification sampled mixes: repetitions to failure at different strain levels from Wohler curve regressions.



Note: MixB not tested.

Figure 4.14: Flexural fatigue results for JMF sampled mixes: repetitions to failure at different strain levels from Wohler curve regressions normalized to Mix A (0% RAP, 0% RAS).

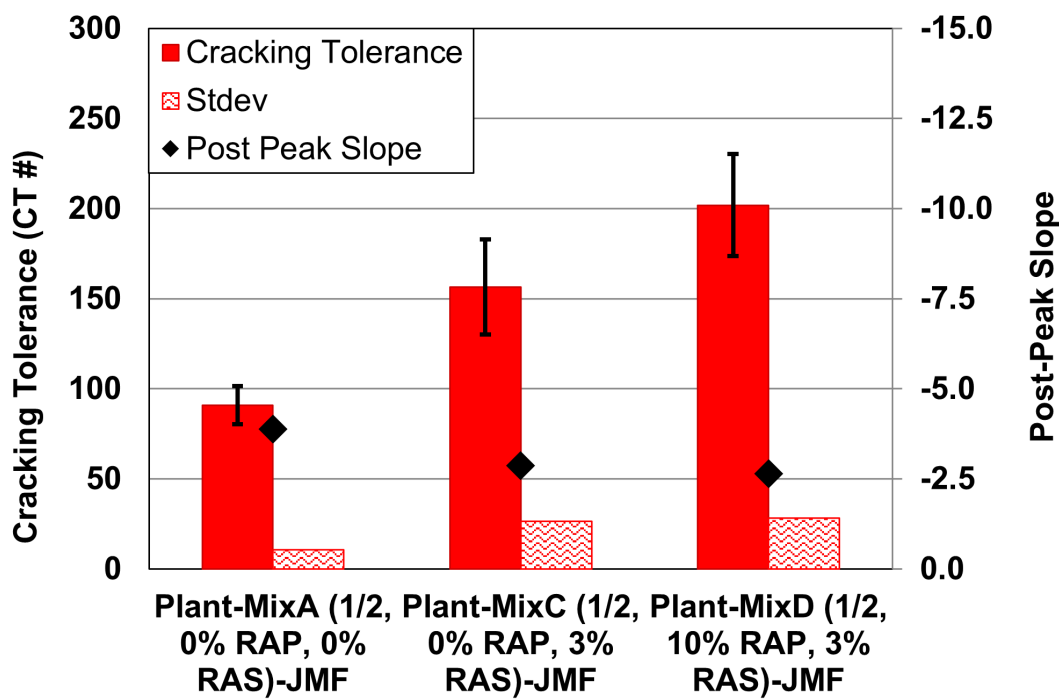
4.3.4 Indirect Tensile Cracking Resistance: IDEAL-CT Test

Figure 4.15 shows the IDEAL-CT results in terms of IDEAL-CT number and post-peak slope. It has been proposed that a larger IDEAL-CT number indicates better cracking resistance under monotonic indirect tensile loading. Research by the UCPRC (22) indicates that the IDEAL-CT number has a strong correlation with flexural stiffness and a weak correlation with fatigue cracking resistance at a given strain. The results show that the JMF verification sample for Mix D had the largest IDEAL-CT number, followed by Mix C, and then control Mix A. A smaller post-peak slope should indicate greater fracture toughness and less brittleness, which showed an inverse ranking for the post-peak slope compared to the IDEAL-CT number for the three mixes.

The IDEAL-CT results for the job mix verification samples show that Mixes C and D met the specification of an IDEAL-CT number greater than that of Mix A.

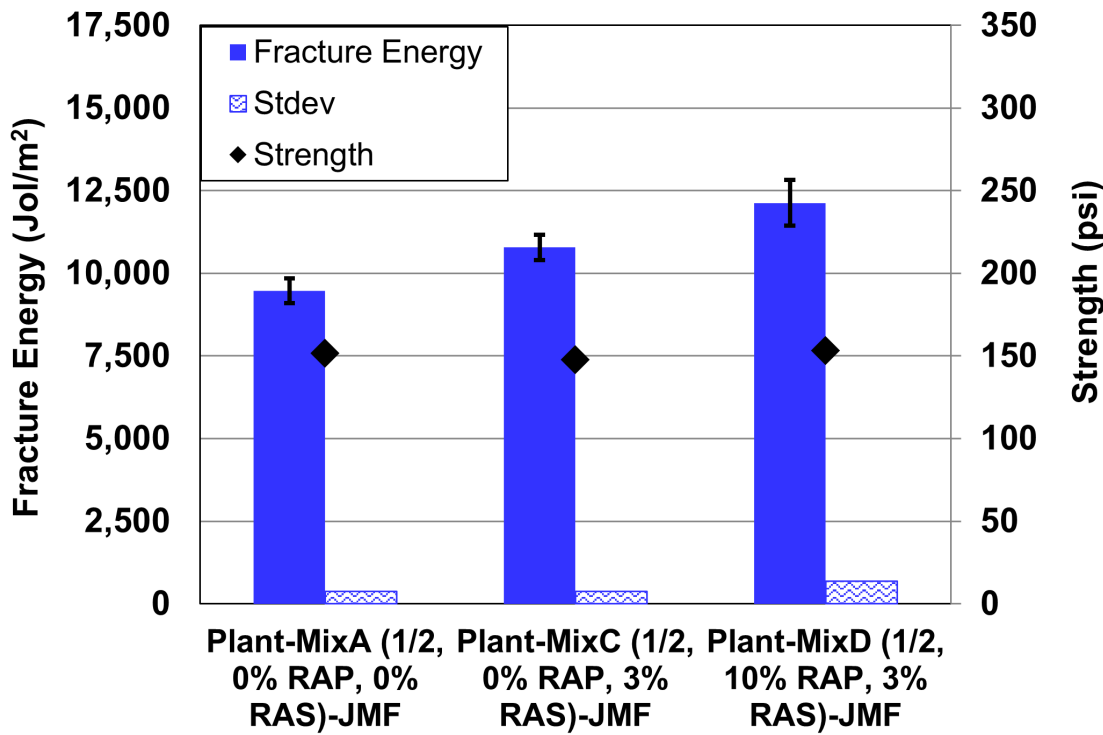
Figure 4.16 shows the Strength value (maximum stress) and fracture energy for the IDEAL-CT test and the three JMF verification sample mixes. Previous UCPRC research has shown that

Strength has a relatively strong correlation with flexural stiffness and largely controls the IDEAL-CT number as well (17). The results showed that the Strength values were very similar for the three mixes. These results correspond to flexural and triaxial dynamic modulus results that show similar stiffnesses at intermediate temperatures and loading frequencies. The fracture energy results rank the mixes the same as the IDEAL-CT number results, as expected since the two parameters have similar definitions.



Note: MixB not tested.

Figure 4.15: IDEAL-CT test results for JMF verification sampled mixes (CT number and post-peak slope).



Note: MixB not tested.

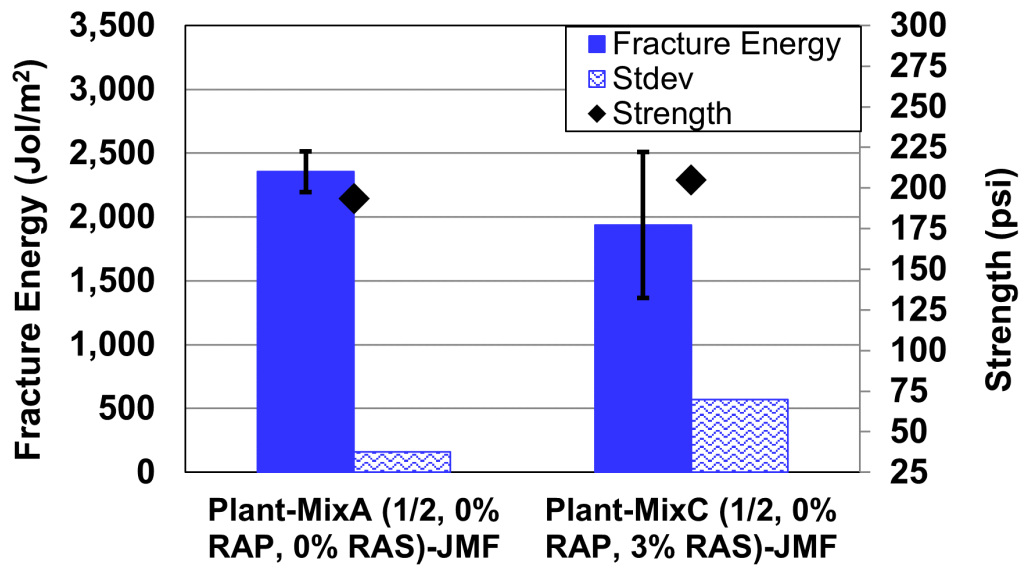
Figure 4.16: IDEAL-CT test results for JMF verification sampled mixes (fracture energy and strength).

4.3.5 Fracture Cracking Resistance: Semicircular Beam Test

Semicircular beam test results from the I-FIT approach for testing and analysis are shown in Figure 4.17 and Figure 4.18 for the JMF verification samples for Mixes A and C. Figure 4.17 shows that the fracture energy of Mix A was somewhat larger than that of Mix C and that the strengths were similar. The fracture energies rank differently compared with the IDEAL-CT values but show similar ranking for strengths with both mixes having the same strengths.

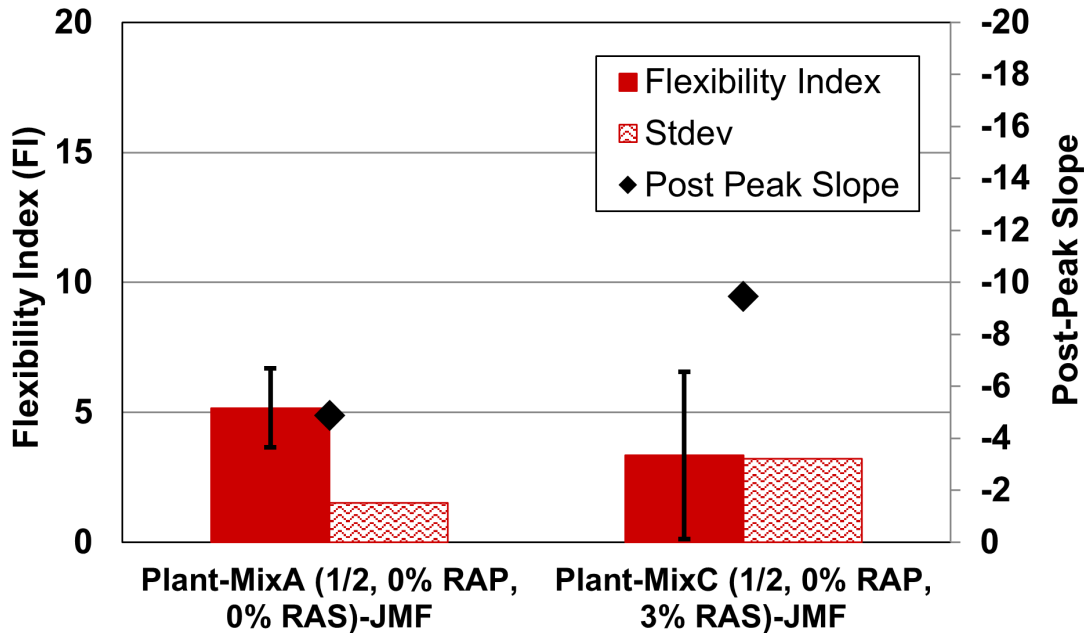
Figure 4.18 shows the flexibility index and post-peak slope values from the I-FIT SCB tests. The ranking of the post-peak slopes for Mixes A and D is the opposite of that from the IDEAL-CT test, with Mix C having a greater post-peak slope than Mix A. The flexibility index number is greater for Mix A than Mix C, which is also a ranking that is the opposite of the IDEAL-CT test. The ranking of the results for Mixes A and C are different from those of the IDEAL-CT rankings, which showed Mix C having greater cracking resistance, while the I-FIT number is larger for Mix A. The lack of correlation between the results from the two tests of the mix samples differs

from other comparisons of IDEAL-CT and I-FIT results for a broader range of materials that showed good correlation between the two parameters.



Note: MixB and MixD not tested.

Figure 4.17: I-FIT test results for JMF verification sample mixes (fracture energy and strength).



Note: MixB and MixD not tested.

Figure 4.18: I-FIT test results for JMF verification sample mixes (flexibility index and post-peak slope).

4.4 Testing of Mixes Sampled During Construction for Quality Assurance

4.4.1 Mix Stiffness: Triaxial and Flexural Dynamic Modulus

Flexural Dynamic Modulus Frequency Sweep Results

The flexural dynamic modulus curves from the QA sample testing for Mixes A, B, C, and D are shown in Figure 4.19, with both QA samples shown and labeled v1 and v2. The QA sample mix stiffness results generally replicate those from binder testing and the JMF verification sample testing for Mixes A, C, and D. As expected from the binder and JMF verification mix testing, all the mixes have similar stiffnesses at reduced frequencies of approximately 1 Hz and faster and increasing differentiation at reduced frequencies less than 1 Hz. Below 1 Hz, Mix A is the softest, followed by Mix B in increasing stiffness, and Mixes C and D being the stiffest, although one of the QA samples from Mix C is softer than Mix B at the slowest frequencies. The relative stiffnesses are shown in Figure 4.20, normalized to the first QA sample for Mix A, which was the softest mix at frequencies slower than 1 Hz. The results in both figures show that the results are very similar for the two QA samples for Mixes B, C, and D and the most variability is between the two samples for Mix A, which had no RAP or RAS.

The normalized results show that the stiffnesses of the mixes with RAS (Mixes C and D) are greater than those of the control mix with no RAS or RAP (Mix A) particularly at slow frequencies (also related to high temperatures) where rutting is an issue. These greater stiffnesses at slow frequencies also typically result in shorter fatigue and reflective cracking lives in thin overlays, and are beneficial for the same distresses in thicker overlays. The stiffness of Mix B with 10% RAP, which is the mix used on the rest of the project and was not tested during JMF mix verification, is about 15% softer than the other mixes at frequencies between 1 and 100 Hz, the normal range of vehicle traffic loading times at constant speeds from boulevards to highways. These results indicate that this mix may have better fatigue and reflective cracking performance for this thin overlay project.

Figure 4.21 shows the Black Space diagram for the QA samples for Mixes A, B, C, and D. Mix A has a higher phase angle at slower frequencies (when lower stiffnesses are occurring), indicating greater propensity for viscous flow and less elastic recovery at those frequencies, which are contributors to increased rutting but potentially beneficial for fatigue and reflective

cracking lives at higher temperatures and slower speeds for a thin overlay. Mixes C and D containing RAS have the lowest phase angles at the same slow frequencies and high temperatures, with Mix B falling between A and C/D.

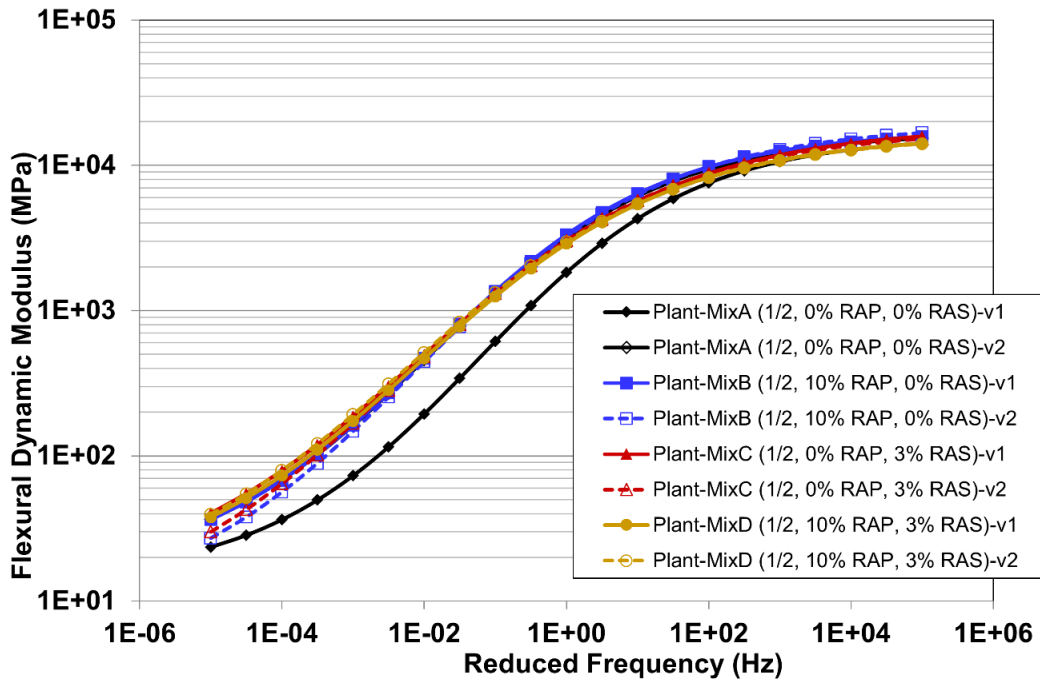


Figure 4.19: Flexural dynamic modulus master curves for QA sampled mixes.

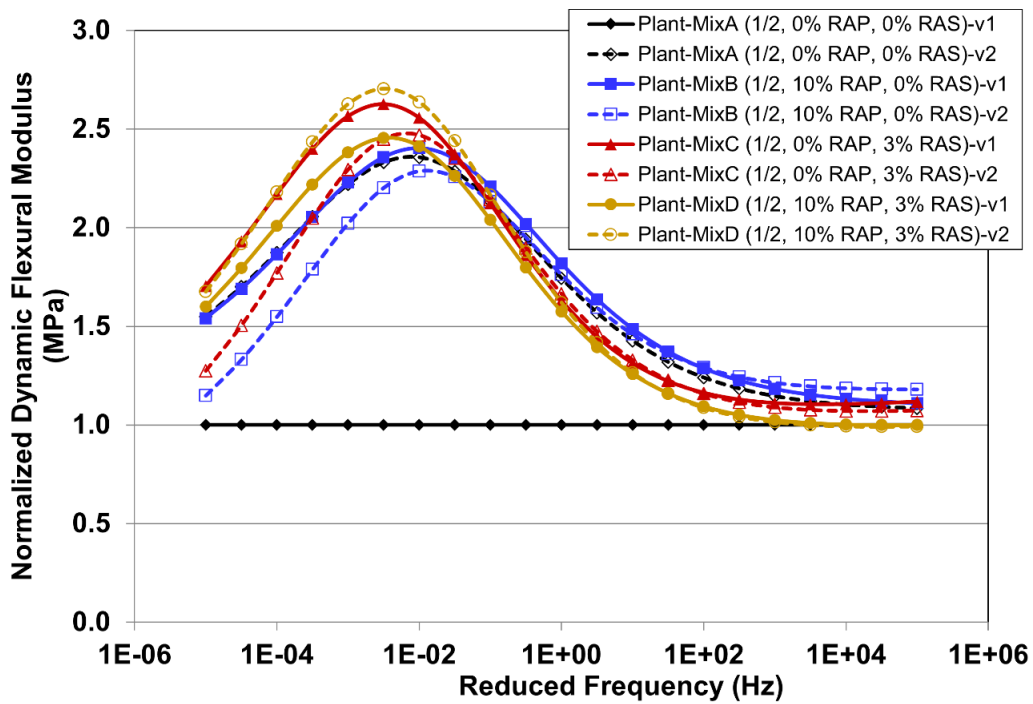


Figure 4.20: Flexural dynamic modulus master curves for QA sampled mixes normalized to Mix A (0% RAP, 0% RAS) first sample (v1).

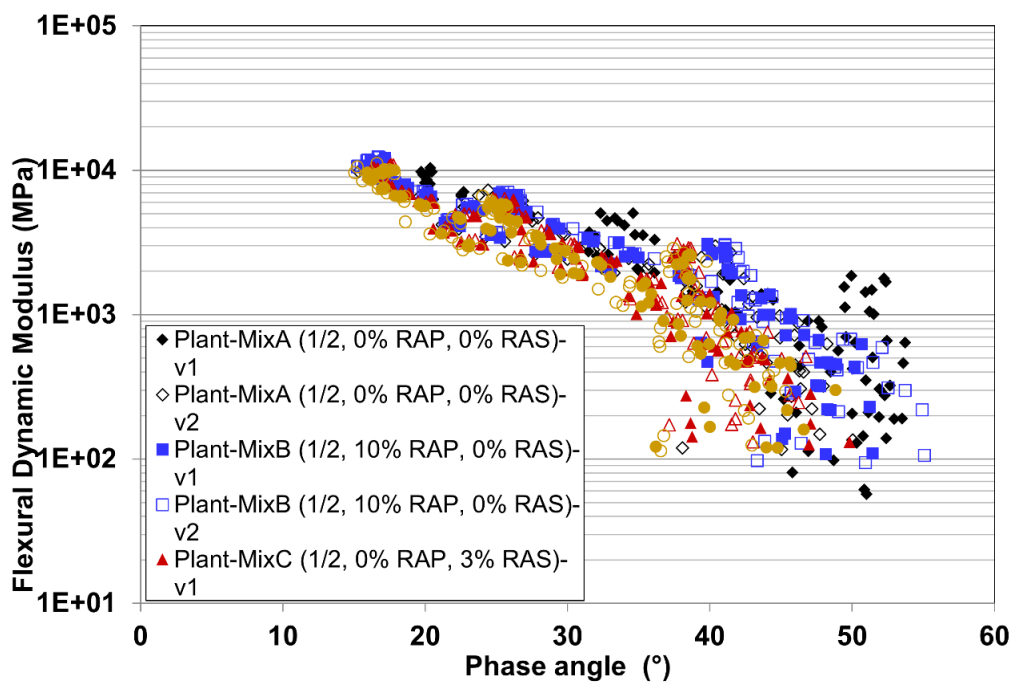


Figure 4.21: Black Space diagram for flexural dynamic modulus master curves for QA sampled mixes.

Triaxial Dynamic Modulus Frequency Sweep Results

Figure 4.22 shows the master mix stiffness curves for the QA samples for Mixes A, C, and D, and Figure 4.23, shows the master stiffness curves for Mixes C and D normalized to that of Mix A. The Black Space diagram for the three mix binders is shown in Figure 4.24. The results are generally consistent with those from the flexural frequency sweeps, as expected, except for the stiffnesses at very slow frequencies for all mixes that do not decrease relative to Mix A, as occurred with the flexural stiffness tests.

As expected, the stiffnesses from the triaxial frequency sweeps shown in these figures are not always the same as those from the flexural sweeps shown previously, and the triaxial stiffnesses are somewhat greater at some frequencies. This result is attributed to the same reasons discussed previously with regard to the JMF verification frequency sweep results.

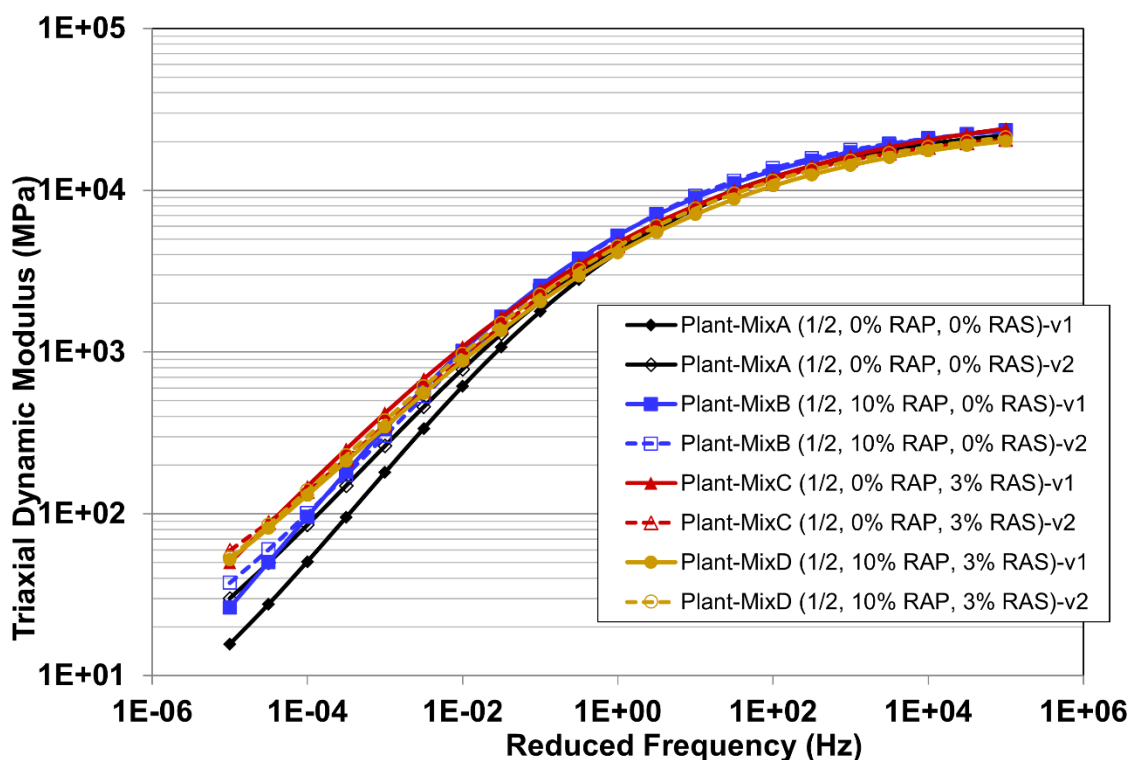


Figure 4.22: Triaxial dynamic modulus master curves for QA sampled mixes.

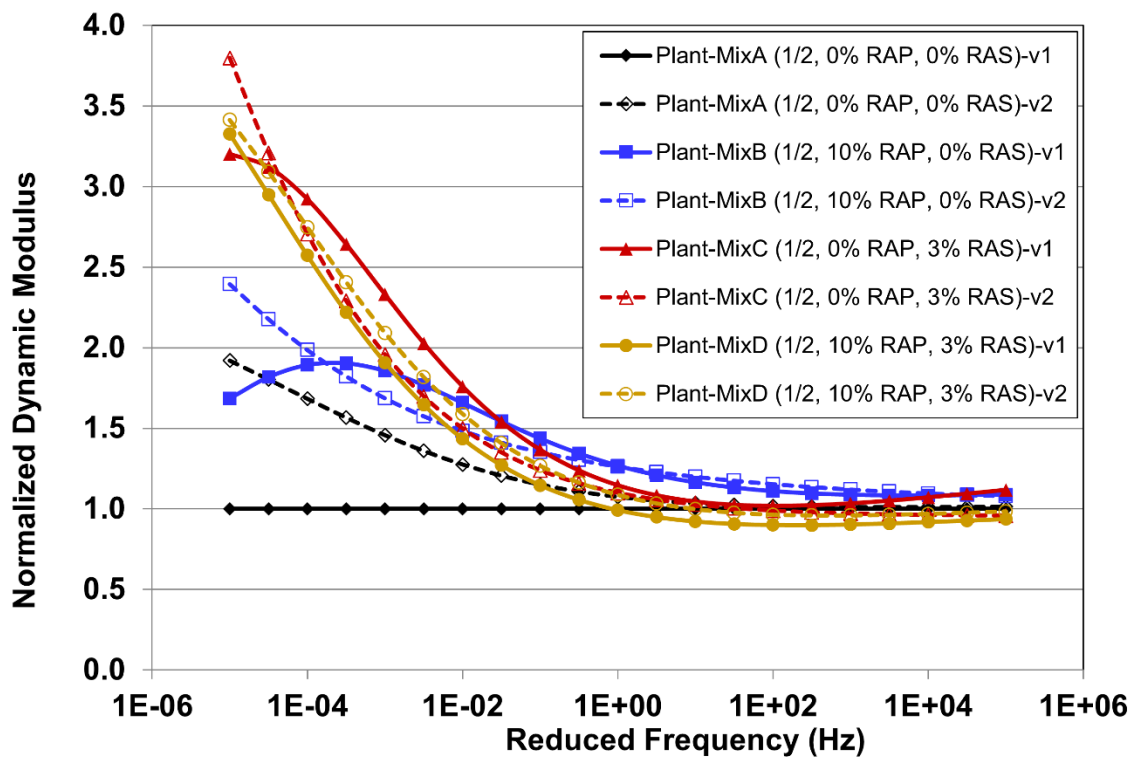


Figure 4.23: Triaxial dynamic modulus master curves for QA sampled mixes normalized to Mix A (0% RAP, 0% RAS) first sample (v1).

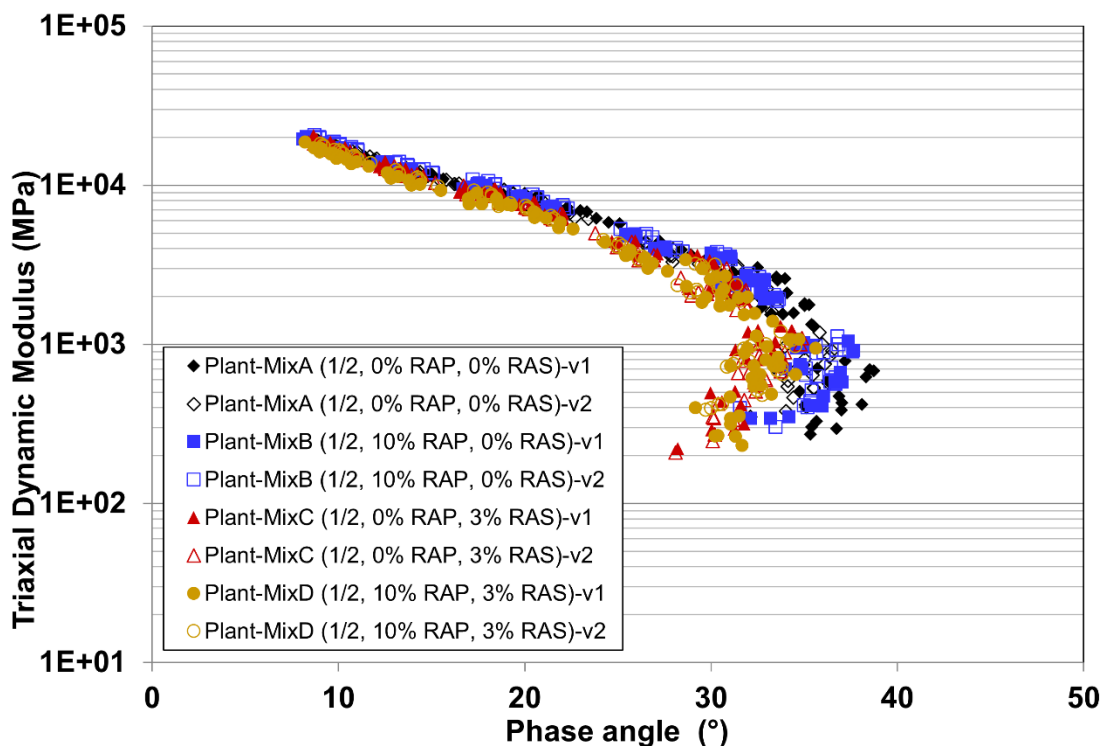


Figure 4.24: Black Space diagram for triaxial dynamic modulus master curves for QA sampled mixes.

4.4.2 Qualitative Assessment of Binder Blending from Comparison Binder and Mix Stiffness Rankings

As noted in the problem statements, the degree of blending of the virgin binder, the RAP and/or RAS binder, and the rejuvenating agent, which increases as a function of time at elevated temperatures, is an important question. If there is insufficient blending, the use of rejuvenating agents and softer virgin binders may result in a mix that is prone to rutting and has an insufficient binder content for fatigue and fracture resistance. Binder extraction and testing results in complete blending of the three binder components. Mix testing produces results that reflect the actual amount of blending that has occurred after mixing, sampling, reheating, and laboratory aging if it is included in the specimen preparation. Mix testing results are also subject to the variable influences of aggregates at different temperatures and frequencies of loading, with less aggregate influence at low temperatures and high frequencies.

A qualitative assessment of the degree of binder blending can be made through comparison of binder stiffness testing rankings with mix stiffness testing rankings. If the rankings are similar, it is an indication that there are no major differences in binder blending.

A qualitative assessment of blending can be made from the comparisons of ranking of binder and mix stiffness results at three frequencies at the reference temperature (20°C) as shown in Table 4.5. The rankings are based on the data in Table 3.1 and Figure 3.9, Figure 4.20, and Figure 4.23. The effects of aggregate on stiffness are generally least at low temperatures and high frequencies. However, because of different temperature susceptibilities of virgin and blended binders, assessment of blending only at those conditions may not give a complete picture. The differences in mix stiffness were greatest at high frequencies, and smaller at low frequencies.

Table 4.5: Ranking of Extracted Binder and Mix Stiffnesses from Quality Assurance Testing

QA Binder Testing (continuous grade temperature ranking [stiffest to softest])	Mix Testing Reduced (frequency [Hz] at 20°C)	QA Mix Testing Flexural Stiffness Ranking (stiffest to softest)	QA Mix Testing Triaxial Stiffness Ranking (stiffest to softest)
Low temperature: B,C,D (stiffest) A (softest)	10 ⁴ Mix stiffness differences small	B (stiffest) A v2 C A v1, D (softest)	B (stiffest) C,A D (softest)
Intermediate temperature: A (stiffest) C B D (softest)	10	B (stiffest) A v2 C D A v1 (softest)	B (stiffest) C,A D (softest)
High temperature: D (stiffest) C B A (softest)	10 ⁻² Mix stiffness differences large	C,D (stiffest) A v2 B A v1 (softest)	C (stiffest) B D A v2 A v1 (softest)

Notes: Mix A (0% RAP, 0% RAS), Mix B (10% RAP, 0% RAS), Mix C (0% RAP, 3% RAS), Mix D (10% RAP, 3% RAS); the two QA samples for Mix A tested for flexural dynamic modulus had different results.

The results at low temperatures, corresponding to high frequencies, showed the most differences between binders and mixes compared with the other temperatures and frequencies. The low temperature binder rankings are very similar except for Mix A with no RAP or RAS which is softest, while the two mix stiffness rankings at high frequency (similar effect to low temperature) indicate that one of the two Mix A samples and Mix D with RAP and RAS and a softer virgin binder and rejuvenating agent are the softest. The fact that the Mix D mix stiffness consistently ranks softer than the Mix D binder stiffness is a potential indicator of incomplete blending in the mix. However, the differences in the mix stiffnesses at this frequency are within 10% of each other, indicating that this mix is not much different from the virgin Mix A and that there is most likely good blending.

The binder results at intermediate and low temperatures (corresponding to intermediate and high frequencies for mix results) indicate similar rankings, which is an indicator of good blending.

4.4.3 Rutting Resistance: Repeated Load Triaxial Test (Unconfined and Confined)

Repeated load triaxial (RLT) test results for the two QA samples for Mixes A, B, C, and D are shown for unconfined conditions in Figure 4.25; averaged across the two QA samples for each mix and unconfined conditions in Figure 4.26; for confined conditions compared with unconfined conditions in Figure 4.27; and averaged for the two samples and confined conditions in Figure 4.28. Figure 4.29 shows the repetitions to 3% permanent deformation for the unconfined testing, and Figure 4.30 shows the repetitions to 5% permanent deformation for the unconfined testing.

The results from RLT testing of the QA sample mixes are similar to those from the JMF verification testing. Figure 4.25 and Figure 4.26 show that Mix A with no RAP and no RAS has the lowest number of unconfined load repetitions to reaching a “flow” condition, indicating rapid axial permanent deformation, followed by Mixes B and D with similar results, and then Mix C, which has the best performance. The permanent axial deformation at the flow condition is similar for all three mixes. Figure 4.27 shows that the repeatability between the two QA samples was good for all mixes except Mix A, where the first sample had a much lower number of repetitions to failure. The confined test results are similar for all sample and mixes except for the first QA sample from Mix A. Figure 4.28 shows average repetitions to the flow condition when in the confined condition, which show similar performance for Mixes B, C, and D, and poorer performance for Mix A, primarily because of the results from the first QA sample. The permanent axial deformations at the flow condition from smallest to largest rank as follows: (1) Mix B, (2) Mix D, (3) Mix C, and (4) Mix A.

The unconfined RLT repetitions to 3% permanent axial strain shown in Figure 4.29 indicate that rutting resistance ranked from Mix A having the worst expected performance, Mix C having the best expected performance, and Mixes B and D falling in between. These results are generally consistent with the stiffness results at slower frequencies (also related to higher temperatures). The results for unconfined RLT repetitions to 5% axial strain shown in Figure 4.30 indicate the same ranking of mixes as those of the repetitions to 3% permanent axial strain.

The repetitions to 3% and 5% permanent axial strain are not shown in the plots for the confined RLT results because the majority of the tests were stopped before reaching those strains. Mix A lasted 11,714 repetitions to 3% permanent strain and Mix C lasted 18,134 repetitions, while Mixes B and D lasted 20,000 repetitions before the test was stopped. Mix A lasted 14,805 repetitions to 5% permanent strain, while the test for Mix C was stopped at 20,000 repetitions before it reached that strain.

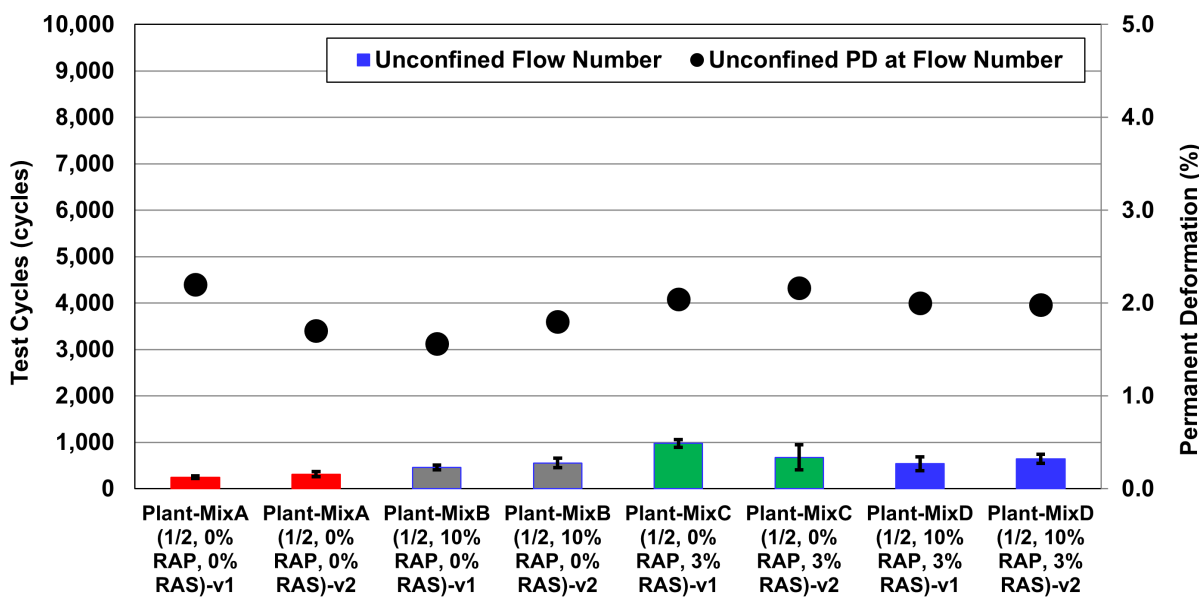


Figure 4.25: Unconfined repeated load triaxial results for QA sampled mixes (flow number and permanent deformation at flow number).

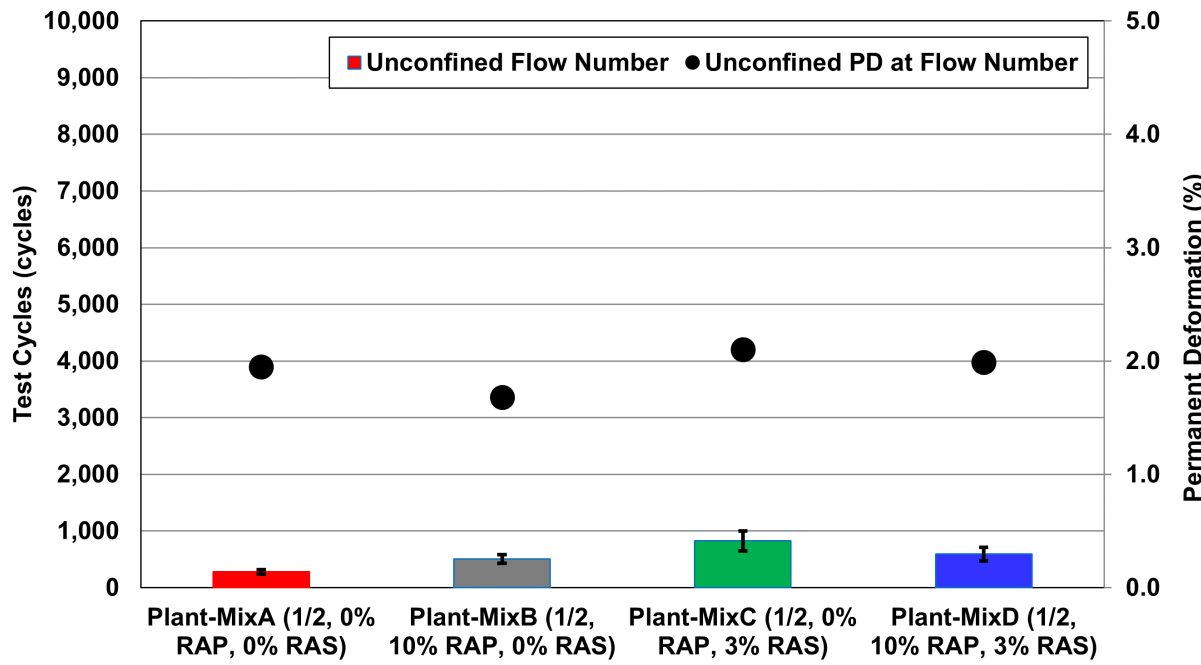


Figure 4.26: Unconfined repeated load triaxial results for QA sampled mixes (average flow number and permanent deformation at flow number).

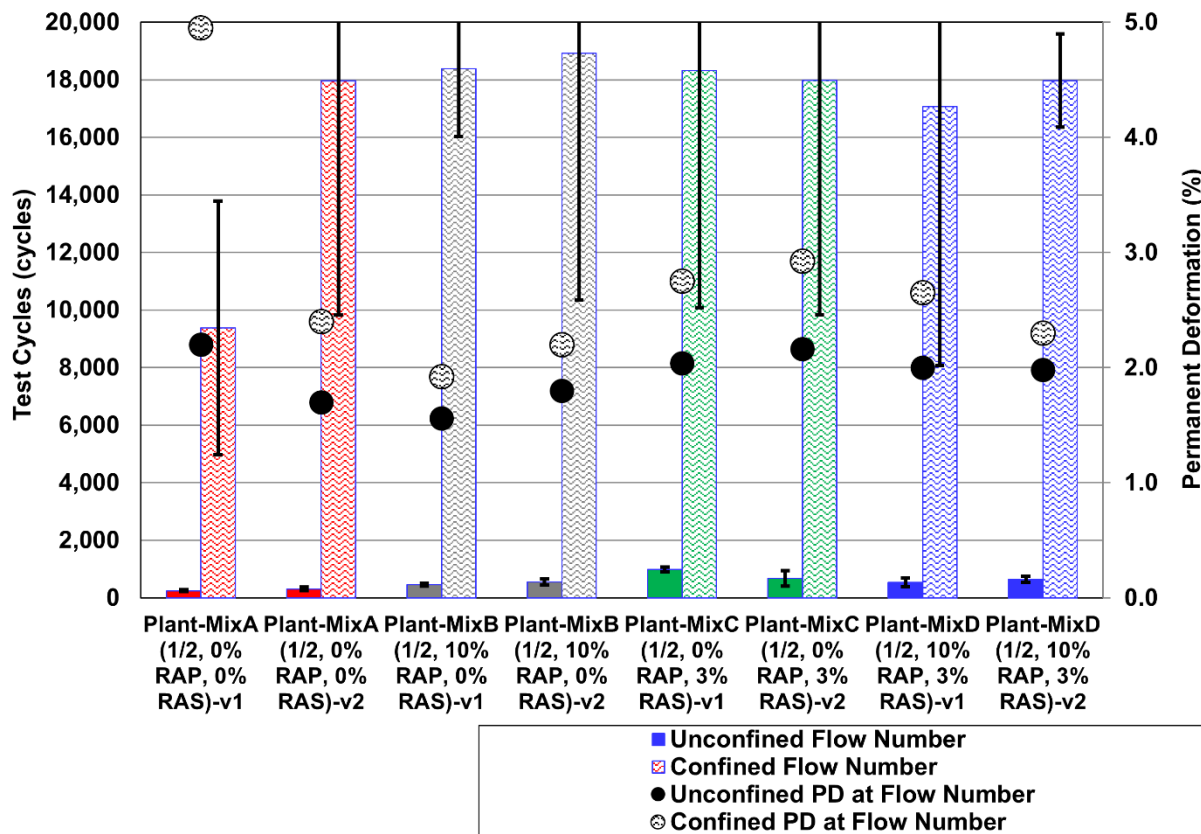


Figure 4.27: Confined repeated load triaxial results for QA sampled mixes (flow number and permanent deformation at flow number).

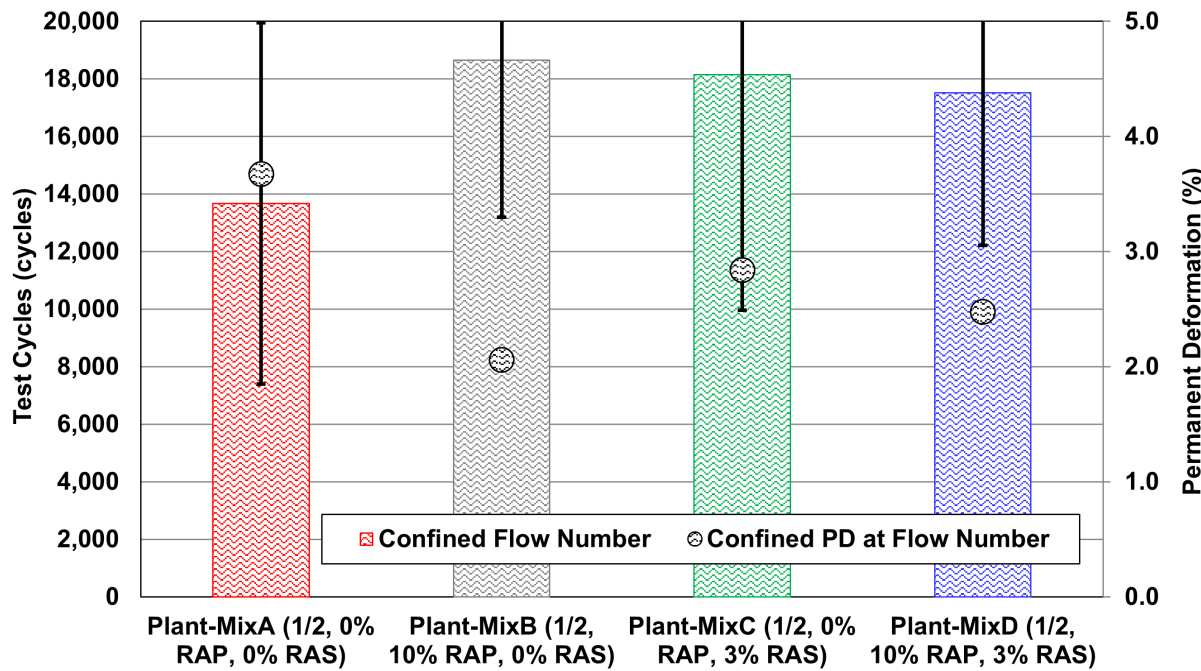


Figure 4.28: Confined repeated load triaxial results for QA sampled mixes (average flow number and permanent deformation at flow number).

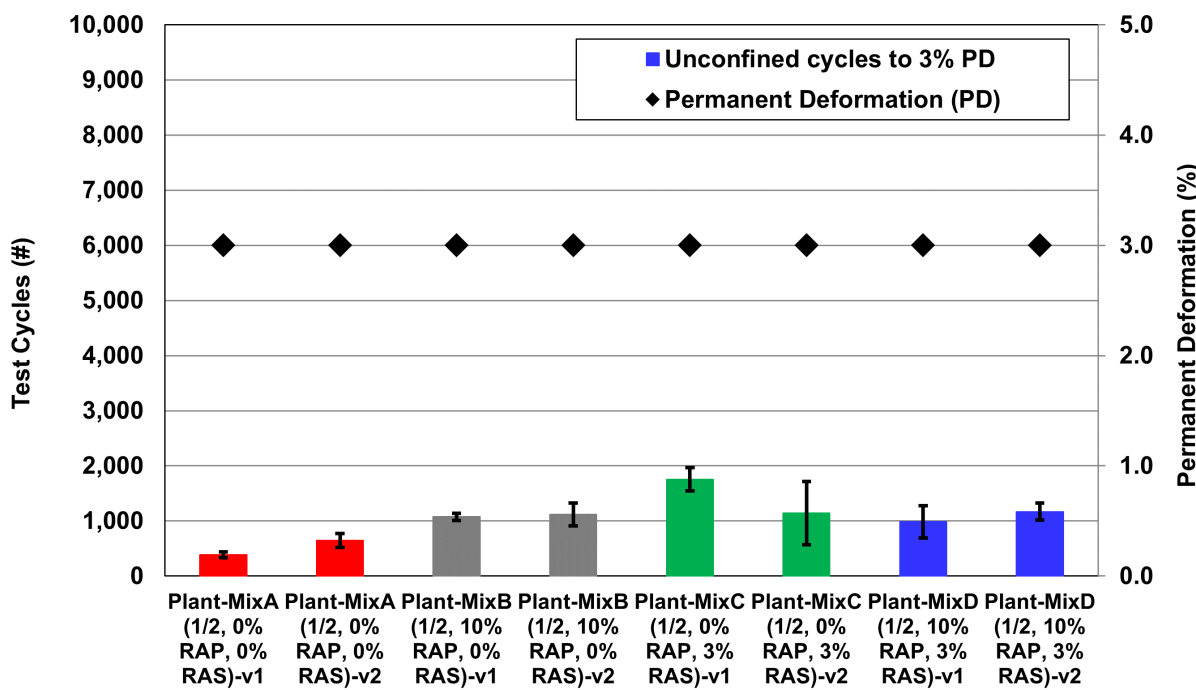


Figure 4.29: Unconfined repeated load triaxial results for JMF verification mixes: load cycles to 3% permanent strain.

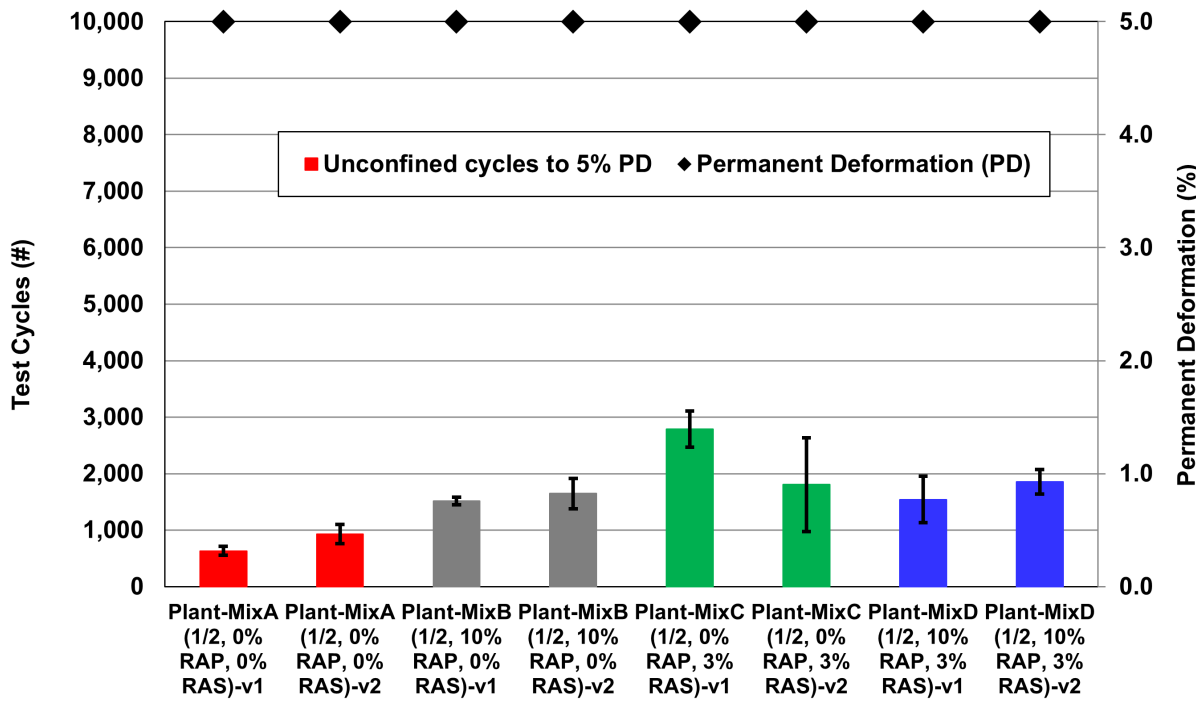


Figure 4.30: Unconfined repeated load triaxial results for QA sampled mixes: load cycles to 5% permanent strain.

4.4.4 Fatigue/Reflective Cracking Resistance: Four-Point Beam Test

Figure 4.31 shows flexural fatigue test results for the two QA samples for each of the four mixes. Also shown on the plots are the Wohler curve trend lines (log of tensile strain versus log of fatigue life). For the range of tensile strain levels used in testing (primarily 375 and 500 microstrain), Mix D with RAP and RAS had the best fatigue lives, followed by Mix C (RAS), Mix A (no RAP or RAS), and Mix B (RAP). These strain levels were selected to survive approximately 1 million and 250,000 cycles to failure. The ranking remained generally consistent across both QA samples for this tensile strain range.

The regressions from Wohler curves have generally been found over many decades of research and practice to provide reasonable estimates when extrapolated in the approximate range of 200 to 700 microstrain, except for polymer and rubber-modified mixes that tend to have much longer fatigue lives than extrapolation would indicate at strains smaller than 200 microstrain. Figure 4.32 shows the same fatigue test data points and the regression lines for the Wohler curve through the combined QA sample data sets for each mix, extrapolated to 200 and

700 microstrain. These results indicate that Mix A had the most sensitivity to tensile strain, with the longest fatigue life at smaller tensile strains and the shortest fatigue life at larger strains. Mix D had the flattest slope, and Mixes B and C were approximately parallel. At larger strains, typical of thin overlays on cracked pavement, Mix D has the best fatigue, followed by Mix C, and then Mixes A and B with similar fatigue performance. Tensile strains in the pavement decrease as the overlay thickness increases and mix stiffness increases in thicker overlays, and the extrapolation indicates that Mixes A and C have the best fatigue lives at small strains, followed by Mix D and then Mix B.

Figure 4.33 shows flexural fatigue testing Wohler curve results for the combined QA sample data sets for the four QA sampled mixes normalized to the results at Mix A for strain levels of 300 to 600 microstrain. The results show that at smaller strains Mixes A, C and D had similar fatigue lives, and Mix B had a lower fatigue life. The plot also shows the greater sensitivity of Mix D to strain, which resulted in the lower fatigue life at 200 microstrain previously shown in Figure 4.32.

Figure 4.34 shows fatigue lives at 300, 400 and 500 microstrain for the JMF and two QA samples for Mix A. The results indicate that the two QA samples approximately matched or exceeded the performance of the JMF verification sample. Similar plots of results are shown for Mixes B, C, and D in Figure 4.35, Figure 4.36 and Figure 4.37, respectively. Mix B did not have a JMF submittal, and the QA results indicated that the second sample had somewhat better fatigue performance. The fatigue performance of both QA samples for Mixes C and D also generally exceeded the fatigue performance of the JMF submittal, except for the 300 microstrain results for Mix D, where the JMF sample had a longer fatigue life.

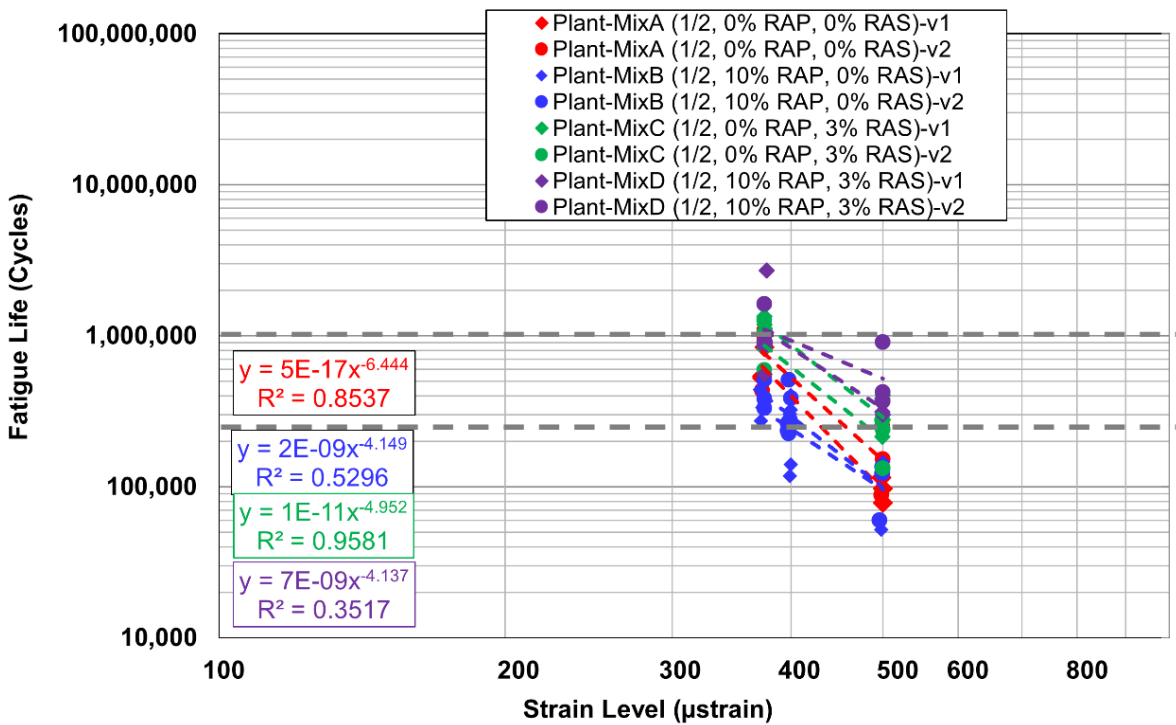


Figure 4.31: Flexural fatigue results for QA sampled mixes (Wohler curve).

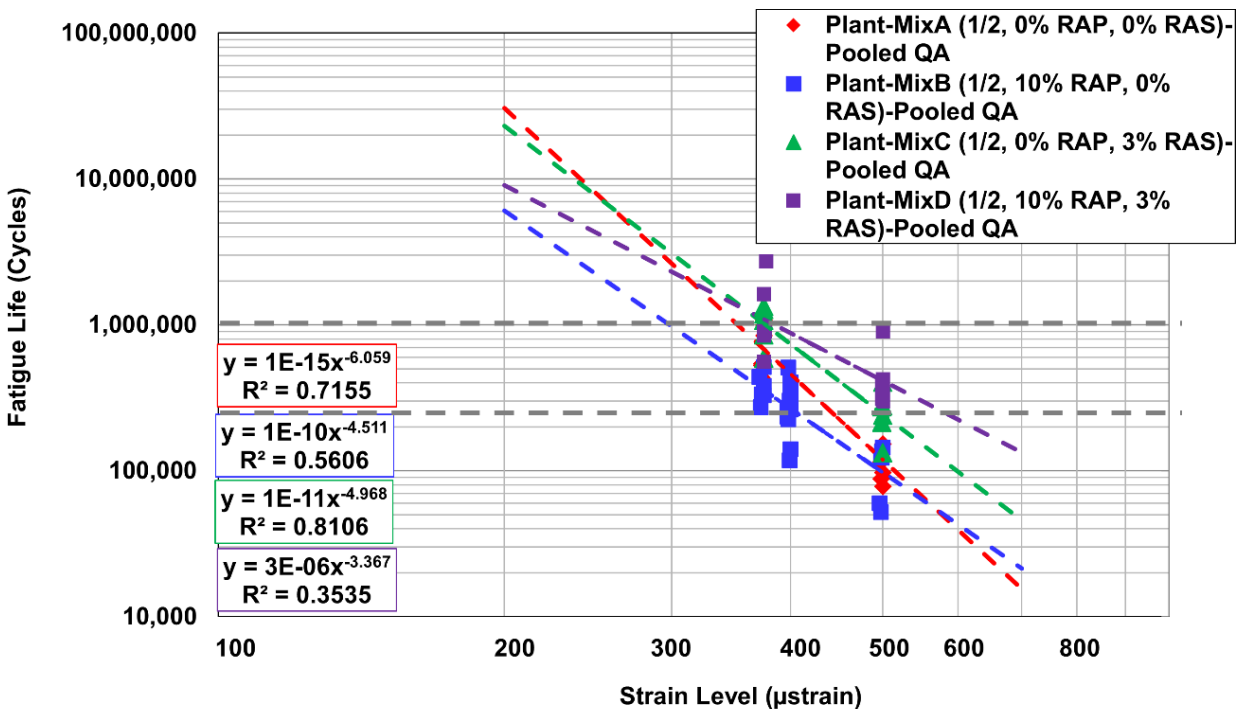


Figure 4.32: Extrapolation of flexural fatigue regression results for QA sampled mixes (Wohler curve).

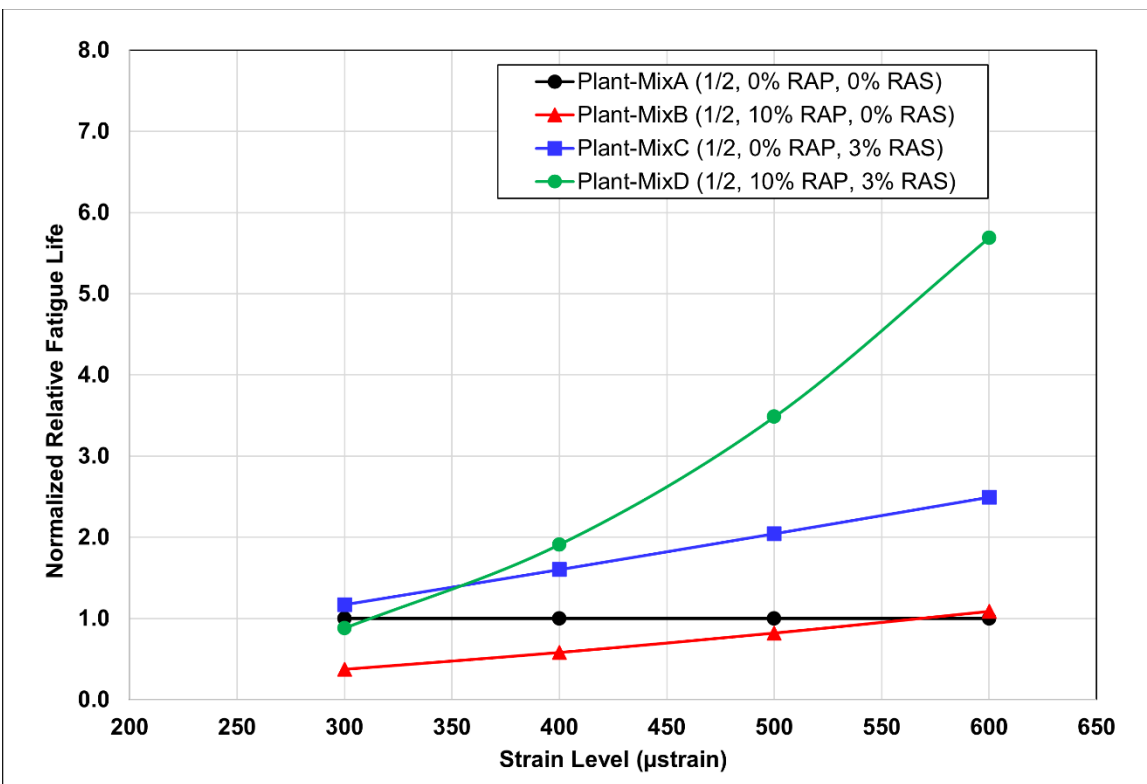


Figure 4.33: Flexural fatigue results for all QA sampled mixes from Wohler curve regression normalized to Mix A.

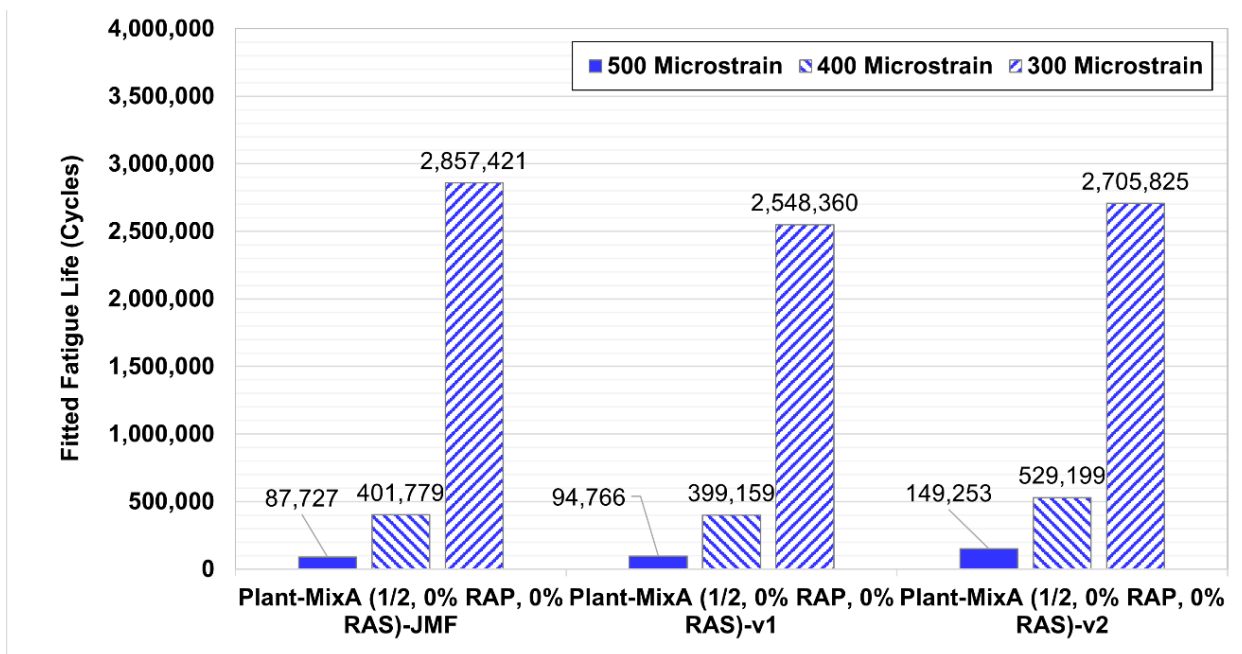


Figure 4.34: Flexural fatigue results for Mix A comparing JMF with first and second QA samples at 300, 400, and 500 microstrain.

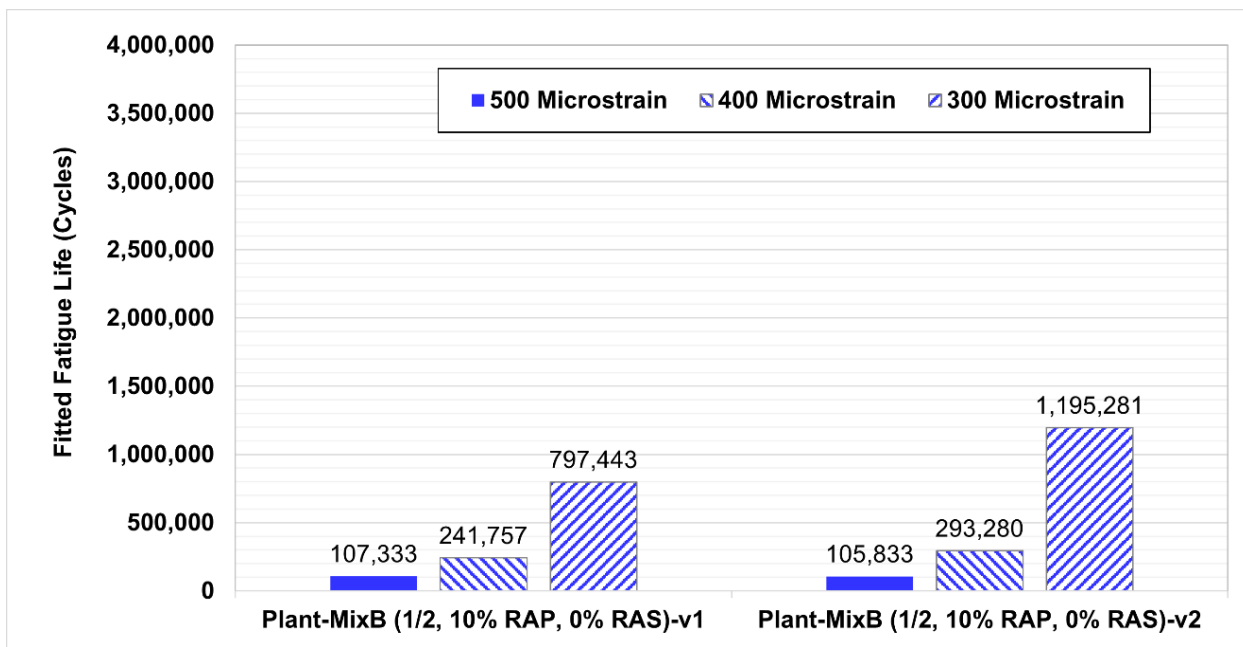


Figure 4.35: Flexural fatigue results for Mix B comparing first and second QA samples (no JMF submittal for Mix B) at 300, 400, and 500 microstrain.

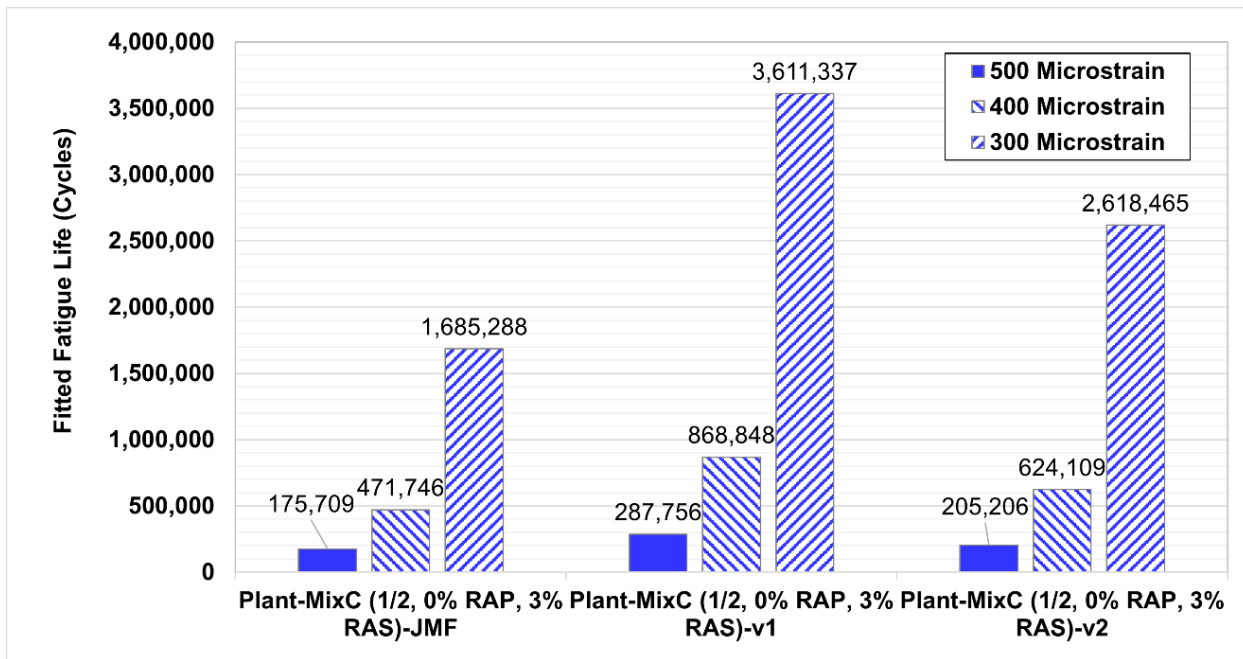


Figure 4.36: Flexural fatigue results for Mix C comparing JMF with first and second QA samples at 300, 400, and 500 microstrain.

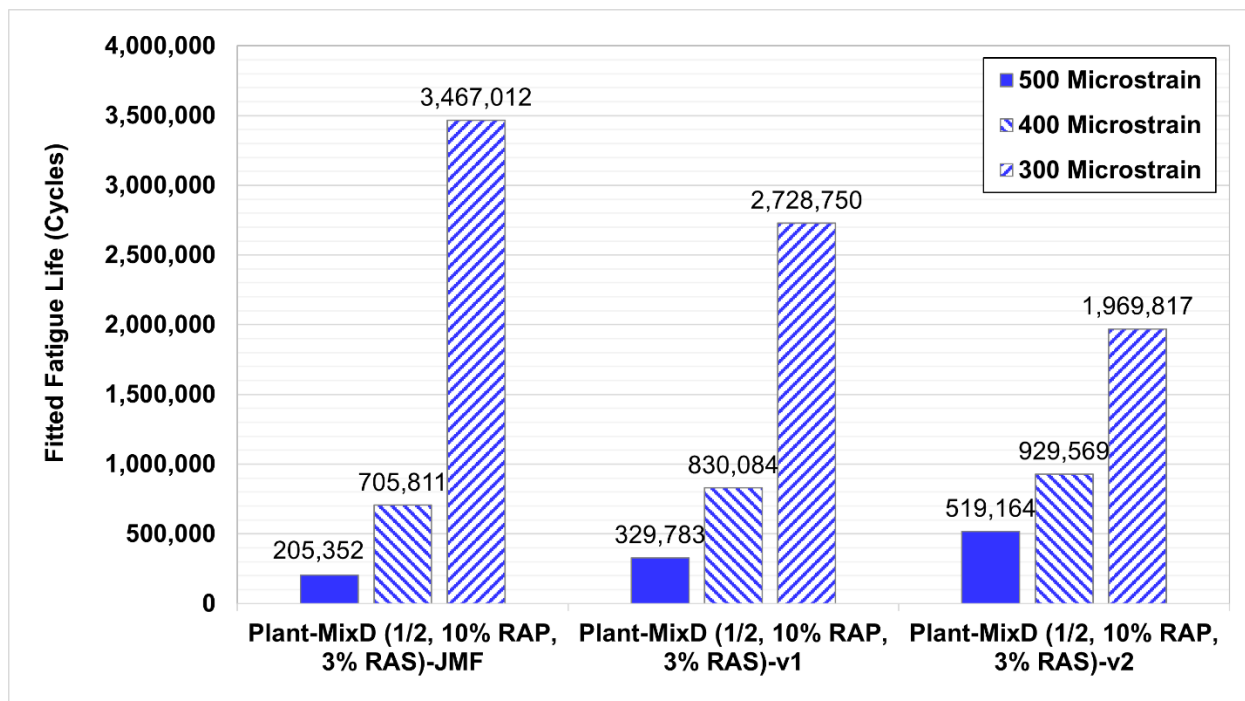


Figure 4.37: Flexural fatigue results for Mix D comparing JMF with first and second QA samples at 300, 400, and 500 microstrain.

4.4.5 Indirect Tensile Cracking Resistance: IDEAL-CT Test

Figure 4.38 shows the IDEAL-CT results in terms of IDEAL-CT number and post-peak slope for the two QA samples for each mix, and Figure 4.39 shows the same results with the results from the two QA samples averaged. The results in Figure 4.38 show large differences between the two QA samples for Mixes A and D, and more consistent results for Mixes B and C. The variability between QA samples for Mix A was seen in most of the results from other tests in this study, while the variability of results between samples for the IDEAL-CT test for Mix D is larger than those seen in the other tests. The average results shown in Figure 4.39 indicate that Mix D has the greatest cracking tolerance, indicated by the IDEAL-CT number, followed by Mixes A and D with similar values, and lastly by Mix B. The post-peak slopes are similar. The QA results show that on average the specification requiring that the IDEAL-CT value for Mixes C and D be greater than that of Mix A was met.

Figure 4.40 shows the strength value (maximum stress) and fracture energy for the IDEAL-CT test for the two QA sample mixes for each of the four mixes. The two QA samples for each mix have similar fracture values, while the strength values show the greatest within-mix variability

for Mixes A and C. The averaged results in Figure 4.41 show similar values for strength and fracture energy for the four mixes, with Mix B having somewhat greater strength on average. The strength results correspond to the flexural fatigue results that showed similar stiffnesses at intermediate temperatures and intermediate loading speeds.

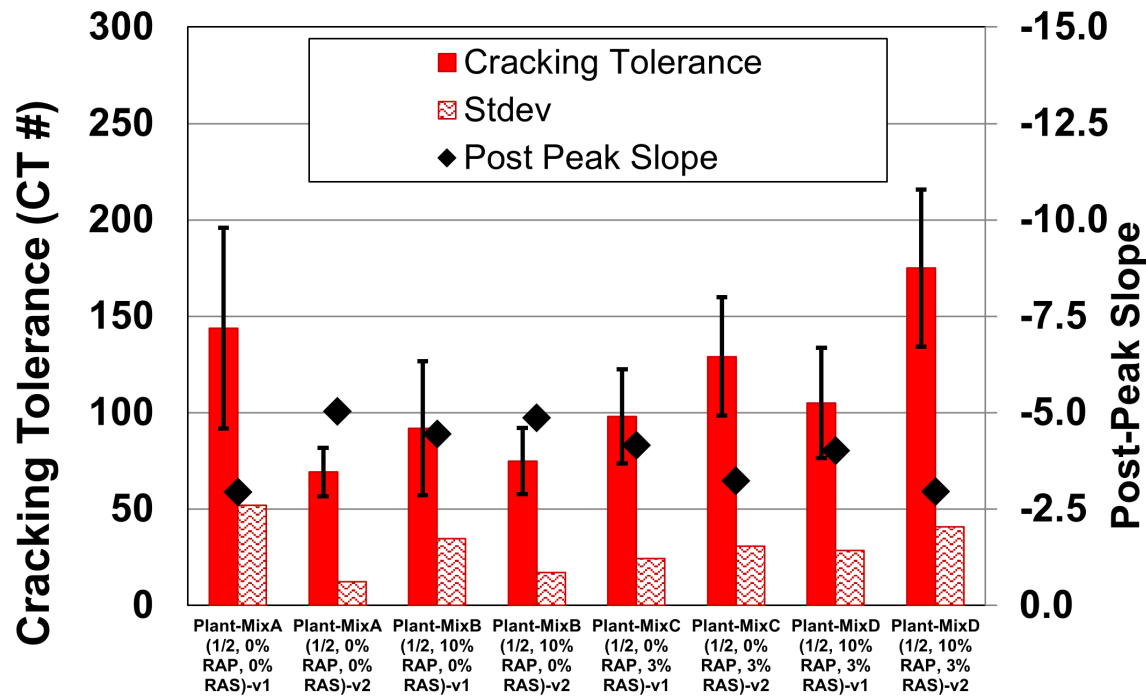


Figure 4.38: IDEAL-CT test results for QA sampled mixes (IDEAL-CT number and post-peak slope).

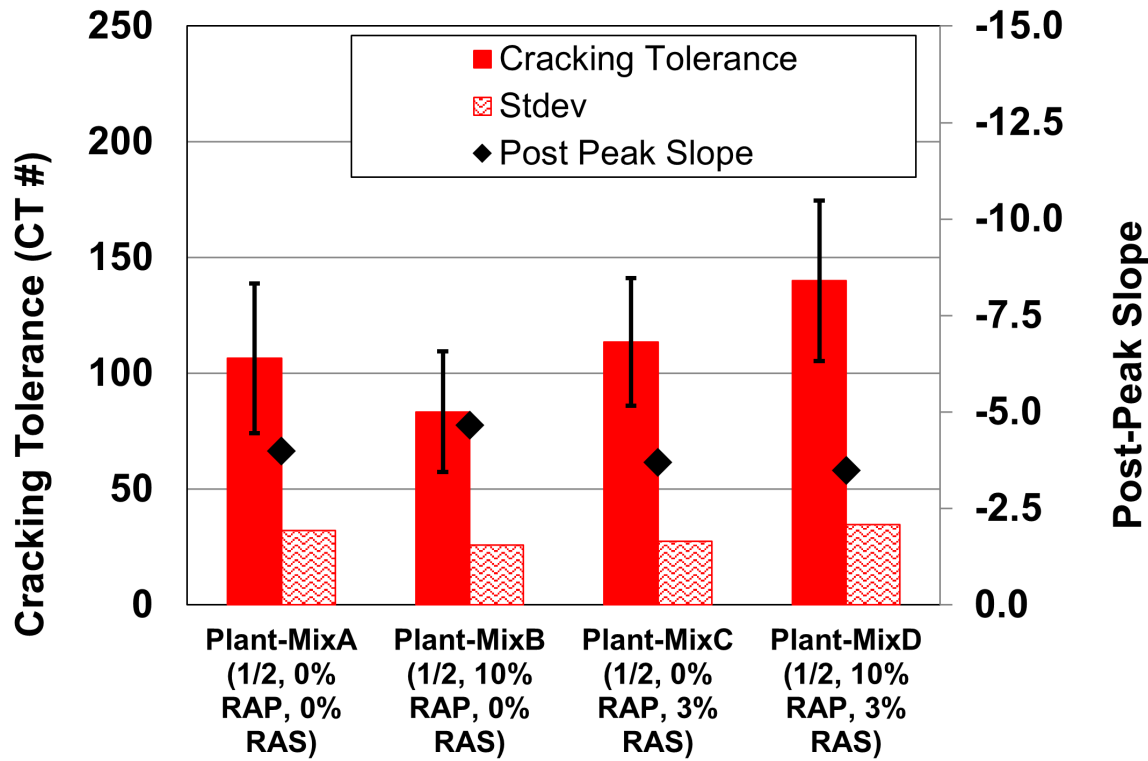


Figure 4.39: Average IDEAL-CT test results for QA sampled mixes (IDEAL-CT number and post-peak slope).

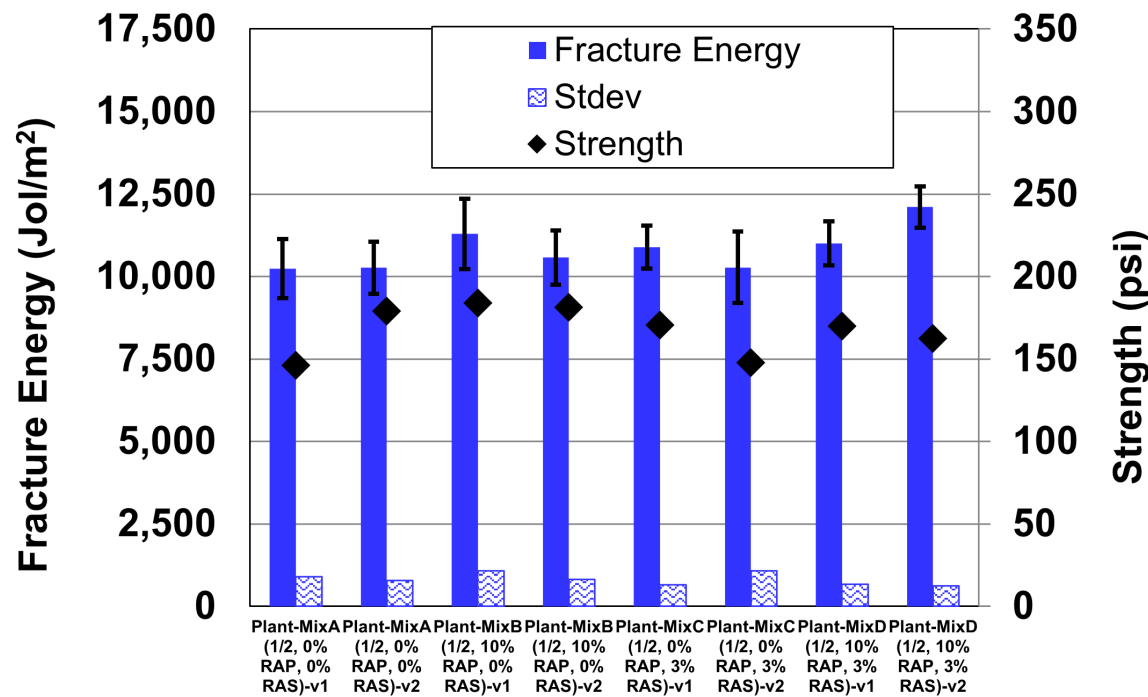


Figure 4.40: IDEAL-CT test results for QA sampled mixes (fracture energy and strength).

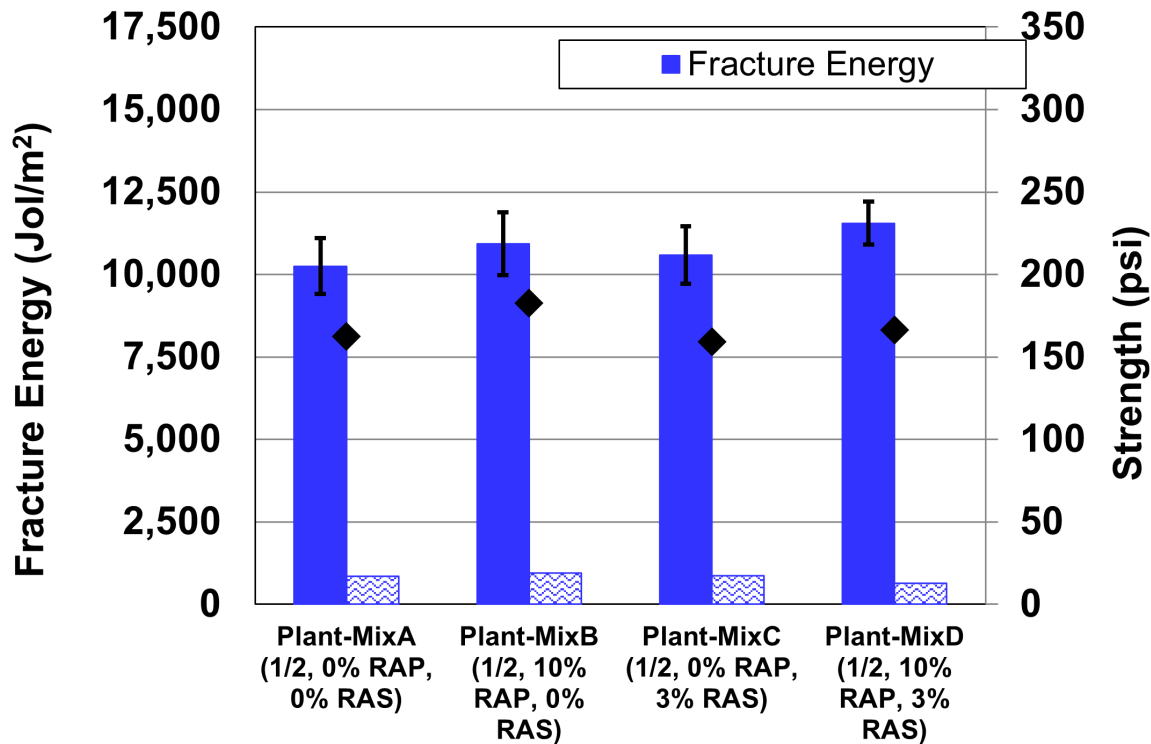


Figure 4.41: Average IDEAL-CT test results for QA sampled mixes (fracture energy and strength).

4.4.6 Fracture Cracking Resistance: Semicircular Beam Test

Semicircular beam (SCB) test results from the I-FIT approach for testing and analysis are shown in Figure 4.42 for the fracture energy and strength for the two QA samples for each of the four mixes, and Figure 4.43 shows the averaged results. The results show similar variability between QA samples for both parameters. The averaged results show that Mixes A, B, and D had similar fracture energies, while Mix C had somewhat lower fracture energy. Compared with the IDEAL-CT test, the SCB test results show similar fracture energies for all four mixes. Mix B had somewhat higher strength than the other three mixes, which all had similar results. The similarity of strength values matches the flexural and triaxial stiffness results, indicating similar stiffnesses at intermediate temperatures and loading frequencies. The IDEAL-CT strength values were also similar to each other and with Mix B having somewhat higher strength.

Figure 4.44 shows the flexibility index and post-peak slope results for the two QA samples for each mix. The variability of both parameters between QA samples was similar across the four mixes. Figure 4.45 shows the average values for the two QA samples. Figure 4.45 shows that

the flexibility index on average is greatest for Mix A, followed by Mixes C and D with similar values, and then Mix B. The post-peak slopes ranked the opposite of the flexibility index. The rankings of the JMF verification samples and the QA samples for Mixes A and C are similar. The flexibility index rankings differ from those of the IDEAL-CT test because the results showed Mix D had the best result instead of Mix A. Both tests ranked Mix B the lowest.

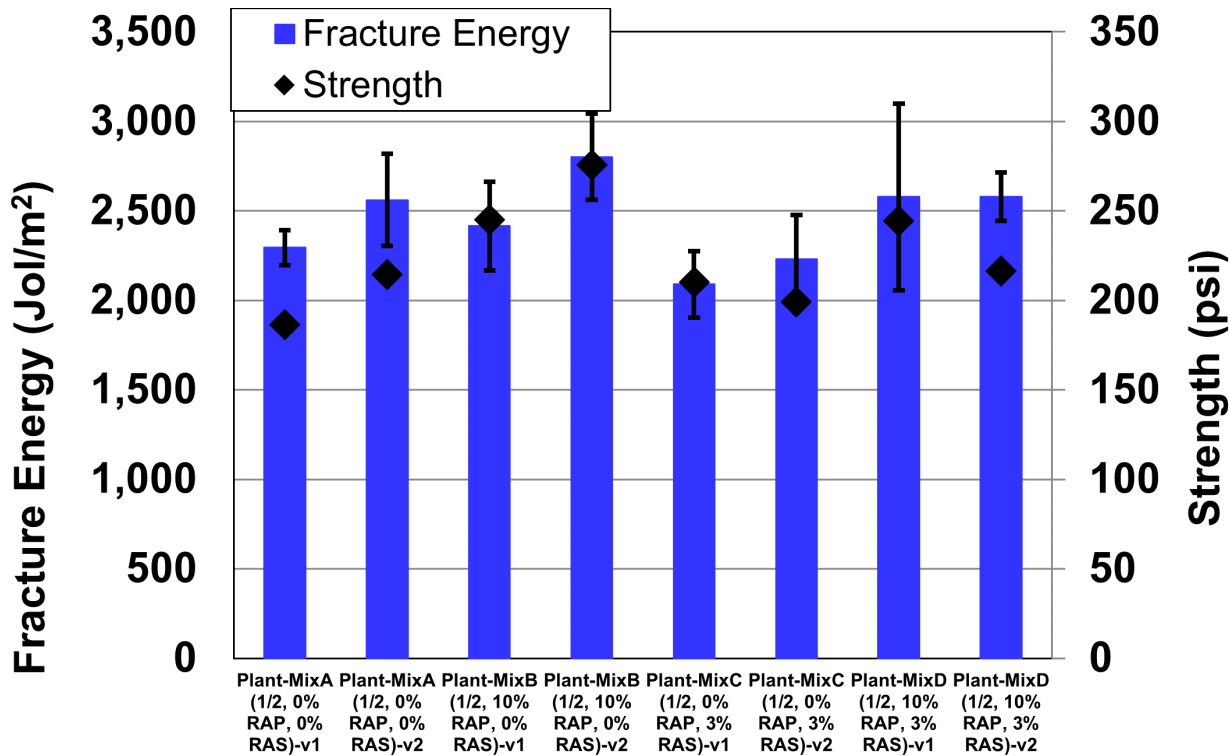


Figure 4.42: I-FIT test results for QA sampled mixes (fracture energy and strength).

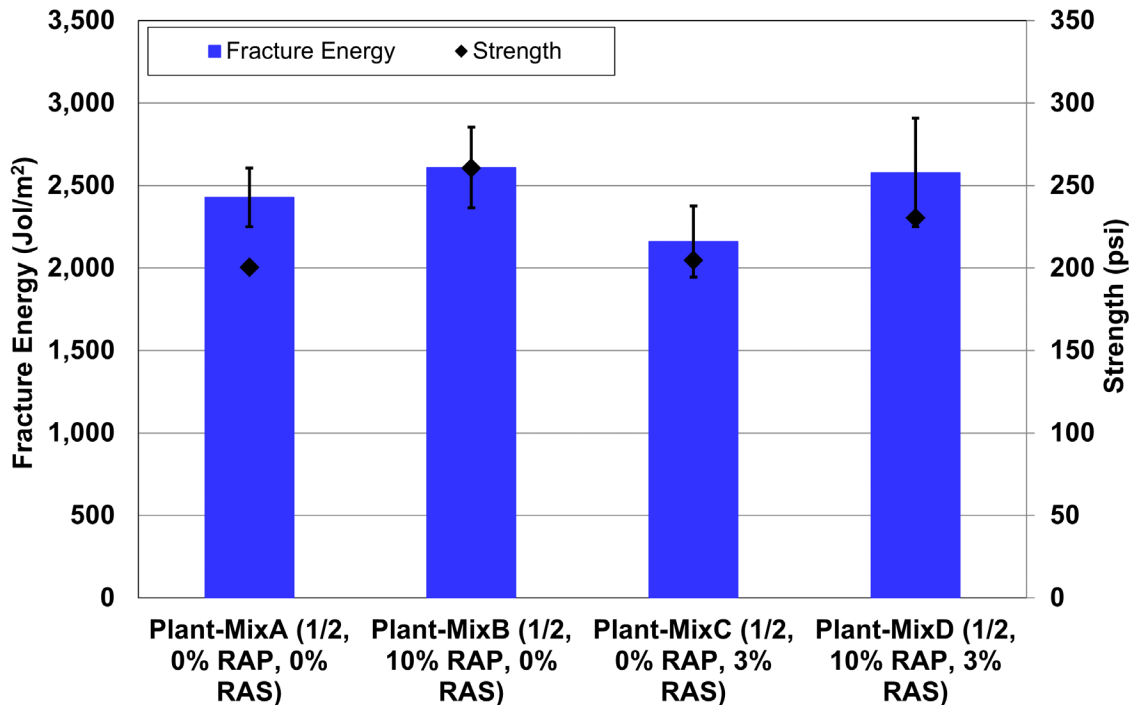


Figure 4.43: Average I-FIT test results for QA sampled mixes (fracture energy and strength).

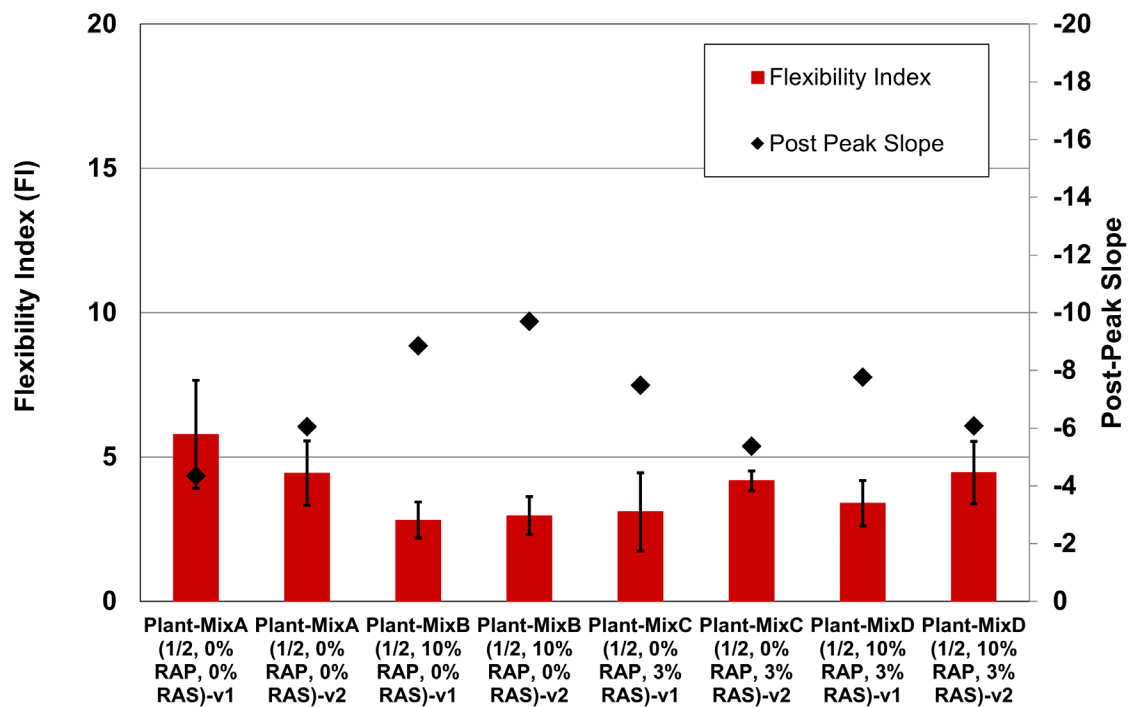


Figure 4.44: I-FIT test results for QA sampled mixes (flexibility index and post-peak slope).

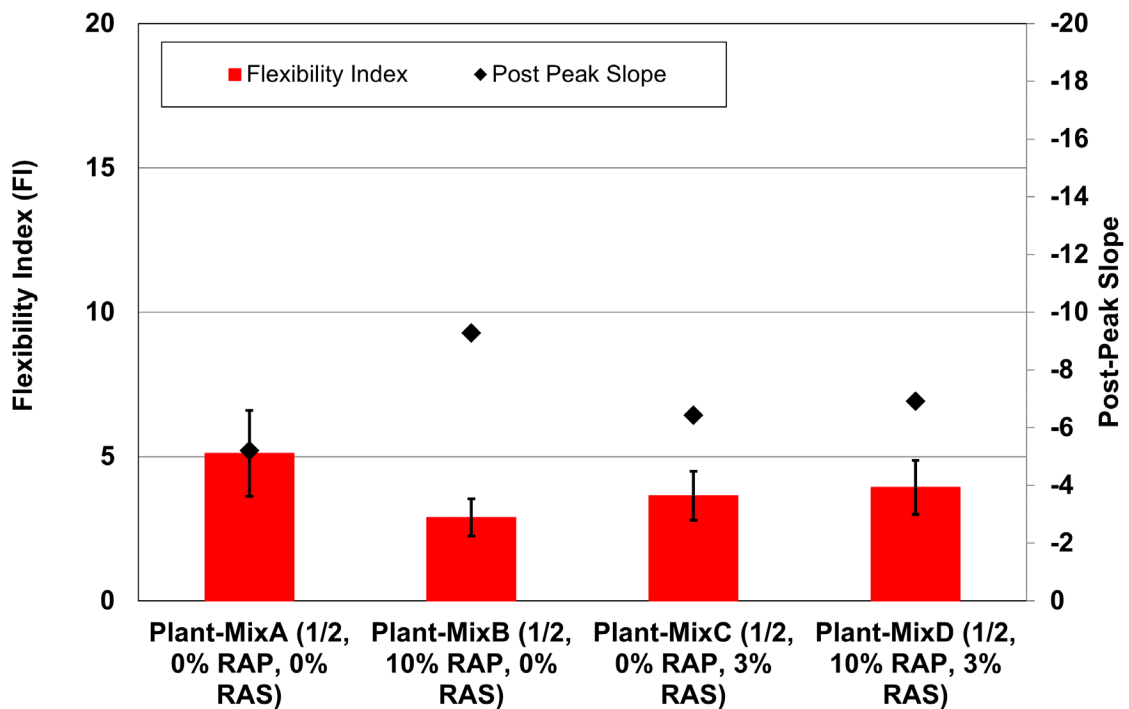


Figure 4.45: Average I-FIT test results for QA sampled mixes (flexibility index and post-peak slope).

5. OBSERVATIONS FROM CONSTRUCTION

5.1 Milling and Post-Milling Condition

The sections were milled prior to placement of the test section material. It could be seen after milling that the existing asphalt varied in thickness. In some locations near the edges of the traveled way, the pre-overlay milling removed all the asphalt and left granular material and subgrade visible. In other locations, remnants of full-depth digouts remained with thicker asphalt than the area outside of the wheelpaths. Both remnant digouts and exposed base are shown in Figure 5.1. Extensive cracking remained in the milled asphalt, indicating that the cracks had been full-depth and there is a likelihood of reflective cracking occurring in the new overlays placed as part of this project, shown in Figure 5.2.

On routes that have had asphalt layers built up over decades of overlay, milling, digouts, and maintenance repairs, variability in the underlying asphalt layers is not uncommon and this resulted in the incomplete removal of existing asphalt lifts. Figure 5.3 shows where portions of the lane had thin remnants of previous lifts while other portions had clean removal of a previous lift. In some cases, the remnants were incompletely bonded to the pavement, and these conditions can result in poor bonding within the overlaid structure.

5.2 Overlay Construction

5.2.1 Plant Operations

There were no problems at the mixing plant that were out of the ordinary for a paving project of this type. Figure 5.4 shows the RAS material in tote bags ready for mixing.

5.2.2 Paving

The design thickness of the overlay was 0.2 ft. Figure 5.5 shows Mix A material from the first day of paving being picked up from the windrow. Figure 5.6 shows one lane paved and the second lane with the tack coat ready for paving on Day 2. There were no problems with the tack coat application. Figure 5.7 shows windrowed Mix D material with RAP and RAS being picked up for paving. The temperature in the windrow was 138°C (280°F). The lumps that can be seen

were soft and fell apart before going through the paver. They did not cause segregation in the mat behind the paver.

Breakdown rolling on Mix D is shown in Figure 5.8. The material “locked up” quickly, and paving crews indicated no problems with compaction. Figure 5.9 shows the compacted mat, and Figure 5.10 shows a close-up. The mat had good surface characteristics and showed no signs of segregation as can be seen in Figure 5.11 during coring.



Figure 5.1: Remnants of digouts remaining in asphalt after milling and milling down to aggregate base in half of the lane.

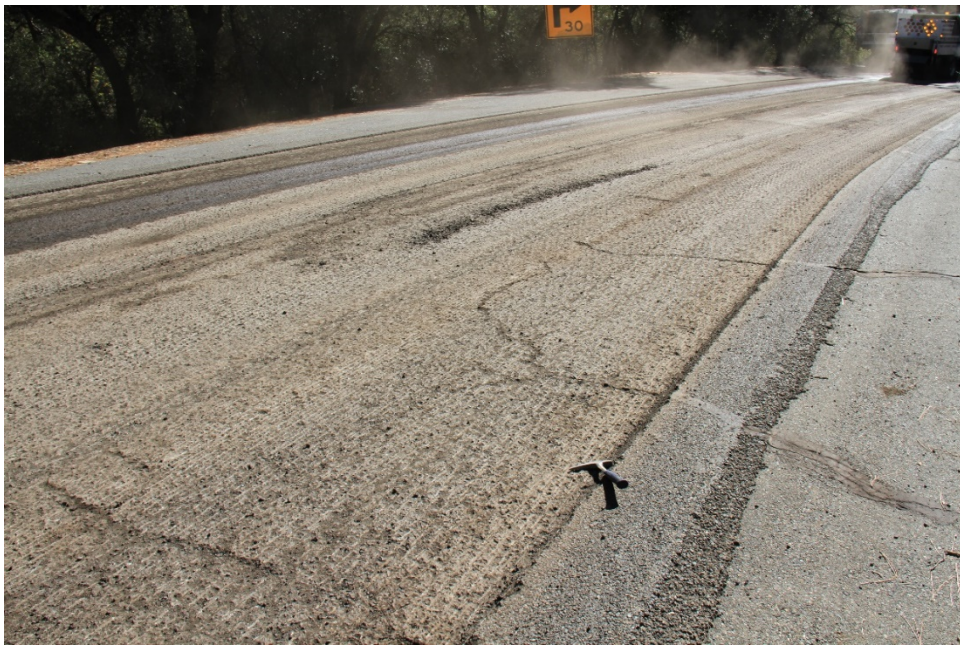


Figure 5.2: Cracking in remaining asphalt after milling.



Figure 5.3: Cracking in remaining asphalt after milling.



Figure 5.4: RAS in tote bags before mixing.



Figure 5.5: Windrow pick up of a mix containing RAS.



Note: Overlay elevation is below elevation of unmilled shoulder.

Figure 5.6: One lane paved with a mix containing RAS (Mix C) and other lane with tack coat before overlay.



Figure 5.7: Windrowed RAP-RAS Mix D material.



Figure 5.8: Breakdown rolling.



Figure 5.9: Compacted mat.



Figure 5.10: Close-up of compacted surface at density test location showing good characteristics and no evidence of segregation.



Figure 5.11: Sampling cores from new pavement.

6. CONCLUSIONS AND RECOMMENDATIONS FROM THE ELD 49 PILOT PROJECT

6.1 Conclusions

The following conclusions are drawn from the data collected during JMF verification and QA testing for four mixes included in the ELD 49 pilot project. For reference, the four mixes can be summarized as follows:

- Mix A, containing 0% RAP and 0% RAS (used as a control mix for this project—although mixes without RAP are not typically used on Caltrans projects)
- Mix B, containing 10% RAP and 0% RAS (mix used on the rest of the paving project outside the test sections and typical of Caltrans HMA mixes in terms of use of RAP and RAS)
- Mix C, containing 0% RAP and 3% RAS
- Mix D, containing 10% RAP and 3% RAS

6.1.1 Performance-Related Properties of the Four Mixes

Conclusions based on the results from the performance-related binder and mix tests are:

- The performance-related properties of the QA sampled extracted binders and mixes were similar to those of the corresponding JMF verification samples. There were no JMF verification samples for Mix B.
- The extracted binders from Mixes B, C, and D had higher high temperature true grades and somewhat higher low temperature true grades compared with the control mix. These results indicate better rutting resistance and a similar or slightly greater risk of low temperature cracking than control Mix A.
- The control Mix A had somewhat better Delta T_c values than Mixes B, C, and D, indicating a somewhat lower risk of aging-induced block cracking. The control Mix A also had less aging under extreme aging conditions, indicating better aging resistance and therefore better block-cracking resistance.
- The extracted binders are fully diffused by the extraction process, while in the mix there may be less than complete diffusion. The extracted binder and mix frequency sweep

results had very similar rankings and trends indicating good diffusion of the RAP, RAS, and virgin binders in Mixes B, C, and D.

- The mixes with RAS (Mixes C and D) and the typical mix (Mix B) had higher binder and mix stiffnesses than the control mix (Mix A) at reduced medium to low frequencies, corresponding to intermediate to high temperatures and intermediate to slow traffic speeds, and similar stiffnesses at high reduced frequencies, corresponding to intermediate to cold temperatures and intermediate to fast traffic speeds. These results indicate that Mixes B, C, and D have a lower risk of rutting at early ages and a similar to lower risk of fatigue and reflective cracking.
- The RLT results indicated that Mixes B, C, and D have a lower risk of rutting than the control Mix A, which corresponds to the binder and mix stiffness results.
- The flexural fatigue results from the JMF verification samples for Mixes C and D had better fatigue lives than those of Mix A for strains of 300 microstrain and greater. Extrapolation of those results to 200 microstrain indicates that the fatigue life of Mix A is as good or better than that of Mixes C and D at smaller strains. The flexural fatigue results at smaller strains are not yet completed for the QA samples but indicated a similar ranking as the JMF sample results at larger strains. Ranking of flexural fatigue results from controlled deformation testing that is typically used is only applicable to fatigue and reflective cracking performance of thin asphalt overlays. For overlay thicker than about 0.2 ft. (60 mm), the interactions of stiffness and controlled deformation fatigue life need to be evaluated using mechanistic-empirical simulation.
- The IDEAL-CT results indicated better cracking resistance for Mixes C and D compared with Mix A, while the flexibility index results indicated better cracking resistance for Mix A compared with Mixes C and D. Both tests showed Mix B had the least cracking resistance. The differences between the four mixes were not large. The strength values from both tests were similar but generally showed Mix B to be somewhat stiffer.
- Qualitative analysis of binder and RAP and RAS blending through comparison of binder and mix stiffness rankings indicates that there was most likely good blending of the virgin binder, rejuvenating agent (where present) and RAP and RAS binders in Mixes B, C, and D.

6.1.2 The Four Mixes and Their Specifications

Conclusions based on this pilot project experience and review of the specifications are the following:

- The mixes submitted for job mix formula verification and tested as part of quality assurance all met the two performance-related specifications; they had IDEAL-CT values that were greater than or equal to those of the control Mix A with no RAP or RAS, and they had Delta T_c values that were greater than -5.
- The contractor used a combination of selection of the PG grade of the base binder and rejuvenating agent to produce mixes that successfully met the specifications.
- It is uncertain how setting the specification for the IDEAL-CT value based on test results for a control mix that has no RAP or RAS can be carried forth into future specifications, due to practical considerations. The use of Mix A as the control for setting specifications resulted in a mix with reduced stiffness at slow frequencies compared with Mix B, a more typical mix. The use of Mix A has some benefits for thin overlays with regard to cracking but may increase risks of rutting at early ages after construction. There are also practical considerations for use of this approach in routine practice.
- Mixes B, C, and D had better high temperature results from binder and mix testing than the virgin Mix A, and generally similar intermediate and low temperature results as Mix A. This indicates that eliminating the practice of requiring same high temperature blended binder properties as a method of avoiding binder testing at intermediate and low temperatures can result in potential gains in rutting resistance at high temperatures without sacrificing low and intermediate temperature properties, if blended binder testing is performed at low and intermediate temperatures as part of binder design.
- Carbonyl content was found to be a good predictor of binder stiffness, the Glover-Rowe parameter related to block cracking, and the crossover modulus related to low temperature creep with aging.

6.1.3 Construction of the Test Sections

Conclusions from observations during construction, including at the mixing plant and at the test sections during paving are the following:

- The asphalt remaining in place after milling had transverse, longitudinal, and wheelpath cracking in it, which may be causes of reflective cracking in the overlays. The existing cracking types and extents need to be considered when evaluating the future cracking performance of the overlays in the test sections. There were also locations where there was no remaining asphalt, which should also be considered.
- There were no problems with mixing or compaction of any of the mixes.
- The surfaces appeared to be similar for all mixes.

6.2 Preliminary Recommendations

The following recommendations are based on the conclusions presented above:

- Use of the high temperature grade to control intermediate and low temperature properties of blended binders should be reconsidered. This approach to specification may increase the risk of rutting without obtaining better cracking resistance.
- Valuable information was gathered in this pilot project, and additional pilot projects for high RAP and RAS should be built and monitored to gain additional information regarding mixes and simplified performance tests. Current mix types containing less than 15% RAP should be used as the control since they represent current practice.
- The testing effort for this project provided valuable data and insight but may not be sustainable for the likely number of future pilot projects in terms of cost. It is suggested that the scope of testing in each pilot project should be evaluated and potentially reduced where possible.
- The potential performance-related tests should continue to be assessed for efficiency, variability, sensitivity to important variables, and practicality.
- The testing for stiffness, fatigue, and fracture properties did not consider the effects of aging in the field, which is important for fatigue cracking performance and as an indicator of long-term aging related cracking. It is recommended that a protocol for laboratory medium-term oven aging (MTOA) of loose mix be developed and included in the testing for future pilot projects. It is also recommended that the mixes in this pilot project be tested again for those properties after MTOA.

REFERENCES

1. Alavi, M. Z., Jones, D., He, Y., Chavez, P., and Liang, Y. 2017. Investigation of the Effect of Reclaimed Asphalt Pavement and Reclaimed Asphalt Shingles on the Performance Properties of Asphalt Binders: Phase 1 Laboratory Testing (Research Report: UCPRC-RR-2016-06). UC Davis: University of California Pavement Research Center. escholarship.org/uc/item/5jq4m661.
2. Pellinen, T.K., Witczak, M.W., and Bonaquist, R.F. 2004. "Asphalt Mix Master Curve Construction using Sigmoidal Fitting Function with Non-Linear Least Squares Optimization." In *Recent Advances in Materials Characterization and Modeling of Pavement Systems*, edited by Tutumluer, E., Najjar, Y.M., and Masad, E., 83–101. Reston, VA: American Society of Civil Engineers.
3. Liang, Y., Wu, R., Harvey, J.T., Jones, D., and Alavi, M.Z. 2019. "Investigation into the Oxidative Aging of Asphalt Binders." *Transportation Research Record* 2673, no. 6: 368–378.
4. Morian, N., Hajj, E., and Sebaaly, P. 2013. "Significance of Mixture Parameters on Binder Aging in Hot-Mix-Asphalt Mixtures." *Transportation Research Record* 2370, no. 1: 116–127.
5. Mohammad, L.N., Cooper, S.B., and Elseifi, M.A. 2011. "Characterization of HMA Mixes Containing High Reclaimed Asphalt Pavement Content with Crumb Rubber Additives." *Journal of Materials in Civil Engineering* 23, no. 11: 1560–1568.
6. Hofko, B., Alavi, M.Z., Grothe, H., Jones, D., and Harvey, J. 2017. "Repeatability and Sensitivity of FTIR ATR Spectral Analysis Methods for Bituminous Binders." *Materials and Structures* 50, no. 3.
7. Lamontagne, J., Dumas, P., Mouillet, V., and Kister, J. 2001. "Comparison by Fourier Transform Infrared (FTIR) Spectroscopy of Different Aging Techniques: Application to Road Bitumen." *Fuel* 80, no. 4: 483–488.
8. Williams, M.L., Landel, R.F., and Ferry, J.D. 1955. "The Temperature Dependence of Relaxation Mechanisms in Amorphous Polymers and other Glass-Forming Liquids." *Journal of the American Chemical Society* 77, no. 14: 3701–3707.
9. Ozer, H., Al-Qadi, I.L., Lambros, J., El-Khatib, A., Singhvi, P., and Doll, B. 2006. "Development of the Fracture-Based Flexibility Index for Asphalt Concrete Cracking Potential Using Modified Semicircle Bending Test Parameters." *Construction and Building Materials* 115: 390–401.
10. Harvey, J., Liu, A., Zhou, J., Signore, J., Coleri, E., and He, Y. 2014. *Superpave Implementation Phase II: Comparison of Performance-Related Test Results* (Research Report: UCPRC-RR-2015-01). Davis and Berkeley, CA: University of California Pavement Research Center. escholarship.org/uc/item/7vg1c54z.

11. He, Y. 2016. "Interaction Between New and Age-Hardened Binders in Asphalt Mixes Containing High Quantities of Reclaimed Asphalt Pavement and Reclaimed Asphalt Shingles." PhD diss. University of California, Davis. proquest.com/openview/fe86c3c2d3a5736f49466890cde58750/1?pq-origsite=gscholar&cbl=18750&diss=y.
12. Pang, C. 2019. "Development of Shift Factors Between Repeated Load Triaxial and Repeated Simple Shear Test Results." MS thesis, University of California Davis. proquest.com/openview/c275721ae6bac8151fbf30c6d64f0106/1?pqorigsite=gscholar&cb=51922&diss=y.
13. Rowe, G. 2011. Prepared discussion response to "Evaluation of the Relationship Between Asphalt Binder Properties and Non-Load Related Cracking" by Anderson, R.M., King, G.N., Hanson, D.I., and Blankenship, P.B. *Journal of the Association of Asphalt Paving Technologists* 80: 615–664.
14. Liu, M. Lunsford, K.M., Davison, R.R., Glover, C.J. and Bullin, J.A. 1996. "The Kinetics of Carbonyl Formation in Asphalt." *AICHe Journal* 42, no. 4: 1069–1076.
15. Tayebali, A., Deacon, J., Coplantz, J., Harvey, J., and Monismith, C. 1994. *Fatigue Response of Asphalt-Aggregate Mixes; Part 1: Test Method Selection* (SHRP-A-404). Washington, DC: Transportation Research Board. onlinepubs.trb.org/onlinepubs/shrp/shrp-a-404.pdf.
16. Sousa, J., Leahy, R., Harvey, J., and Monismith, C. 1994. *Permanent Deformation Response of Asphalt Aggregate Mixes; Part 1: Test Method Selection* (SHRP-A-415). Washington, DC: Transportation Research Board. onlinepubs.trb.org/onlinepubs/shrp/SHRP-A-415.pdf.
17. Ullidtz, P., Harvey, J., Tsai, B.W. and Monismith, C. 2008. "Calibration of Mechanistic Empirical Models for Flexible Pavements Using the WesTrack Experiment." *Journal of the Association of Asphalt Paving Technologists* 77: 591–630.
18. Harvey, J., Guada, I., and Long, F. 2000. "Effects of Material Properties, Specimen Geometry, and Specimen Preparation Variables on Asphalt Concrete Tests for Rutting." *Journal of the Association of Asphalt Paving Technologists* 69: 236–280.
19. Witczak, M.W., Kaloush, K., Pellinen, T., El-Basyouny, M., and Von Quintus, H. 2002. *Simple Performance Test for Superpave Mix Design* (NCHRP Report 465). Washington, DC: Transportation Research Board.
20. Zhang, Y., Luo, R., and Lytton, R.L. 2012. "Characterizing Permanent Deformation and Fracture of Asphalt Mixtures by Using Compressive Dynamic Modulus Tests." *Journal of Materials in Civil Engineering* 24, no. 7: 898–906.
21. Harvey, J., Weissman, S., and Monismith, C. 2009. "Rutting Characterization of Asphalt Concrete Using Simple Shear Tests." In *Modeling of Asphalt Concrete*, edited by Y. Richard Kim, 269–316. Reston, VA: American Society of Civil Engineers.
22. Jiao, L., Harvey, J., Wu, R. Elkashaf, M., Jones, D., and Liang, Y. Forthcoming. *Preliminary Study on Developing a Surrogate Performance-Related Test for Fatigue Cracking of*

Asphalt Pavements (Research Report: UCPRC-RR-2021-02). Davis and Berkeley, CA:
University of California Pavement Research Center.